CANADIAN THESES ON MICROFICHE

I.S.B.N.

THESES CANADIENNES SUR MICROFICHE

National Library of Canada
Collections Development Branch

Canadian Theses on
Microfiche Service

Ottawa, Canada
K1A 0N4

Bibliothèque nationale du Canada
Direction du développement des collections

Service des thèses canadiennes
sur microfiche

NOTICE

The quality of this microfiche is heavily dependent upon the quality of the original thesis submitted for microfilming. Every effort has been made to ensure the highest quality of reproduction possible.

If pages are missing, contact the university which granted the degree.

Some pages may have indistinct print especially if the original pages were typed with a poor typewriter ribbon or if the university sent us a poor photocopy.

Previously copyrighted materials (journal articles, published tests, etc.) are not filmed.

Reproduction in full or in part of this film is governed by the Canadian Copyright Act, R.S.C. 1970, c. C-30. Please read the authorization forms which accompany this thesis.

THIS DISSERTATION
HAS BEEN MICROFILMED
EXACTLY AS RECEIVED

AVIS

La qualité de cette microfiche dépend grandement de la qualité de la thèse soumise au microfilmage. Nous avons tout fait pour assurer une qualité supérieure de reproduction.

S'il manque des pages, veuillez communiquer avec l'université qui a conféré le grade.

La qualité d'impression de certaines pages peut laisser à désirer, surtout si les pages originales ont été dactylographiées à l'aide d'un ruban usé ou si l'université nous a fait parvenir une photocopie de mauvaise qualité.

Les documents qui font déjà l'objet d'un droit d'auteur (articles de revue, examens publiés, etc.) ne sont pas microfilmés.

La reproduction, même partielle, de ce microfilm est soumise à la Loi canadienne sur le droit d'auteur, SRC 1970, c. C-30. Veuillez prendre connaissance des formules d'autorisation qui accompagnent cette thèse.

LA THÈSE A ÉTÉ
MICROFILMÉE TELLE QUE
NOUS L'AVONS REÇUE

NL-339 (r. 82/08)

Canada

NUCLEAR MAGNETIC RESONANCE STUDIES OF THE INTERACTION OF LOCAL ANESTHETICS WITH MEMBRANES AND MOTIONS IN SOLID n-ALKANES

Eric Charles Kelusky
M.Sc., Brock University

Thesis submitted to the School of Graduate Studies, University of Ottawa, in partial fulfillment of the requirements for the Degree of Doctor of Philosophy in Chemistry

Ottawa, Ontario
April, 1983

Perhaps the worst plight of a vessel is to be caught in a gale on a lee shore. In this connection the following . . . rules should be observed:
1. Never allow your vessel to be found in such a predicament . . .

CALLINGHAM,
Seamanship: Jottings for the Young Sailor

ABSTRACT

The work presented in this thesis represents an investigation of two problems. The first is a study of the interaction of two local anesthetics, tetracaine (TTC) and procaine (PRC), with phosphatidylethanolamine (PE) and phosphatidylcholine (PC) model membranes and with membranes of human erythrocytes and *Acholeplasma laidlawii* B. The second problem is an investigation of the motions of the long chain n-alkanes in their various solid phases.

The interaction of tetracaine and procaine with multilamellar dispersions of phosphatidylethanolamine has been investigated using ^2H NMR of specifically deuterated anesthetics. Tetracaine is found to partition more strongly than procaine into the lipid. The ^2H NMR spectra show a Pake doublet and a narrow line, with the former corresponding to membrane bound anesthetic and the latter to anesthetic which is free in solution. The integrated areas of the narrow line and the Pake doublet correspond to the concentrations of free and bound anesthetic predicted from the partition coefficients. There is no strong pH dependence for the quadrupole splittings of TTC, suggesting a similar depth of penetration into the PE bilayer over the entire pH range. The data are consistent with a model in which TTC acts as a wedge to

stabilize the phosphatidylethanolamine bilayer against transition to a hexagonal structure. The spin lattice relaxation times (T_1) are generally shorter in the membrane than in solution, suggesting slower motions, particularly for the aromatic ring of TTC.

The binding of tetracaine and procaine with multilamellar dispersions of egg phosphatidylcholine has been reexamined. The ^2H NMR line shapes of specifically deuterated local anesthetics are found to be very dependent on the attainment of a true equilibrium condition. The equilibrium could most properly be reached by the use of repeated freeze-thaw-vortex cycles. The data for tetracaine are consistent with the three site exchange model proposed earlier [Y. Boulanger, S. Schreier, L.C. Leitch and I.C.P. Smith, Can. J. Biochem. 58, 986 (1980)]. Tetracaine is in slow exchange between a strongly bound site and a weakly bound site and in fast exchange between the weakly bound site and free in solution. The slow exchange rate is estimated, from temperature and dilution studies, to be approximately 1.5×10^3 s^{-1} at pH 5.5 and slightly faster at pH 9.5. Comparison of the quadrupole splittings in PC with those seen in PE suggest that the location of the strongly bound site is very dependent on the anesthetic charge. This is in contrast to egg PE, where the molecular shapes appear to be the dominant factor in the anesthetic location.

The influence of TTC and PRC on a bilayer of specifically deuterated DMPE was studied by ^{2}H and ^{31}P NMR. Tetracaine is observed to penetrate into the hydrocarbon region while PRC does not. Tetracaine also induces changes in the conformation of the ethanolamine headgroup. It appears that both the charged and uncharged forms of TTC penetrate to the same depth in the PE bilayer. As with the studies of labelled TTC in egg PE, it is apparent that it is the molecular shape, not the charge, which is important in anesthetic - PE interactions.

At low pH the *net* diffusion rate (a combination of the TTC and PE rates) is slow on the ^{2}H NMR time scale, resulting in the observation of two populations of DMPE. This is the first example of a slow lateral diffusion and it likely arises from increased headgroup interactions between PE's and between PE and TTC.

The interaction of TTC and PRC with membranes of human erythrocytes and *Acholeplasma laidlawii* B was also studied. Exchange rates of anesthetics between biological membranes and water are proposed to be much faster than in the model membrane cases and the quadrupole patterns are therefore not observed. However the spectra do indicate that TTC penetrates into the hydrocarbon region while PRC does not. There is no major difference between the results at high and low pH, suggesting a similar depth of penetration for both charged and uncharged TTC. It is

also proposed that the TTC molecule sits somewhat higher in the bilayer of a biological membrane than in model bilayers.

The ^2H NMR spectra of perdeuterononadecane and several specifically deuterated nonadecanes were examined in solid phases I (orthorhombic) and II (rotator). In phase I the central portion of the chain is static on the time scale of 10^{-5} seconds; however, the chain ends are subject to torsional motions. In phase II, the chains undergo hindered rotation. The phase II spectra of the methylene groups, located in the centre of the chain, can be simulated with a model in which the rigid chain undergoes 82° jumps between equivalent sites. However, this model is inadequate for the methyl and methylene groups near the chain ends. The data suggest higher amplitudes of torsional motion in these positions.

Studies of the C_{21} n-alkane, specifically deuterated at positions 2, 4, 6 and 11, confirm the rigid central portion of the chain in phase I. There is clear evidence for motions at the ends of the chains. These motions are consistent with small angle jumps which increase in size with proximity to the end of the chain, and which persist down to $-20^{\circ}C$.

The C_{21} alkane chain in phase II, like the C_{19}, undergoes hindered rotation, and again not as a rigid

rotator. The chains undergo jumps of 82° at the centre, but this increases slightly starting at carbon 6, and reaches 86° for the final methylene. The jump angle is also observed to be temperature dependent in phase II; increasing by 4° over the phase II temperature range. Superimposed on the chain jumping is an off axis motion which correlates with the appearance of gauche rotamers.

For the C_{35} n-alkane, ^{2}H NMR cannot detect any motions in the low temperature solid phases. In phase II the alkane undergoes restricted jumps just slightly smaller than those observed for the C_{19} and C_{21}.

ACKNOWLEDGEMENTS

I would like to express my gratitude to the many people in the Molecular Biophysics Group who have provided assistance during my stay at the NRC. In particular, I wish to thank Dr. Keith W. Butler for answering many biological questions; Dr. R. Andrew Byrd for his help with the NMR experiments and Dr. Harold Jarrell for advice on synthetic procedures. I also wish to thank Drs. David G. Cameron and Hector L. Casal for their insights and suggestions on alkanes. The support, friendship and suggestions of my fellow students have been most gratefully appreciated. I wish to thank the National Research Council, Guest Worker Program for allowing me to work at the NRC, the Natural Sciences and Engineering Research Council for their financial support and Mrs. Yvonne Rowe for the typing of this thesis.

Finally, I wish to express my appreciation to my supervisor, Dr. Ian C.P. Smith for his support and advice during my stay at the NRC.

TABLE OF CONTENTS

TABLES

FIGURES

ABBREVIATIONS

BPC	borate-phosphate-citrate buffer
C_{19}	nonadecane
C_{19}-d_{40}	perdeuterononadecane
C_{19}-2-d_2	2,2-dideuterononadecane
C_{19}-10-d_2	10,10-dideuterononadecane
C_{19}-1,19-d_6	1,1,1,19,19,19-hexadeuterononadecane
C_{21}	heneicosane
C_{21}-2-d_2	2,2-dideuteroheneicosane
C_{21}-4-d_2	4,4-dideuteroheneicosane
C_{21}-6-d_2	6,6-dideuteroheneicosane
C_{21}-11-d_2	11,11-dideuteroheneicosane
C_{35}	pentatriacontane
C_{35}-18-d_2	18,18-dideuteropentatriacontane
CSA	chemical shift anisotropy
DMF	dimethylformamide
DMPC	1,2-dimyristoyl-sn-glycero-3-phosphocholine
DMPE	1,2-dimyristoyl-sn-glycero-3-phosphoethanolamine
1-[2'-$^2H_2$]DMPE	1-[2'-$^2H_2$]-myristoyl-2-myristoyl-sn-glycero-3-phosphoethanolamine
2-[2'-$^2H_2$]DMPE	1-myristoyl-2-[2'-$^2H_2$]-myristoyl-sn-glycero-3-phosphoethanolamine
2-[4'14'-$^2H_5$]-DMPE	1-myristoyl-2-[4'14'-$^2H_5$]-myristoyl-sn-glycero-3-phosphoethanolamine

3-[1',2'-$^2H_4$]DMPE	1,2-dimyristoyl-sn-glycero-3-phospho-[1'2'-$^2H_4$]-ethanolamine
DPPC	1,2-dipalmitoyl-sn-glycero-3-phosphocholine
DPPE	1,2-dipalmitoyl-sn-glycero-3-phosphoethanolamine
egg PC	phosphatidylcholine from eggs
egg PE	a semisynthetic phosphatidylethanolamine made from egg PC
ESR	electron spin resonance
FID	free induction decay
GC/MS	gas chromatography/ mass spectrometry
GPC·$CdCl_2$	sn-glycero-3-phosphocholine cadmium chloride adduct
K_p	partition coefficient
lyso-MPC	1-myristoyl-sn-glycero-3-phosphocholine
NMR	nuclear magnetic resonance
PA	phosphatidic acid
PC	phosphatidylcholine
PE	phosphatidylserine
PRC	procaine (see figure 11 for labelled structures)
PRC-d_2	2-dimethylaminoethyl-4-aminobenzoate-3,5-d_2
PRC-d_4	2-diethyl-1,1,1',1'-d_4-aminoethyl-4-amino-benzoate
PS	phosphatidylserine
TTC	tetracaine (see figure 11 for labelled structures)
TTC-d_2	2-dimethylaminoethyl-4-butylaminobenzoate-3,5-d_2
TTC-d_3	2-dimethylaminoethyl-4-butyl-4,4,4-d_3-aminobenzoate

TTC-d_6	2-dimethyl-d_6-aminoethyl-4-butylaminobenzoate
TTC-d_9	2-dimethylaminoethyl-4-butyl-1,1,2,2,3,3,4,4,4-d_9-aminobenzoate

CHAPTER I

INTRODUCTION

I.1 Membranes: Biological and Model

The biological membrane represents a complex structure-function correlational problem in the study of living organisms. The membrane acts both as a site for biochemical activity and as a barrier between the intra and extracellular environments. In its role as a barrier the membrane is selective, rejecting the passage of some materials while actively transporting others.

This multi-functional facet of the membrane arises as a consequence of its composition and structure. The membrane is known to be composed of both phospholipids and neutral lipids as well as proteins and carbohydrates. Its organization is now generally accepted to conform to the fluid mosaic model of Singer and Nicolson (1). In this model (Figure 1) the lipids form a bilayer structure with their nonpolar, hydrocarbon regions facing inwards and their polar, hydrophilic groups facing outwards to the intra and extracellular media. The proteins are located within this lipid matrix, either spanning it completely (intrinsic) or facing one side only (extrinsic). Cell surface receptors and antigens would reside on the hydrophilic surfaces of the bilayer.

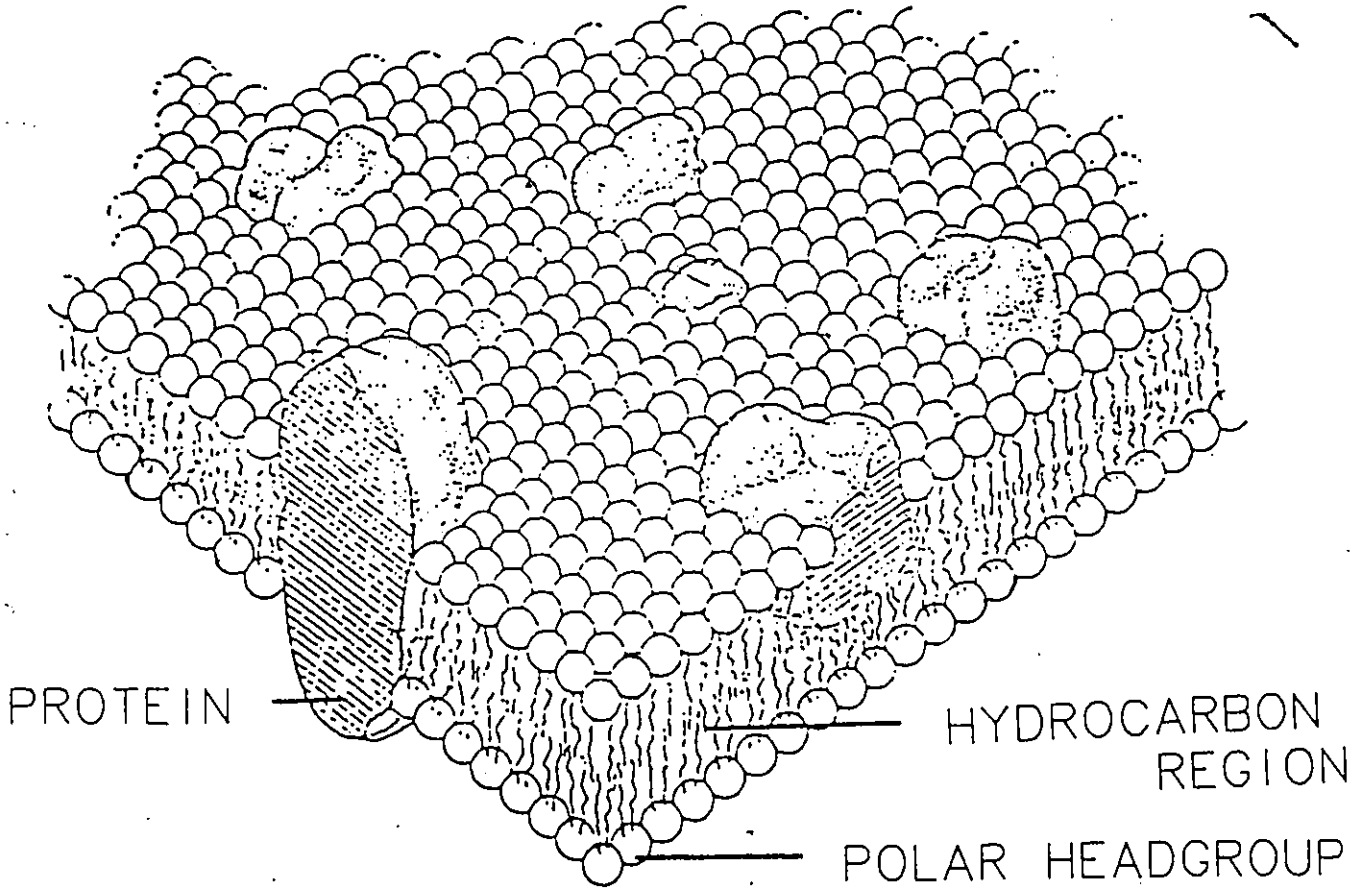

Figure 1. The bilayer structure of the biological membrane proposed in the Fluid Mosaic Model (1).

In many biological membranes the bulk of the bilayer lipids are phospholipids. These compounds consist of a glycerol backbone with fatty acid esters at the first two positions and a phosphate at the third. The phosphate, in turn, can be esterified to a variety of different alcohols, thus defining the different classes of phospholipids. Figure 2 shows the general structure of the phospholipids and the more common headgroups. The fatty acids can have varying chain lengths and degrees of unsaturation, however, in natural lipids it is most common for the unsaturated lipids to occupy the 2 position of the glycerol backbone. The presence of the nonpolar, hydrocarbon region and the polar phosphate headgroup gives the phospholipid its so-called amphipathic character. It is this character which allows it to form the bilayer arrangement in natural membranes.

In many studies of membrane structure and function it is desirable to simplify the system by making model membranes, out of a single phospholipid, and therefore, studying only one membrane component at a time. Dispersions of phospholipids in water can take several forms depending on geometrical and thermodynamic considerations (2, 3). The most common form is the liposome or multi-lamellar dispersion (Figure 3A) in which the phospholipids are arranged in concentric bilayers, much as in the manner of an onion skin. Water is located

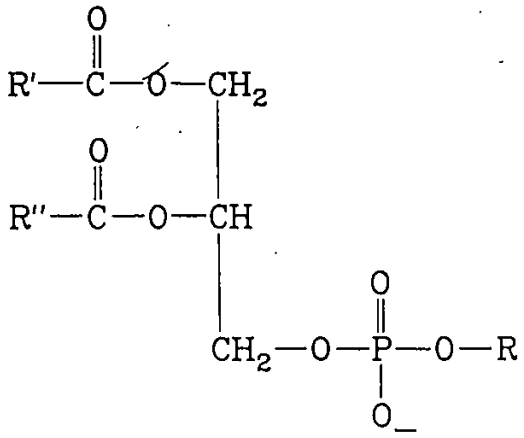

In real lipids, R' and R'' are usually saturated and unsaturated acyl chains, respectively.

–R	PHOSPHOLIPID	
–H	Phosphatidic acid	PA
$-CH_2-\underset{\displaystyle \overset{+}{N}H_3}{\underset{|}{CH}}-CO_2^-$	Phosphatidylserine	PS
$-CH_2CH_2\overset{+}{N}H_3$	Phosphatidylethanolamine	PE
$-CH_2CH_2\overset{+}{N}(CH_3)_3$	Phosphatidylcholine	PC

Figure 2. Structures of the common phospholipid classes.

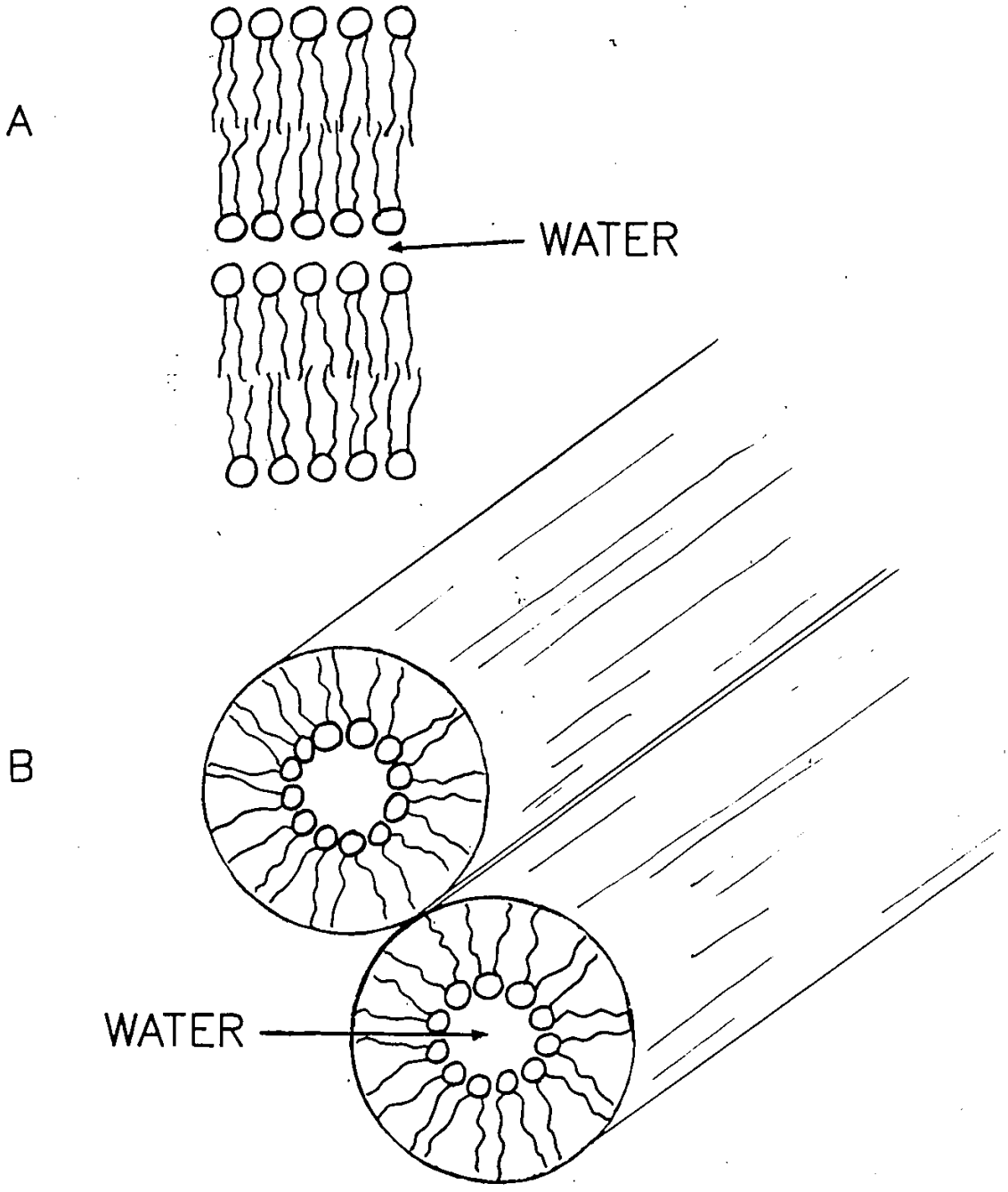

Figure 3. Two common phases for phospholipids. A) bilayer (multilamellar), B) inverted hexagonal.

between successive layers, in contact with only the hydrophilic, polar regions of the lipid. This structure most closely mimics the bilayer arrangement in natural membranes and thus represents a good model system.

Several other lipid phases are possible, including inverted hexagonal, hexagonal and micellar. In the inverted hexagonal form (Figure 3B) the phospholipids are arranged in a cylindrical tube with the headgroup facing inward. Water is located in the central region of this tube. This form occurs in several lipids, including phosphatidylethanolamines, but has not been observed in natural membranes. However, the hexagonal phase has been implicated in several membrane processes including membrane fusion (4).

I.2 Theories of Local Anesthetic Action

Local anesthetics encompass a wide range of chemical structures and have the common characteristic of being able to block nerve conduction. Chemicals observed to possess such activity include amino-carbamates, amino-ketones, alcohols, ureas, thioethers, and simple amines. For general clinical use, amino-esters such as procaine and tetracaine are often used (Figure 4). In North America, amino-amides such as lidocaine and mepivicaine have replaced the amino-esters for most clinical uses because of the absence of allergic reactions (5, 6).

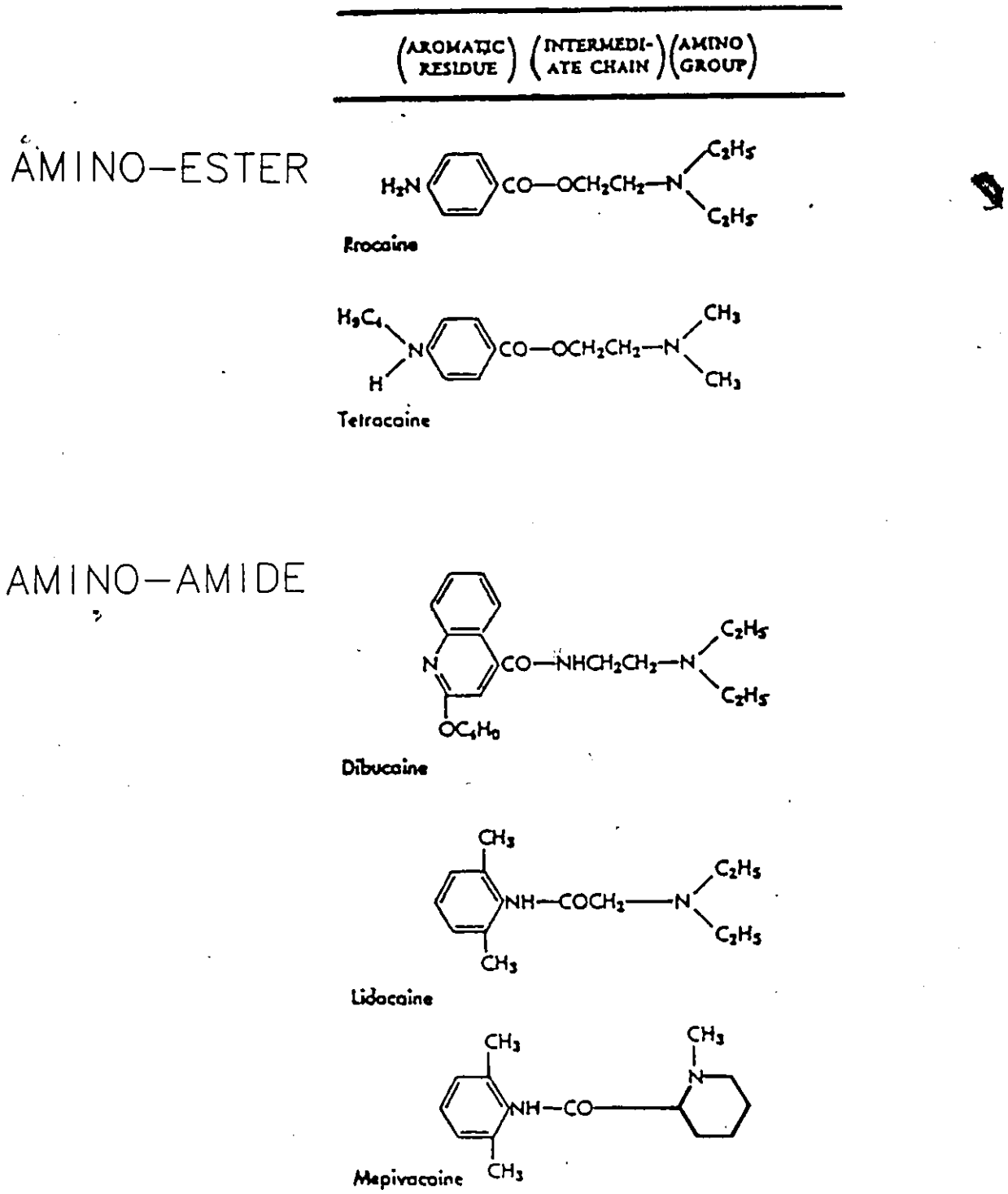

Figure 4. Some common amino-ester and amino-amide local anesthetics.

Local anesthetics exert their major pharmacological action by interupting the excitation-conduction process of peripheral nerve fibers. During periods of inactivity a resting potential of approximately -70 mV exists across the cell membrane. This voltage difference, across the membrane, arises from the ionic composition of the intra and extracellular fluids. At rest, the extracellular concentrations of sodium and chloride are 140 meq/L and 110 meq/L respectively, while the concentration of potassium is 3-5 meq/L. Conversely, the intracellular fluid has a high concentration of potassium (110-170 meq/L) and low concentrations of sodium and chloride (5-10 meq/L) (5). This ionic differentiation arises in part from the attraction of potassium ions to the negative charges localized on the inside of the membrane. This attraction acts to overcome the tendency of potassium to diffuse across the bilayer while for sodium and chloride ions the membrane acts as an impermeable barrier.

For the propagation of a nerve signal, excitation initially causes a slow depolarization of the membrane. When a critical, or threshold potential is reached, a very rapid depolarization occurs, leaving the membrane with a positive potential of approximately 40 mV. The slow depolarization results from the inward flow of sodium ions at a rate slightly greater than the outward flow of potassium.

Since the resting membrane is normally impermeable to sodium, the nerve stimulus must open a small portion of the sodium channels, which exist in the nerve membrane, to allow sodium ions in. This net inward flow of positive charge will slowly cancel the net negative charge in the intracellular environment (Figure 5A).

When the threshold potential is reached (also called a firing threshold) there is a cascade of sodium channels opening. An extremely rapid influx of sodium ions results and the potential quickly becomes positive (+40 mV). The cell responds quickly to restore the local cation concentrations by increasing the potassium permeability and closing the sodium gates. During this repolarization the total cation concentrations are quickly restored, however, an excess of sodium is left in the intracellular fluid and an excess of potassium in the extracellular fluid. These levels are restored by the active transport of sodium and potassium through the Na^+/K^+ pump.

Local anesthetics could act to prevent propagation of the nerve impulse by interfering with this sequence in several places. The anesthetic could act to lower the resting potential, raise the firing threshold or alter the rates of depolarization or repolarization. Experiments on isolated nerves have shown that neither the resting (7) nor the firing potentials (5) are significantly affected

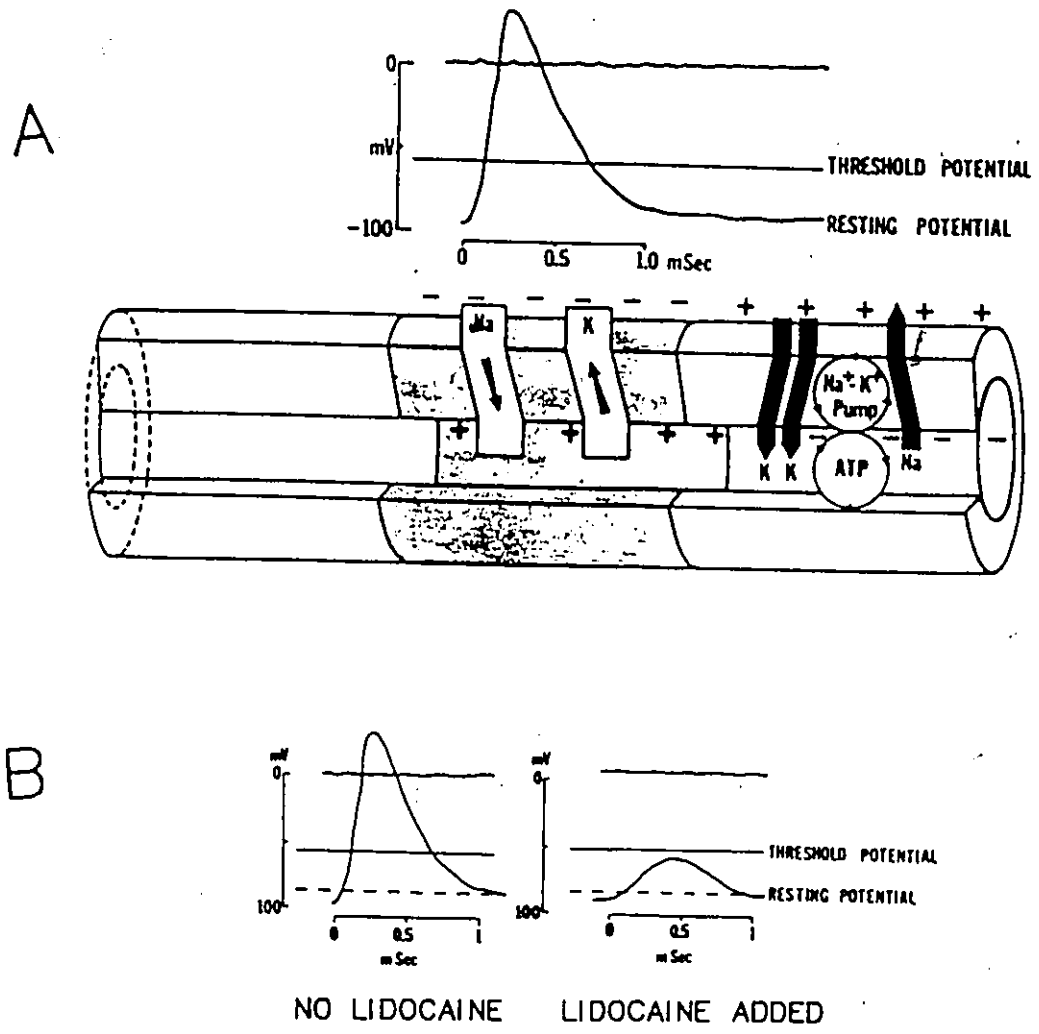

Figure 5. (A) Electrochemical response of the nerve membrane during signal propagation.
(B) Effect of the local anesthetic lidocaine on the firing sequence of the nerve membrane.

by local anesthetics. Rather, the depolarization rate is seen to decrease with increasing anesthetic addition. If a sufficient quantity of anesthetic is added, the firing potential will not be reached and the nerve impulse will be terminated (Figure 5B). The local anesthetics appear to be acting to close the sodium channels and prevent the influx of sodium ions required for depolarization.

There are many theories on the mechanisms by which local anesthetics inhibit the sodium influx, but they can be generally classified into two main areas. First, the anesthetic may act to block the sodium channel directly (9) or bind to the protein (at a specific receptor) in such a way as to alter the protein's conformation and close the channel (10). The second general classification is known as the lipid hypothesis and encompasses a variety of models for anesthetic action. In general, all of these models involve anesthetics interacting with the lipid and altering a physio-chemical property of the lipid matrix. This altered property results in a modification of the protein conformation which closes the sodium channel.

The interaction of local anesthetics directly with the sodium channel has been demonstrated conclusively only with the biotoxins, tetrodotoxin and saxitoxin (11, 12). These toxins block the outside opening (13) of the sodium channel, but even subtle modifications of their structures

will nullify their anesthetic activity (14). Anesthetics have also been shown to cause conformational and structural changes in proteins such as hemoglobin (15).

Many authors have proposed a specific receptor (16) located on the inside of the membrane (17), in (18) or near the sodium channel (10). It is proposed that it is the charged form of the amine type anesthetics which interacts with these sites (17). However, the strict conformational requirements on the biotoxins, which definitely interact with the sodium channel and the general structural variability found among local anesthetics (some of which are never charged) makes a specific sodium channel-anesthetic interaction difficult to rationalize for all of the known anesthetics.

The so-called lipid hypothesis of anesthetic action dates back to the beginning of this century when Meyer (19) and Overton (20) were able to show a strong correlation between anesthetic potency and lipid solubility. Subsequent work has added a great deal of thermodynamic evidence to the theory of a site of anesthetic action with lipid character (21, 22, 23). The lipid hypothesis now encompasses a number of specific models involving anesthetic-lipid interactions.

The first model involves changes in phase transitions and fluidity. Experiments have shown that anesthetics, at

clinical concentrations, depress the phase transition temperatures of model membranes by 2-5°C (24, 25) and increase the fluidity of model and real membranes (26, 27, 28). An increase in fluidity as a cause of anesthesia is unlikely since a strong fever will cause a rise in temperature which gives a comparable fluidity change (22). Changes in the phase transition have been suggested to result in local domains of gel and liquid crystal. This gives a lateral phase separation which can then close the sodium channel (29). However, this seems an unlikely mechanism for a real membrane which will have cholesterol and unsaturated fatty acids. The former acts to eliminate the transition and the latter to lower the phase transition temperature well below physiological temperatures. The red cell membrane, which has a similar composition to the membrane of the giant squid nerve (30) shows no phase transition down to -5°C (31).

It has been suggested that the actual lipids of importance are those immediately in contact with the protein (a lipid annulus). Lee (32) has proposed that these lipids exist in the gel state and the anesthetic causes a transition to the liquid crystalline state. The increased fluidity forces the sodium channel to close, inhibiting the propagation of the nerve signal. Although many authors have proposed a boundary lipid for proteins, of the general

type required for the annulus, only ESR results have shown indications of lipids in contact with a protein (33, 34). ^{2}H NMR experiments, on several lipid/protein systems, have not shown a boundary lipid. It has been suggested that the lipids are in exchange between protein-bound and bulk lipid at a rate which is fast on the ^{2}H NMR time scale (10^{-3}-10^{-5}s), but slow on the ESR time scale (10^{-10}-10^{-8}s) (35). It is difficult to reconcile this requirement for rapid exchange with Lee's lipid annulus model. Lee's model requires lipids which are more strongly bound and, indeed, in the gel state.

While all of the current theories explain some aspects of the mechanism of anesthesia, they are all deficient in some manner. Protein and specific receptor models certainly have some strong evidence in their favour, but the wide range of structures (both charged and neutral) which exhibit anesthetic potency seem to rule against them. Theories involving physio-chemical changes in the lipid certainly show excellent correlation with anesthetic potency, but are those changes significant in a real membrane?

A recent model of a sodium channel has been proposed which allows for a heterogeneous site of anesthesia (22). The sodium channel is proposed to be a single, trans-membrane protein, with a subunit on the axoplasmic side to facilitate inactivation of the channel (36) and with at

least three hydrophobic arms extending out into the bilayer (Figure 6). The arms have a negative charge on the ends and in the resting state are repelled from the intracellular side by the large negative potential (Figure 6A). On depolarization, the transmembrane potential approaches neutral and the arms move across the bilayer creating the sodium channel. Because of the altered potential, this conformation represents a new free energy minimum (Figure 6B) for the sodium channel. When the arms make contact with the inner side of the membrane, and sodium ions are flowing in, the inactivation processes start (Figure 6C) with a conformation change. As repolarization occurs the arms return to their original position (Figure 6D) and when the initial ionic concentrations are restored, the resting state is re-attained (Figure 6A).

This model of the sodium channel represents a heterogeneous site of anesthesia. Anesthetics which appear to have some specificity of charge (like quaternary salts) could interact with the inner end of the sodium channel or the protein arms in Figure 6A. Biotoxins could interact at the pore opening and hydrophobic anesthetics could partition into the lipid, near the arms, and prevent the sodium channel from opening.

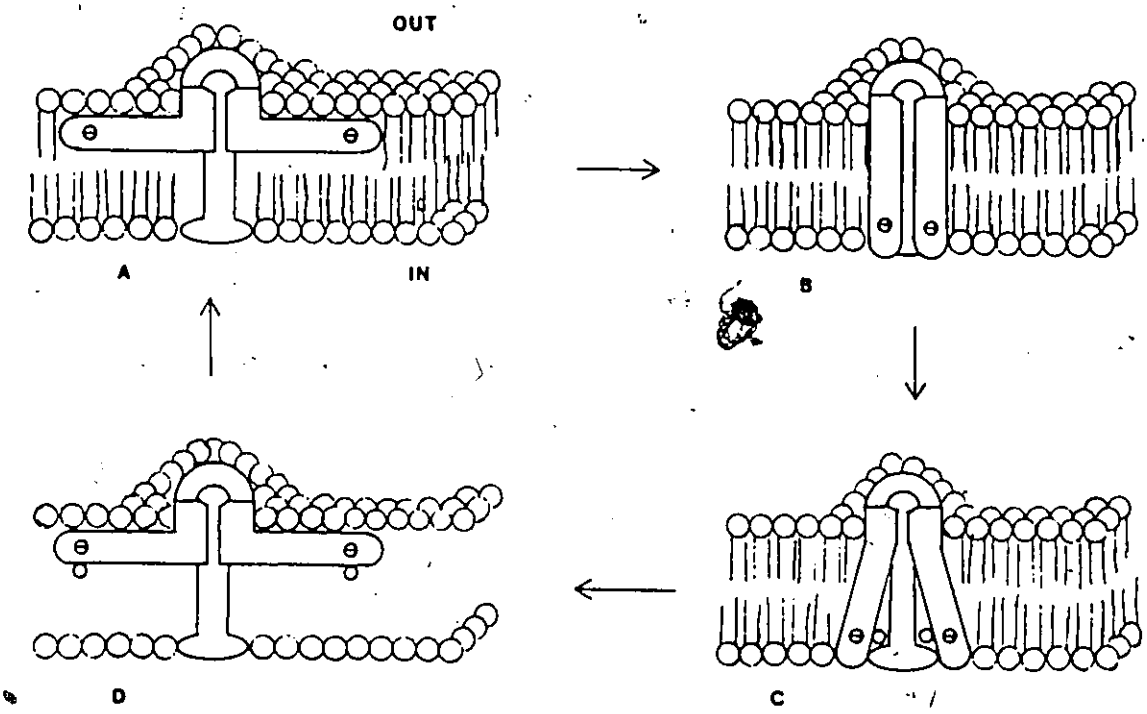

Figure 6. Trudell's model for the sodium channel (20). (A) Resting state with the negative arms at the extracellular surface. (B) Conducting state after depolarization. (C) Inactivated channel. (D) Channel during repolarization. A direct change to state B is not possible until repolarization is complete.

I.3 Alkanes

The solid state behaviour of the n-alkanes has been the subject of much interest in recent years. These compounds represent simple models for the more complicated chain behaviour found in membranes, liquid crystals and polymers. In particular, model and biological membranes are known to undergo phase transitions involving the hydrocarbon chains.

The long chain n-alkanes, containing an odd number of carbon atoms, are known to undergo solid-solid phase transitions prior to melting (37, 38, 39). Figure 7 shows the transition temperatures of the odd n-alkanes as a function of chain length (39). For the n-alkanes of from 9 to 23 carbons there is only one solid-solid phase transition. This is from the low temperature, phase I to the high temperature, phase II (also called rotator or hexagonal). The low temperature phase has chains which are all trans and packed parallel to each other in an orthorhombic unit cell. The high temperature phase is characterized by an expansion of the unit cell dimensions (40) and the onset of hindered rotation about the chain long axis (41-43).

The motions of the alkane chains in phase II has been the subject of much research and speculation, since Müller first reported the existence of phase II in 1932

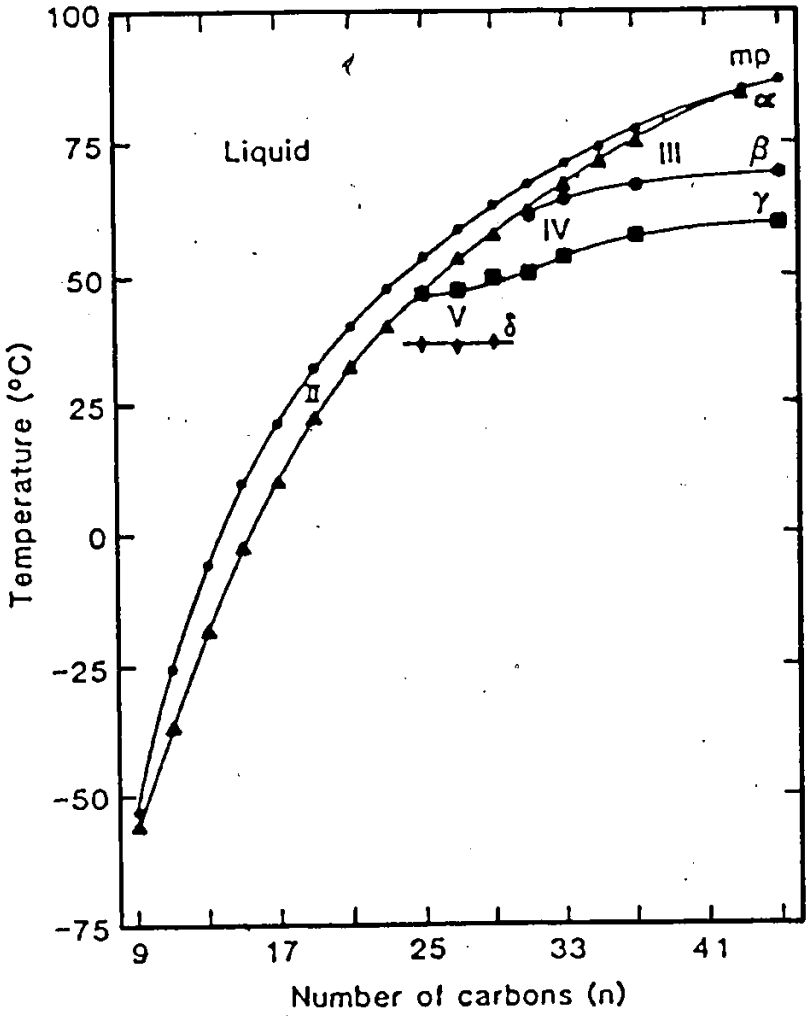

Figure 7. Transition temperatures of the odd n-alkanes. The solid-solid transition curves α, β, γ and δ separate crystalline phases I, II, III, IV and V (39).

(37). Müller identified the chain packing as hexagonal, but assumed a hindered rotation about the chain long axis. This type of packing would give a freely rotating alkane chain and later work has shown that the packing is, in fact, not quite hexagonal (40, 44). Andrew has suggested that the hindered rotation involves a cooperative molecular motion around the long axis of the chain, much as in the manner of a set of meshed gears (41). A ^{1}H NMR spin relaxation study of the C_{19} n-alkane showed that the relaxation of the methylene protons has contributions from two mechanisms (42). These are proposed to be a fast rotational reorientation of the entire alkane as a rigid rotator and a slow diffusion of the alkane. This fast reorientation has a mean jump time much less than 10^{-9} seconds. This corresponds to inelastic neutron scattering results which indicate that the alkane chains exist in an all-trans configuration and reorientation has a mean jump time of approximately 3.5×10^{-12} seconds (43).

For n-alkanes longer than C_{23} there are from one to three other solid phases between phase I and phase II (38, 39, 44). These phases are characterized by increases in the concentration of non-planar alkanes, but there is no hindered rotation. This hindered rotation is limited to the last solid phase observed prior to melting (phase II), however, the phase II exists over a much narrower temperature range than is found in the shorter alkanes.

Phase II is also characterized by the presence of conformational disorder in the form of gauche rotamers (39, 45, 46). Snyder (46) has shown that for specifically deuterated C_{21} n-alkanes the gauche rotamer distribution varies with chain position and temperature. Figure 8 shows the gauche concentration, in phase II, as a function of position at two temperatures. The gauche concentration is observed to increase from less than 1% to more than 8% as the label was moved from position 11 (chain centre) to position 2 (penultimate carbon). The gauche concentration is also very sensitive to temperature, doubling for all positions when the temperature is raised by only $6^{o}C$ within Phase II.

I.4 Deuterium Nuclear Magnetic Resonance in Membranes

Deuterium (^{2}H) is a low abundance isotope of hydrogen which has a nuclear spin quantum number of I = 1. Deuterium also has a small nuclear quadrupole moment which makes it an excellent probe for anisotropic systems, like membranes. By chemical synthesis, deuterium can be incorporated to levels in excess of 95%, overcoming the problem of low natural abundance. The ability to deuterate specifically a lipid, or other molecule in the membrane, makes the ^{2}H NMR experiment tractable.

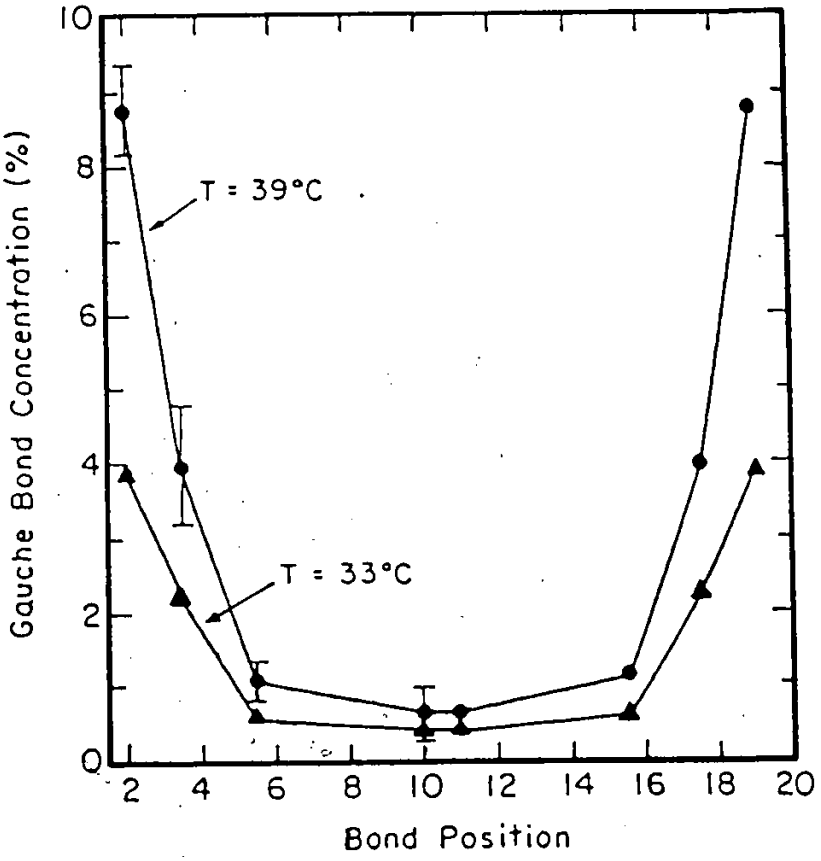

Figure 8. Variation of gauche concentrations with bond position, for C_n n-alkanes at two temperatures in phase II (46).

The nuclear quadrupole moment is a measure of the lack of spherical symmetry in the charge distribution inside the nucleus. For a C-^{2}H bond, the bonding electrons produce an inhomogeneous field (an electron field gradient, $\vec{\nabla}$) which interacts with the charge distribution inside the deuterium nucleus. This electrostatic (quadrupolar) interaction is of relatively low energy for deuterium and can be treated as a small perturbation on the nuclear Zeeman interaction (47). The latter is the interaction between the deuterium nuclear magnetic moment and the static magnetic field. The Hamiltonian for the deuterium nucleus in a magnetic field is the sum of the Zeeman and quadrupolar terms.

$$\mathcal{H} = \mathcal{H}_Z + \mathcal{H}_Q \qquad (1)$$

Solution of the Hamiltonian (47) yields three energy levels and two quantum-mechanically allowed transitions.

For a single crystal the ^{2}H NMR experiment will show two lines, for the two allowed transitions, with a spacing of:

$$\Delta\nu = \frac{3}{4}\frac{e^2qQ}{h}(3\cos^2\theta - 1) \qquad (2)$$

where $\Delta\nu$ is the quadrupole splitting and e^2qQ/h is the static quadrupole coupling constant. The angle θ is the

angle between the C-^{2}H bond, which is the direction of the largest component of the electric field gradient tensor, and the applied magnetic field.

In liposomes and biological membranes the phospholipids undergo several types of motion. If these motions are fast relative to the quadrupole coupling constant (170 kHz) there will be an averaging of the electric field gradient tensor. In particular, phospholipids undergo rapid (10^7-10^{10} sec^{-1}) rotation about their long axis (48) and this averages the electric field gradient tensor perpendicular to the long axis. The result of the axially symmetric motion is that the largest component of the electric field gradient tensor is now parallel to the axis of rotation (the director). Also, because liposomes and real membranes have rates of rotation (tumbling) slower than 3×10^5 sec^{-1} (49), all possible orientations of the lipid with respect to the static field are detected. However, the probability of any one orientation will be a function of sin 0', where 0' is the angle between the director and the applied field. The effect on the ^{2}H NMR spectrum is demonstrated in Figure 9 where the lipids in the membrane or liposome are shown at several orientations with respect to the magnetic field H_0. Each orientation gives rise to a doublet and the total spectrum is the sum of all orientations, with the intensity scaled by sin 0'. This is simply

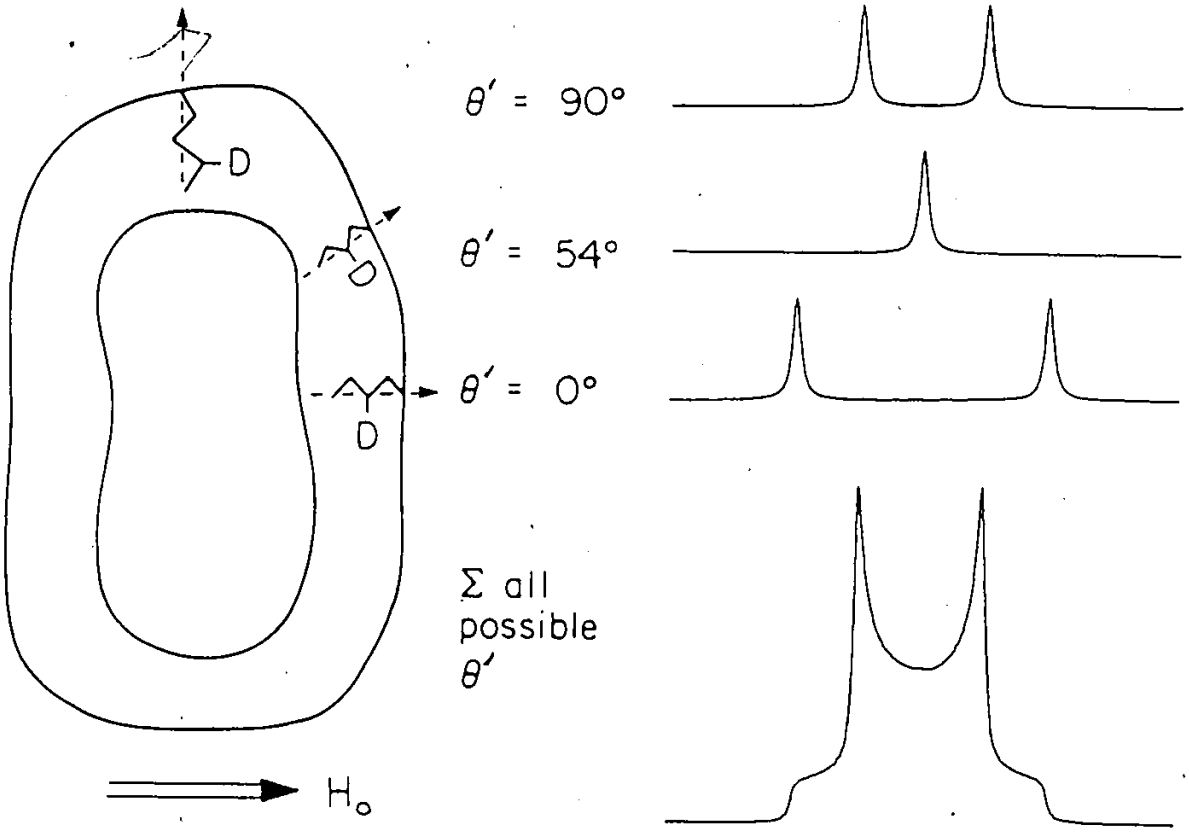

Figure 9. The origin of the ^2H NMR powder spectrum. The angle θ′ is between the director (broken line) and H_o.

because there are more lipids with their directors at 90^{o} to the field than parallel to the field ($\theta' = 0$).

If lipids were rigid molecules, with no motions other than fast rotation about the director, a quadrupole pattern would be observed with a splitting of approximately 60-64 kHz (half the splitting observed for the rigid solid). However, phospholipids are not rigid molecules; they can undergo oscillations about the rotation axis and they can undergo local segmental motions (interconversion between gauche and trans rotamers). These motions reduce the observed quadrupole splitting by averaging the electric field gradient tensor. These anisotropic fluctuations modulate Equation 2 as,

$$\Delta\nu = \frac{3}{2}\frac{e^2qQ}{h}\frac{1}{2}(3\cos^2\theta'-1)\frac{1}{2}<3\cos^2\alpha-1>\frac{1}{2}<3\cos^2\gamma-1> \qquad (3)$$

where γ is the angle between the C-^{2}H bond and the instantaneous chain orientation, α is the angle between the instantaneous segmental chain orientation and the director of the motion, $\hat{n}$ (normal to the bilayer surface) and the angular brackets indicate a time or ensemble average. The angles are shown in Figure 10 and correspond to those of Peterson (50) and Dufourc (51).

For a quadrupole pattern, a quadrupole splitting is measured (when $\theta' = 90^{o}$)

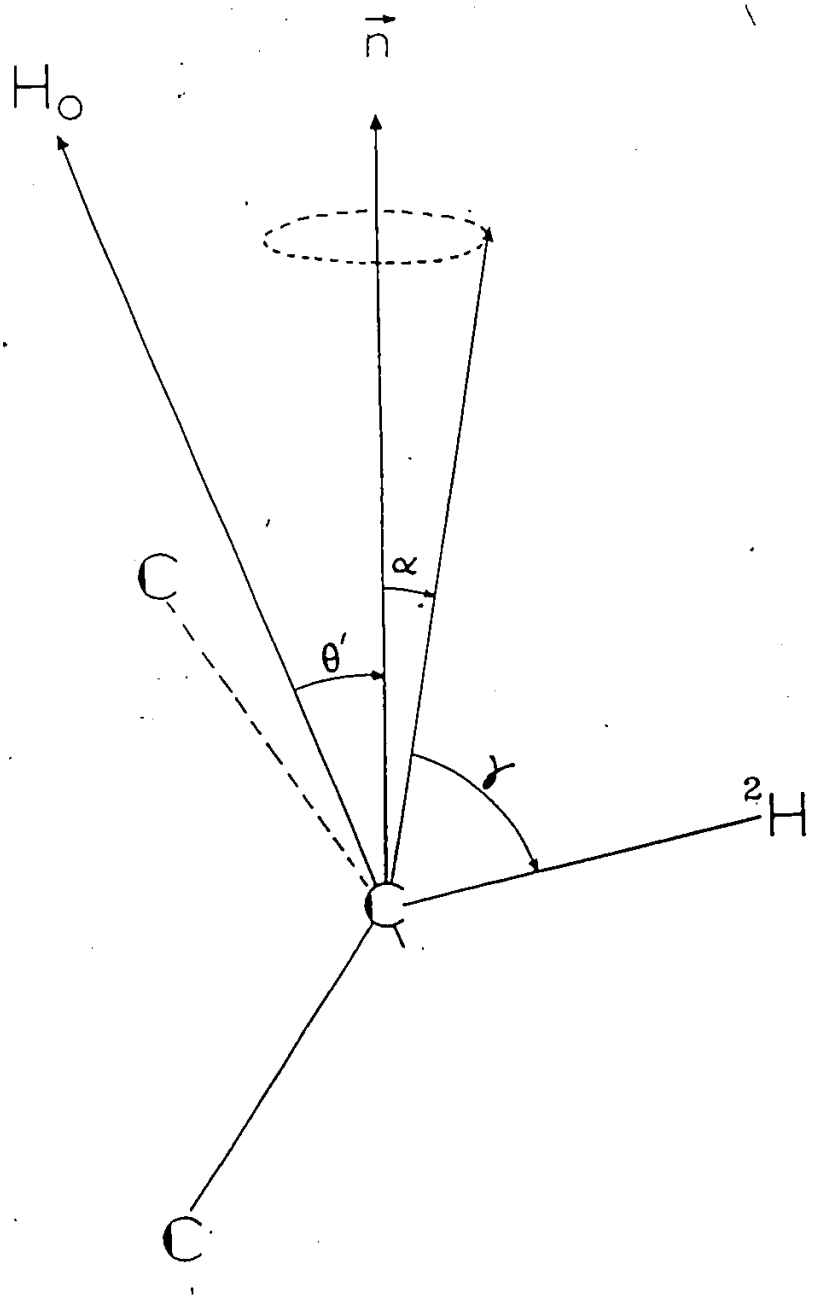

Figure 10. Angles defining the orientation of the C–^{2}H bond. See text for details (50,51).

$$\Delta\nu_Q = \frac{3}{4}\frac{e^2qQ}{h}\frac{1}{2} < 3\cos^2\alpha - 1 > \frac{1}{2} < 3\cos^2\gamma - 1 > \quad (4)$$

The two terms in brackets represent the anisotropic fluctuations and are referred to as the S_{C-^2H} order parameter. For a non-rigid molecule these two terms cannot be separated and Equation 4 can be rewritten as:

$$\Delta\nu_Q = \frac{3}{4}\frac{e^2qQ}{h} S_{C-^2H} \quad (5)$$

For a rigid molecule like cholesterol (52, 53) or cyclopropane (51) the angle γ, between the $C-^2H$ bond and the director, is fixed and Equation 4 becomes:

$$\Delta\nu_Q = \frac{3}{4}\frac{e^2qQ}{h}\frac{1}{2} < 3\cos^2\alpha - 1 > \frac{1}{2} (3\cos^2\gamma - 1) \quad (6)$$

The term $\frac{1}{2} < 3\cos^2\alpha - 1 >$ is referred to as the molecular order parameter, S_{mol}. It is of interest since it describes the anisotropic motion of the entire molecule. For a perfectly ordered system, $S_{mol} = 1$ while for a system undergoing isotropic motion $S_{mol} = 0$.

The use of ^2H NMR in biological studies has grown exponentially over the last ten years. Studies of deuterated lipids, proteins, cholesterol and drugs in both model and biological membranes have been undertaken. The field has been extensively covered in several excellent reviews (47, 48, 54-57).

I.5 Scope of the Studies

This present work has been devoted to the study of two problems. The first, and major problem, was a study of the interaction of two common local anesthetics, tetracaine and procaine, with model and biological membranes. The second problem investigated was the nature of the motions and the phase behaviour of solid n-alkanes.

The molecular mechanism of anesthesia is still not well understood. There are several theories and models for the action of local anesthetics (see Section I.2), but by far the most reasonable is Trudell's concept of a heterogeneous site of anesthetic action (22). This model suggests that lipid soluble anesthetics, like TTC and PRC, could interact with the lipid matrix. This would, in turn, prevent the sodium channel in the nerve membrane from opening, effectively terminating the propagation of the nerve signal.

The interaction of tetracaine and procaine with PE model membranes was studied by ^{2}H NMR. Specifically deuterated tetracaines, procaines and DMPE's were prepared and used to determine the location of the anesthetics in the bilayer, the nature of the anesthetic exchange and TTC's lateral diffusion. Differences between the protonated and unprotonated forms of the anesthetics were studied. The interaction of labelled TTC and PRC with PC model membranes

was also reexamined. This model system was studied earlier by other workers, but with some conflicting interpretations of the anesthetic exchange (58-61).

Finally, the techniques and results obtained from the investigation of model systems were applied to a study of two real membranes. The interaction of labelled TTC and PRC with membranes of human erythrocytes and *Acholeplasma laidlawii* B, was studied by ^2H NMR. The influence of TTC and PRC ON *A. laidlawii* B, grown on specifically deuterated oleic acids, and on erythrocytes doped with perdeuterated palmitic acid, was also examined. In addition, the nature of the anesthetic exchange and the location of the anesthetic in the membrane were studied.

The second major problem examined was the phase behaviour and motions of solid n-alkanes. Longer n-alkanes are known to undergo a series of solid-solid phase transitions prior to melting (37, 38, 39). These transitions are characterized by changes in crystal packing and the onset of various motions. The temperature dependence of the ^2H NMR spectra of specifically labelled C_{19}, C_{21} and C_{35} n-alkanes enabled the types of motions in the solid phases to be characterized much more fully than they have been previously. These motions were modelled and the ^2H NMR spectra were simulated. The variation of these motions, as a function of chain position, was determined through a study of specifically deuterated C_{21} n-alkanes.

CHAPTER II

EXPERIMENTAL METHODS

II.1 Materials

Crude egg phosphatidylcholine, phospholipase A_2 (Crotaleus adamanteus), procaine hydrochloride, tetracaine hydrochloride and myristic acid were purchased from Sigma Chemical Company. Bovine phosphatidylserine was obtained from lipid products. Tetrabutylammonium hydroxide, dicyclohexylcarbodiimide, 4-dimethylaminopyridine and deuterium-depleted water were purchased from Aldrich Chemical Company. Bromobutane-d_9 and ^2H_2O were obtained from Merck, Sharp and Dohme. The deuterated local anesthetics TTC-d_6, TTC-d_3, PRC-d_4 and PRC-d_2 (see Figure 11) were the generous gift of Dr. Yvan Boulanger. Ion exchange resins were Amberlite CG-50(H^+) and IRA-45(OH^-). Raney Active Nickel Catalyst (#28) was purchased from Grave Davidson Chemicals. Alumina (Activity 1) was purchased from Woelm and silicic acid from Bio Rad. All other chemical were reagent grade.

The perdeuterononadecane (C_{19}-d_{40}) was purchased from Merck, Sharp and Dohme (Montreal, Quebec). The 2,2-dideuterononadecane (C_{19}-2-d_2), 10,10-dideuterononadecane (C_{19}-10-d_2), and 1,1,1,19,19,19-hexadeuterononadecane (C_{19}-1,19-d_6) were the generous gift of Dr. L.C. Leitch.

Purity was greater than 99% for these compounds by GLC. The specifically deuterated C_{21} and C_{35} n-alkanes were the generous gift of Dr. C.A. Elliger and their synthesis has been described elsewhere (62). The C_{21}-11-d_2 was approximately 95%, by GLC, while the others (C_{21}-6-d_2, C_{21}-4-d_2, C_{21}-2-d_2 and C_{35}-18-d_2) showed purity greater than 99% in all cases. Less than 3.5% of the methylenes were CHD according to the mass spectra (62).

II.2 Syntheses

Egg Phosphatidylcholine

Egg PC was isolated by a method adapted from Singleton (63). Thirty, extra large, fresh brown eggs were obtained and the yolks were separated. Acetone (1 L) was added to the yolks and the mixture was homogenized for 5 minutes and filtered through a Buchner funnel (Whatman No. 1 filter paper). The filtered solid was rehomogenized with acetone 3 more times. The remaining solid was homogenized for 5 minutes with 750 mL of 95% ethanol and filtered. The solid was again homogenized with 750 mL of ethanol, filtered and the filtrate was stored in the freezer under N_2. The filtrate was distilled under reduced pressure (temperature < 30°C) to remove the ethanol and then lyophilized to remove residual water.

The lipid was dissolved in 200 mL of anhydrous ether and precipitated with 800 mL of acetone. After sitting for one hour in the freezer, the supernatant was decanted and the ether/acetone precipitation was repeated three further times. The residual acetone was dried under a stream of N_2.

The lipids were dissolved in 100 mL of $CHCl_3$ and applied to a column of 500 g of Alumina (Woelm Activity 1). The lipids were eluted with 1250 mL of $CHCl_3$ and then 1250 mL of $CHCl_3/CH_3OH$ (90/10). As the $CHCl_3/CH_3OH$ mixture begins eluting, 100 mL fractions were collected under a stream of nitrogen. Fractions were checked by TLC, with a PC standard, and those containing just egg PC were collected and dried by reduced pressure distillation. The PC was dissolved in 50 mL of $CHCl_3$ and samples were stored under N_2 at -20°C. Yields from 30 eggs ranged between 6 and 11 g. The fatty acid analysis for the egg PC is reported in Table 1.

Partially Purified Phospholipase D

The procedure is adapted from Davidson and Long (64). The inner, light green leaves of a fresh Savoy cabbage (300 g) were homogenized for 4 minutes with 400 mL of water. The homogenate was filtered through cheesecloth and centrifuged at 13000 x g for 20 minutes. The supernatant was decanted off, heated to 55°C for 5 minutes and then placed

in an ice bath. The supernatant was again centrifuged at 13000 x g for 20 minutes, decanted and placed in an ice bath. Acetone (2 L, cooled to -15°C) was added and the solution was allowed to sit for 15 minutes at 0°C. The precipitate was collected by centrifugation at 13000 x g for 20 minutes, dissolved in 60 mL of water and centrifuged again. The sample was then lyophilized dry and stored at -20 C° under N_2. Several preparations yielded activities of 5 to 20 units/mg of crude phospholipase. (One unit will hydrolyse 1 μmole of choline/hour, at pH 5.6 and 37°C.)

Semisynthetic Egg Phosphatidylethanolamine

Ethanolamine (14 g) in 50 mL of water and 1.48 g of $CaCl_2.H_2O$ was titrated with glacial acetic acid to pH 5.6. Crude phospholipase D (500 mg) was added to the solution. Egg PC (4 g) dissolved in 100 mL of diethyl ether was added to the ethanolamine and the mixture was stirred vigorously at 37°C. After 15 and 30 minutes, 200 mg portions of phospholipase D in 3 mL of H_2O were added. The reaction was monitored by TLC and after better than 75% of the PC was converted, 200 mL of 0.1 M EDTA (pH 7.0) was added to stop the reaction (65).

Ether was removed under reduced pressure and the lipids were extracted by the method of Bligh and Dyer (66). The total lipids were applied to a silicic acid column and

eluted with a chloroform/methanol gradient (0, 5, 10, 15, 20, 25% methanol). Diacylphosphatidic acids were eluted first, followed by PE and then PC. Fractions were collected under a stream of N_2 and those containing only PE were combined, dried by reduced pressure distillation (< 30°C) and recrystallized with hexane/cold acetone. Purity was checked by TLC, with spots visualized with phosphate and ninhydrin sprays. The yield of pure semisynthetic egg PE was 2.3 g (62.9%). The fatty acid composition of the semisynthetic PE (hereafter called egg PE) showed good agreement with the egg PC starting material (Table 1) indicating negligible oxidation. The PE was occasionally contaminated with ethanolamine. This was removed by stirring the PE in distilled water, centrifuging and lyophilizing the PE.

sn-Glycero-3-phosphocholine Cadmium Chloride Adduct

Aqueous tetrabutylammonium hydroxide (100 mL, 40 wt %) was lyophilized and then dissolved in 150 mL of methanol (67). Crude egg PC (100 g, from Sigma) was dissolved in 1.0 L of anhydrous ether and filtered through glass wool. The tetrabutylammonium hydroxide was added to the egg PC and the mixture was allowed to stand for 6 hours. The supernatant was decanted off and the remaining brown precipitate was washed with three 50 mL portions of ether.

Table 1

FATTY ACIDS OF EGG PC AND THE SEMISYNTHETIC EGG PE[a] (%)

	16:0	16:1	18:0	18:1	18:2	20:4	Others
egg PC	30.4	1.8	14.4	29.6	16.6	5.3	1.9
semisynthetic egg PE	32.5	2.1	12.5	32.7	16.6	2.4	1.2

a Average of three analyses.

Absolute ethanol (250 mL) was added to the precipitate and the mixture was refluxed for 15 minutes. Celite (1 g) was added, the mixture was filtered, cooled and the supernatant was decanted off. The remaining precipitate was dissolved in 75 mL of boiling water. Cadmium chloride (12.8 g), celite (2 g) and activated charcoal (0.5 g) were added and the mixture was refluxed for 10 minutes. The reaction mixture was filtered through a scintered glass funnel while still hot and then diluted with 750 mL of ethanol and placed in a freezer at $-20^{\circ}C$ overnight. The product was collected on a scintered glass funnel, washed with absolute ethanol (100 mL), benzene (100 mL) and anhydrous ether (100 mL). The yields varied from 5 to 13 g and the product was checked by ^{1}H NMR.

1,2-Dimyristoyl-*sn*-glycero-3-phosphocholine

The title compound was prepared by a method modified from Gupta (68). Dicyclohexylcarbodiimide (6.05 g, 30 mmoles) was dissolved in 100 mL of dry CCl_4 and added to a solution of 13.7 g of myristic acid (60 mmoles) in 400 mL of dry CCl_4 (69). After six hours the solution was filtered and the solvent was distilled off under reduced pressure. The remaining solid was recrystallized from hot acetone (250 mL) to yield 10.5 g of myristic anhydride (79%).

The cadmium chloride adduct of *sn*-glycero-3-phosphocholine (3 g, 4.8 mmoles) was dispersed in very dry DMF (750 mL) and warmed slightly to aid in dissolving. Myristic anhydride (4.5 g, 10.2 mmoles) and 4-dimethylaminopyridine (1.3 g, 10.6 mmoles) were added to the suspension which was then sealed under dry nitrogen. The reaction was stirred vigorously for four hours and the reaction was monitored by TLC. The DMF was removed under reduced pressure and dried overnight on a vacuum line.

The DMPC was dissolved in 500 mL of a 5:4:1 mixture of $CH_3OH/CHCl_3/H_2O$ and passed through a mixed bed ion exchange column. The lower half of the column contained 25 g of Amberlite CG-50(H^+) resin and the upper half contained 25 g of Amberlite IRA-45(OH^-). The column was then washed with a further 300 mL of the same solvent mixture. The chloroform and methanol were removed on a rotory evaporator (with care to avoid foaming) and the water was removed by lyophilization. The remaining solid was dissolved in a minimum of $CHCl_3$ and applied to a silicic acid column (250 g, Bio Rad). Elution was carried out with 2 bed volumes of $CHCl_3$; 1 bed volume of 25/75 $CH_3OH/CHCl_3$ and then 50/50 $CH_3OH/CHCl_3$ until all of the DMPC was collected. Fractions containing DMPC (identified by TLC and visualization with phosphate spray) were collected and dried to

yield 3.5 g (74%) of DMPC. Elemental analysis: calculated: C 62.12, H 10.72, N 2.01, found: C 61.58, H 10.40, N 2.02.

[1,2-$^2H_4$]-Ethanolamine

Ethanolamine (30 g) was stirred in 20 mL of ^2H_2O followed by distillation at reduced pressure to remove water. This was repeated twice, to yield $^2H_2NCH_2CH_2O^2H$ (70). Raney nickel catalyst in ^2H_2O was made by washing 50 g of Raney Active Nickel Catalyst in water (#28, Grave Davidson Chemicals) in four 30 mL portions of ^2H_2O. Half of this Raney nickel suspension and the deuterium exchanged ethanolamine were combined with 40 mL of ^2H_2O and the sample was refluxed for two hours. The ^2H_2O was then distilled off and 50 mL of fresh ^2H_2O and 25 g of fresh Raney nickel suspension were added. The sample was refluxed a further two hours, cooled and filtered. The remaining active nickel catalyst was decomposed with 6 N HCl. Water was removed by reduced pressure distillation and the ethanolamine was distilled at 75°C (9 mm) to yield 8.1 g (24%) of [1,2-$^2H_4$]-ethanolamine. Deuterium incorporation was greater than 90% (by ^1H NMR) for both positions, if two exchanges were run.

1,2-Dimyristoyl-*sn*-glycero-3-phospho-[1',2'-$^2H_4$]-ethanolamine

[1,2-$^2H_4$]-ethanolamine (6.8 g) was added to 25 mL of water and titrated to pH 5.6 with glacial acetic acid. Phospholipase D (160 mg) and 0.69 g of $CaCl_2.H_2O$ were added to the ethanolamine solution (65). DMPC (1.85 g) was added to 100 mL of anhydrous ether and stirred vigorously. The ethanolamine solution was added to the DMPC solution and the mixture was stirred under a condensing column while the temperature was maintained at 37°C. Additional portions of phospholipase D (100 mg in 2 mL of water) were added after 15 and 30 minutes. After two hours, 100 mL of 0.1 M EDTA (pH 7.0) was added to stop the reaction. The remaining ether was removed on a rotory evaporator and the DMPE was extracted and purified in the manner described for the egg PE synthesis. The reaction yielded 890 mg of the headgroup labelled 3-[1',2'-^2H]-DMPE (52% yield based on DMPC). The TLC showed only one spot using ninhydrin and phosphate sprays. Elemental analysis (% of H includes both ^1H and ^2H): calculated: C 61.95, H 11.03, N 2.19, found: C 61.85, H 10.58, N 2.03.

[2-$^2H_2$]-Myristic Acid

Myristic acid (11.4 g) was neutralized with 0.1 M NaOH in 150 mL of water. The solution was heated until it

turned clear (90°C) and was then lyophilized. The sodium salt was placed in a high pressure rocking bomb with 1 g of NaO^2H and 100 mL of ^2H_2O (71). The bomb was sealed and heated to 200°C for three days. The resulting mixture was lyophilized, and the exchange was repeated. After the second exchange the product was acidified with 300 mL of 6 N HCl and extracted with chloroform. The extract was dried and recrystallized twice from hot acetone to yield 7.1 g of [2-$^2H_2$]-myristic acid. The melting point was 53.5-53.7°C (corrected, literature 53.8°C) (72). Mass spectral analysis showed a 99% incorporation of deuterium.

[4,14-$^2H_5$]-Myristic Acid

[12-$^2H_3$]-Lauric acid (2 g) was deuterated at the α position by ^2H_2O exchange in a high pressure bomb (see the synthesis of [2-$^2H_2$]-myristic acid for details). The deuterated acid was dissolved in 30 mL of anhydrous ether and added dropwise to a suspension of 0.5 g of $LiAlH_4$ in 20 mL of anhydrous ether (73). The reaction mixture was refluxed for three hours and the reduction of the acid to the alcohol was monitored by IR. On completion, water (50 mL) was added to the mixture with cooling. Sulfuric acid (10 mL, 10%) was added and the product was extracted with ether. The ether was removed to yield 1.9 g of the alcohol.

The lauryl alcohol, triethylamine (1.1 mL) and CH_2Cl_2 (50 mL) were cooled to -15°C. Methanesulfonyl chloride (0.6 mL) in 6 mL of CH_2Cl_2 was added dropwise with vigorous stirring and the reaction mixture was left overnight at 5°C (74). The product was washed with water, dried over Na_2SO_4 and the CH_2Cl_2 was removed on a rotory evaporator. The mesylate was distilled at 160-170°C (1 mm) and the product was identified by ^1H NMR (4.1 ppm (s,2H), 3.0 ppm (s,3H), 1.2 ppm (m,18H)).

Diethyl malonate (1.2 g) in dry xylene (40 mL) was added to 0.16 g of NaH in 40 mL of dry xylene and the mixture was left overnight, yielding a white precipitate (75, 76). The mesylate, dissolved in 5 mL of xylene, was added dropwise to the sodium diethyl malonate at 110°C and stirred for four hours. The xylene was removed on a rotory evaporator and the residue was heated to 80°C for 2 hours with 40 mL of 5% KOH in 80% ethanol. The ethanol was removed and 5 mL of water was added. The solution was made acidic with 2N H_2SO_4 and extracted with 60 mL of ether. The ether solution was washed with water until a neutral pH was obtained, dried over Na_2SO_4 and then the ether was removed.

The product was placed in a two-necked flask with N_2 flowing through one neck and a water aspirator on the other. The flask was placed in an oil bath at 125°C and heated to 165°C where the temperature was maintained until

the evolution of CO_2 ceased (≈ 2 hours). The product was distilled at 180°C (0.5 mm) to yield 0.83 g. GC of the methyl ester showed 97% myristic acid and the mass spectrum indicated a 99% incorporation of deuterium.

1-Myristoyl-*sn*-glycero-3-phosphocholine

The title compound was prepared by the action of phospholipase A_2 on DMPC (77, 78). The DMPC (2.5 g) was dissolved in 8 mL of methanol and 200 mL of ether. Phospholipase A_2 (Crotaleus adamanteus) (50 mg), in 10 mL of a buffer of 0.22 M NaCl, 0.02 M $CaCl_2$ and 1 mM EDTA (pH 7.5) was added to the DMPC. The mixture was stirred vigorously and the reaction was monitored by TLC. Two further additions of phospholipase A_2 (2 x 50 mg), after 30 and 60 minutes, were sufficient to drive the reaction to completion. The lyso-MPC was purified on a silicic acid column using a chloroform/methanol gradient. Fractions containing only the lyso (one spot on TLC) were collected and dried to yield 1.4 g (81%). Elemental analysis: calculated: C 56.51, H 9.91, N 2.99, found: C 56.23, H 9.68, N 3.07.

1-[2'-$^2H_2$]-Myristoyl-2-myristoyl-*sn*-glycero-3-phosphocholine

The cadmium chloride adduct of *sn*-glycero-3-phosphocholine (3 g, 6.9 mmoles) was dissolved in 10 mL of water, lyophilized and placed on a drying gun for 2 days. The

GPC.$CdCl_2$ was dispersed in 75 mL of very dry DMF and warmed slightly. The anhydride of [2-$^2H_2$]-myristic acid (4.5 g) and 1.8 g of 4-dimethylaminopyridine were added and the mixture was stirred vigorously under dry N_2 for 3 hours. The DMF was removed and the product was passed through a mixed bed ion exchange column (Amberlite CG-50(H^+) and IRA-45(OH^-)). The product was converted to the lyso with phospholipase A_2 (see procedure for lyso-MPC preparation) and purified by column chromatrography to yield 2.2 g of 1-[2'-$^2H_2$]-myristoyl-*sn*-glycero-3-phosphocholine.

The lyso-MPC (2.2 g, 4.5 mmoles) was dried and dissolved in 75 mL of dry chloroform. Myristic anhydride (2.2 g, 5 mmoles) and 4-dimethylaminopyridine (0.51 g, 5 mmoles) were added and the reaction was sealed under dry N_2 and stirred vigorously. The resulting DMPC was purified on a silicic acid column to yield 2.8 g (59% based on GPC.$CdCl_2$). Elemental analysis: calculated: C 63.59, H 10.96, N 2.06, found: C 63.02, H 11.11, N 2.46.

1-Myristoyl-2-[2'-$^2H_2$]-myristoyl-*sn*-glycero-3-phosphocholine

Lyso MPC (2.2 g, 4.5 mmoles) was dissolved in 75 mL of dry chloroform. The anhydride of [2-$^2H_2$]-myristic acid (2.2 g, 5.0 mmoles) and 4-dimethylaminopyridine (0.51 g, 5 mmoles) was added under dry nitrogen and the reaction was stirred vigorously. The product was purified on silicic

acid to yield 2.7 g of 2-[2'-$^2H_2$]-DMPC (57%). Elemental analysis: calculated: C 63.58, H 10.96, N 2.06; found: C 63.11, H 10.88, N 2.40.

1-Myristoyl-2-[4'14'-$^2H_5$]-myristoyl-*sn*-glycero-3-phosphocholine

Lyso-MPC (750 mg) was dispersed in 25 mL of very dry chloroform. The solution was warmed slightly to aid in dissolving the lyso-MPC. The anhydride of [4,14-$^2H_5$]-myristic acid (750 mg) and 4-dimethylaminopyridine (170 mg) were added, the vessel was sealed under dry N_2 and the reaction was stirred vigorously. The labelled DMPC was purified by column chromatography to yield 800 mg of product (71%). TLC showed only one spot.

1-[2'-$^2H_2$]-Myristoyl-2-myristoyl-*sn*-glycero-3-phosphoethanolamine,

1-Myristoyl-2-[2'-$^2H_2$]-myristoyl-*sn*-glycero-3-phosphoethanolamine,

1-myristoyl-2-[4',14'-$^2H_5$]-myristoy -*sn*- glycero-3-phosphoethanolamine

The labelled DMPE's were prepared by phospholipase D mediated headgroup exchange, as described in the egg PE synthesis. The PE's were purified on silicic acid columns and yields were typically over 80%. Products showed only one spot on TLC and were visualized with ninhydrin and phosphate sprays. Melting points and elemental analysis are listed below.

1-[2'-$^2H_2$]-DMPE: M.p. 194-195°C (lit. m.p. 195-196°C (79))

calculated: C 62.14, H 10.74, N 2.19
found: C 62.07, H 10.53, N 2.32

2-[2'-$^2H_2$]-DMPE: M.p. 192-193°C (lit. m.p. 195-196°C (79))

calculated: C 62.14, H 10.74, N 2.19
found: C 61.79, H 10.58, N 2.31

2-[4',4'-$^2H_5$]-DMPE: M.p. 191-192°C (lit. m.p. 195-196°C (79))

calculated: C 61.84, H 11.17, N 2.18
found: C 61.59, H 10.98, N 2.29

Tetracaine-d_9

Potassium p-aminobenzoate (1.23 g, 7 mmole) was dissolved in 10 mL of water. 1-Bromobutane-d_9 (1 g, 6.85 mmoles) was added and the mixture was refluxed for five hours (80). The pH was adjusted to 6.0 with concentrated HCl, the mixture was filtered and the precipitate was washed with methylene chloride. The deuterated N-butyl-p-aminobenzoic acid and the unreacted p-aminobenzoic acid were esterified by refluxing in absolute ethanol saturated with HCl. The ethanol was evaporated, the esters were dissolved in water and sodium acetate was added to precipitate ethyl N-[1,2,3,4-$^2H_9$]-butyl-p-aminobenzoate. The ester was then transesterified (by stirring overnight) with 100 mL of dimethylaminoethanol and 0.1 g of sodium ethoxide. Ethanol and excess dimethylaminoethanol were removed under reduced pressure, the residue was dissolved in ether and

TTC-d_9 was extracted with 0.1 N HCl. The TLC showed only one spot with I_2 staining. ^1H NMR (2.25 ppm (s, 6H), 3.6 ppm (t, 2H), 4.6 ppm (t, 2H), 7.2 ppm (m, 4H).

II.3 Membrane Preparations

Isolation of Erythrocyte Ghosts

Erythrocyte ghosts were isolated in a procedure modified from Dodge (81) and Burton (82). Out-of-date blood and malarial-area blood were obtained from the Canadian Red Cross. Samples were centrifuged (5900 x g (average) for 8 minutes) and the plasma and buffy coat were aspirated off, leaving packed red cells. The centrifuge tubes were refilled with phosphate wash buffer and shaken gently. The samples were again centrifuged and the buffer and remaining buffy coat were aspirated off. Packed red cells were placed in a 5 mM lysing solution (5 mL lysing solution to 1 mL packed red cells) and allowed to stand for 2 hours at 5°C. The solution was centrifuged for 20 minutes (36900 x g (average)) and the buffer was aspirated off. The procedure was repeated using a 2.5 mM lysing solution until the packed membranes were white and the solution was clear (4-6 lysings). The packed ghosts were then lyophilized dry. One unit of blood typically yielded 200 to 300 mg of dry ghosts. The total fatty avid analysis is reported in Table 2.

The phosphate wash buffer for red cells was made from $Na_2HPO_4 \cdot 7H_2O$ (23.9 g/L) and $NaH_2PO_4 \cdot H_2O$ (2.88 g/L) in distilled water. The pH was adjusted to 7.4 with HCl and the buffer was stored at 5°C. The 5 mM lysing solution was made from $Na_2HPO_4 \cdot 7H_2O$ (1.34 g/L), the pH was adjusted to 7.4 and the solution was stored at 5°C.

Extraction of Lipids from Ghosts

The total lipids were extracted from the red cell ghosts (81, 83, 84). Methanol (250 mL) was added to a suspension of 220 mg of ghosts in 25 mL of water and the mixture was stirred for 5 minutes with N_2 bubbling. Chloroform (250 mL) was added and the mixture was stirred for a further 5 minutes. The mixture was filtered into a round bottom flask and the extraction was repeated twice more. The bulk of the solvent was removed on a rotory evaporator with the temperature kept at less than 30°C. The remaining mixture was extracted with 250 mL of chloroform. Methanol (50 mL) and 40 mL of 0.1 N KCl in water were added and the mixture seprated into 2 phases. The chloroform phase was separated, the volume was reduced to 25 mL and the lipids were stored at -15°C. TLC of the total lipids, with known standards, showed the presence of PC, PE, PS sphingomyelin and cholesterol (81).

Incubation of Ghosts with Palmitic Acid-d_{31}

Perdeuterated palmitic acid (50 mg) was sonicated in 20 mL of buffer until it formed a milky suspension (4). The buffer was made up with NaCl (6 mM), KCl (6 mM), $MgSO_4.7H_2O$ (5 mM), $CaCl_2.H_2O$ (2 mM) and Tricine (20 mM) and a pH of 6.8. The sonicated acid was added to a suspension of 400 mg of ghosts in 100 mL of the same buffer. The mixture was incubated at 37°C, with shaking, for one hour. The ghosts were recovered by centrifuging at 37000 x g for 30 minutes. The palmitic acid which failed to enter the membrane was observed to form a small pellet at the bottom of the centrifuge tube. The ghosts were separated from the acid, washed with water, centrifuged and lyophilized. The ghosts containing the perdeuterated acid, as well as an unincubated sample, were analyzed for total fatty acids by GC (Table 2). Perdeuterated palmitic acid was observed to have a slightly shorter retention time and so could be observed separately from the non-deuterated palmitic acid. Perdeuterated stearic acid gave a quantitatively similar result. The perdeuterated palmitic acid accounted for 10.5% of the total fatty acids and this corresponds to approximately 3% of the total dry ghost weight (81).

Table 2

TOTAL FATTY ACIDS IN GHOSTS AND INCUBATED GHOSTS[a] (%)

	14:0	16:0	16:0-d_{31}	18:0	18:1	18:2	20:4	22:6	Others
ghosts	2.4	26.3	-	18.8	18.1	12.0	19.2	0.5	2.7
ghosts + 16:0-d_{31}	2.1	23.8	10.5	16.5	15.7	9.6	15.8	0.3	5.7

a Average of 3 runs.

Acholeplasma laidlawii B Growth

Acholeplasma laidlawii B was grown at 37°C in a tryptose browth, initially free of fatty acids. This was supplemented with [5-$^2H_2$]-eleic, [18-$^2H_3$]-oleic and unlabelled oleic acid. The [5-$^2H_2$]-oleic acid and the [18-$^2H_3$]-oleic acid were the generous gift of Dr. A.P. Tulloch (85, 86, 87). The cells were harvested in the late log phase, osmotically lysed in distilled water, lyophilized and stored at -15°C. More complete details on growths and preparations of membranes can be found in reference 88. The distribution of fatty acids was determined by GC of the methyl esters and is reported in Table 3.

II.4 Experimental Techniques

Partition Coefficients

Partition coefficients (K_p) for egg PE were measured by dispersing the PE and anesthetic in a borate-phosphate-citrate buffer at the pH of interest. Samples were heated to 65°C, vortexed, freeze-thawed several times and centrifuged. The concentration of anesthetic in the supernatant was determined spectrophotometrically (TTC, λ_{max} = 285 nm; PRC, λ_{max} = 307 nm) (89) and the partition coefficient was calculated according to:

Table 3

FATTY ACID ANALYSIS FOR THE

ACHOLEPLASMA LAIDLAWII B GROWTHS (%)

	12:0	14:0	16:0	18:0	18:1
[5-$^{2}H_{2}$]-oleic	1.8	4.7	26.3	2.6	54.3
[18-$^{2}H_{3}$]-oleic	2.6	6.5	23.6	3.1	59.0
unlabelled	3.4	16.4	48.3	11.1	10.2

$$K_P = \frac{[A_l]}{[A_w]} = \frac{\text{concentration of anesth. in lipid}}{\text{concentration of anesth. in water}} \qquad (7)$$

Since K_P shows strong ionic strength and concentration dependence (90) the values of K_P were determined at concentrations similar to those of the NMR experiments.

Partition coefficients for natural membranes were determined by dispersing the membrane and anesthetic in BPC buffer and vortexing extensively. Samples were centrifuged and the anesthetic concentration was determined spectrophotometrically. The BPC buffer was made up with citric acid (3.8 mM), boric acid (2.9 mM), sodium hydroxide (17.1 mM) and 85% H_3PO_4 (2.4 mM) and the pH was adjusted to 5.5, 7.0 and 9.5 with concentrated HCl.

Fatty Acid Analysis

The lyophilized membrane (10 mg) or dry lipid (5 mg) and 40 µg of heptadecanoic acid were added to 4.5 mL of methanolic HCl (14 mL acetyl chloride and 250 mL methanol) and the mixture was refluxed for 2 hours. Water (0.5 mL) was added and the esters were extracted with distilled hexane (2 mL). The esters were analyzed on a Hewlett-Packard 5710A gas chromatograph with a 15% diethylglycosuccinate column at 175°C.

NMR Sample Preparation

For studies of labelled anesthetics in phosphatidylethanolamine, the egg PE, in a chloroform/methanol solution, was dried under a stream of nitrogen until the volume was reduced to 0.5 mL. This solution, and the deuterated anesthetic were placed in a 10 mm NMR tube with a 5 mm capillary at the open end. The remaining solvent was blown off under a stream of nitrogen and the sample was dried on a vacuum line for 12 hours. Buffer was added and the NMR tube was sealed off on the vacuum line. The sample was then vortexed extensively and heated above the bilayer-hexagonal transition temperature of 65°C (91) to ensure complete hydration of the PE (92). In order to attain complete equilibration of the anesthetic, each sample was then subjected to five freeze-thaw-vortex cycles (61, 93). Samples prepared in this manner gave very reproduceable results and did not change, even on standing at 15°C for several months.

The buffer was a borate-phosphate-citrate buffer, identical in concentration to the one used for the partition coefficient studies, but made up in deuterium depleted water to minimize the H^2HO signal. The pH's of several of the NMR samples were checked in order to ensure that a correct pH was maintained. The ^2H NMR spectrum of the BPC buffer alone was run under the same conditions as the other NMR experiments. The resulting spectrum indicated that H^2HO

contributed <1% to the intensity of the central narrow line observed in the ^2H NMR spectra of the deuterated anesthetics.

For studies of labelled DMPE's and labelled anesthetics in egg PC, a similar procedure was used. However, the samples were not sealed under vacuum. Labelled hydrocarbons were run in sealed 10 mm NMR tubes.

Membrane samples of NMR experiments were prepared by adding BPC buffer (in ^1H_2O) to a known weight of lyophilized membrane and anesthetic, and vortexing extensively. The buffer to membrane ratio was always chosen to be in excess of 4:1 (w/w).

^2H NMR

The ^2H NMR spectra were obtained in a Bruker CXP-300 spectrometer operating at 46.063 MHz using homebuilt 10 mm and 7 mm solenoid coil probes (R.A. Byrd, unpublished). Spectra were acquired using the quadrupole echo sequence (94), with full phase cycling of the rf pulses as shown below, (173)

$$90^\circ_A - \tau_1 - 90^\circ_B - \tau_2 - \text{echo} \qquad (8)$$

where A and B represent a phase shift of 90°. The 90° pulse lengths were typically 5.5 μsec for the 10 mm coil and 3

μsec for the 7 mm coil. The pulse spacing (τ_1) was generally 50-60 μsec and the recycle time was at least 5 x T_1. The frequency of the spectrometers was set at the centre of the powder pattern (Larmor frequency) and the spectra were acquired with quadrature detection. The phase relationship between the transmitter and the detector was carefully adjusted so that all of the signal was in only one of the quadrature channels. The channel containing only noise was zeroed, resulting in a 'folding' about the Larmor frequency and a $2^{1/2}$ improvement in signal-to-noise. Spectra were checked with and without folding in order to ensure that no distortions in the line shape were introduced.

Since τ_1 was chosen to be larger than τ_2, several data points were acquired prior to the exact top of the echo. Spectra were 'left-shifted' until the first data point corresponds to the top of the echo and then the spectra were Fourier transformed. On the Nicolet 1280 data station, an interpolation was often performed on the FID in order to provide a more exact determination of the echo maximum.

For the broad powder patterns observed in the solid alkanes, the spectral distortions arising from finite pulse lengths are important (95). To minimize the distortion, an echo sequence with pulses $<90^{\circ}$ was used (96, 97). Typically, a $45\text{-}60^{\circ}$ pulse was used (2.75-4.0 μsec with a 10 mm coil) in these echo experiments. This procedure resulted in a

loss of intensity, however, more rapid pulsing was also possible.

Spin lattice relaxation times (T_1) were determined using a modified inversion recovery sequence (98):

$$180^{\circ} - \tau_{VD} - 90^{\circ}_{A} - \tau_1 - 90^{\circ}_{B} - \tau_2 - \text{echo} \qquad (9)$$

where τ_{VD} is a variable delay to allow partial relaxation. Typically 12 to 14 values of τ_{VD} were chosen, with at least five of the values on each side of the zero crossing. The data were fitted graphically to the relationship:

$$M_{\infty} - M_{\tau_{VD}} = M_{\infty} e^{-\tau_{VD}/T_1} \qquad (10)$$

where M_{∞} and $M_{\tau_{VD}}$ are the magnitudes of the z component of the magnetization after times of 5 x T_1 and τ_{VD}, respectively.

Spectral de-Paking (99) was done on a Nicolet 1280 data station connected to the Bruker ASPECT-2000 (R.A. Byrd and M. Rance, unpublished). Three iterations on 750 data points gave good convergence. Moments of the ^2H NMR spectra (100) were calculated on the Nicolet 1280. Moments were calculated from the centre of the spectrum to a point where no signal is detected. A similar calculation is then done from the centre to the next 10 successive points and the results are averaged to give the reported moments.

The sample temperature was controlled by passing heated air or cold nitrogen gas into an insulated glass dewar, which enclosed the sample and coil. Samples were allowed to equilibrate for 15 to 30 minutes at a given temperature prior to acquisition.

^{31}P NMR

The ^{31}P NMR experiments were performed on a Bruker CXP-300 spectrometer operating at 121.47 MHz. A high power probe with a 10 mm solenoid coil, doubly tuned for ^{31}P and ^{1}H was used (R.A. Byrd, unpublished). Spectra were acquired using a Hahn echo (101).

$$90^{\circ}_{A} - \tau_1 - 180^{\circ}_{B} - \tau_2 - \text{echo} \qquad (11)$$

which refocusses the chemical shift interactions. The use of this echo sequence, coupled with phase cycling of the pulses gives undistorted line shapes (102). The phase cycling involved 16 cycles of the echo experiment with varying phases on the 90° and 180° pulses. (X, Y, Y, X, -X, Y, -Y, X, X, -Y, Y, -X, -X, -Y, -Y, -X, -X, X, -Y, Y, X, X, Y, Y, -X, -X, -Y, -Y, X, -X, Y, -Y). This phase cycling eliminated the errors arising from mis-set pulse angles.

Unlike ^{2}H spectra, ^{31}P spectra are asymmetric and thus it is not possible to adjust the phase such that all of the

signal is in one channel. Instead, the phase is adjusted such that at the time the echo occurs, there is a signal maximum in one channel and a zero crossing in the other. More complete details of this operation can be found in reference 102.

Proton decoupling was used for all spectra and was achieved with the low-power decoupler on the Bruker CXP-300. Gated broadband decoupling was used with the decoupling field on from the start of the echo 90° pulse until the end of the acquisition. A ^{1}H field strength of 1.9 gauss gave complete decoupling.

Spectra were acquired with a 125 kHz sweep width and a recycle time of 2 seconds. This was generally found to be greater than five times the ^{31}P spin lattice relaxation time.

CHAPTER III

CHARACTERIZATION OF THE BINDING OF TETRACAINE AND PROCAINE WITH PHOSPHATIDYLETHANOLAMINE

III.1 Introduction

If the sodium channel in the nerve membrane is of the form described by Trudell (22, see Section I.2), the strong correlation between anesthetic potency and hydrocarbon solubility, first reported by Meyer (19) and Overton (20), makes a study of anesthetic - lipid interactions quite important. Such anesthetic - lipid interactions could inhibit the movement of the hydrophobic arms during depolarization (Figure 6), preventing propagation of the nerve signal. Since the exact nature of the anesthetic - lipid interaction required for such inhibition is unknown, it is necessary to examine the interaction of anesthetics with different lipid classes. Since amino-ester and amino-amide anesthetics are known to act preferentially on the inside surface of the membrane, (10, 17, 18) and since PE is known to be distributed preferentially on the intracellular side of the membrane (103, 104), a study of the interaction of TTC and PRC with PE is appropriate.

The influence of local anesthetics on PE model membranes has been studied only sparingly to date. Local

anesthetics have been observed to depress the gel-liquid crystal phase transition temperature of DPPE by several degrees (25, 105). Cullis has shown, by ^{31}P NMR, that local anesthetics alter the polymorphic phase behaviour of PE and mixtures of PE with other lipid classes (106, 107, 108). The anesthetics act to inhibit the transition of PE from lamellar to inverted hexagonal, but it is difficult to imagine any way in which this is a significant element in anesthesia. Dibucaine has been observed, by ^{2}H NMR, to alter the headgroup conformation of specifically deuterated DPPE in a manner analogous to the action of cations, like Ca^{2+} (109).

The interaction of local anesthetics with other lipids has been the subject of more extensive studies, by a number of techniques, including ESR (28, 110, 111, 112), high resolution NMR (113), neutron diffraction (114) and a rather novel study by polarized light-absorption spectroscopy (115). All these studies suggest that the anesthetic intercalates partially into the lipid bilayer.

A recent ^{2}H NMR study of the interaction of deuterated tetracaine and procaine with PC indicated that TTC exists in both a strongly bound and a weakly bound environment, as well as free in solution (58, 59). The strongly bound site was characterized by quadrupole splittings arising from deuterium incorporated at several positions on the tetracaine

molecule. Tetracaine was found to be intercalated into the bilayer, with a deeper penetration observed at pH 9.5, when the anesthetic is primarily uncharged (58, 60). Later work on the effect of attaining a true equilibrium on the ^2H NMR line shape showed that repeated freeze-thaw cycles eliminated the quadrupole patterns observed for PRC-d_4 and TTC-d_6 at most pH values (61). (See Figure 11 for the structures of PRC-d_2, PRC-d_4, TTC-d_2, TTC-d_3, TTC-d_6 and TTC-d_9.) It was suggested that when a true equilibrium was obtained, TTC was in fast exchange between a single bound site and free in solution.

In this work, the interaction of TTC and PRC with PE has been studied by obtaining the ^2H NMR spectra of labelled anesthetics in multilamellar dispersions of PE. A semisynthetic PE (made from egg PC by phospholipase D mediated headgroup exchange and hereafter called egg PE) was used and experiments were performed at both pH 5.5 and 9.5 in order to compare the differences in the charged and uncharged forms of the anesthetic.

III.2 Results and Discussion

Partition Coefficients (K_p)

The partition coefficients for procaine and tetracaine in egg PE are reported in Table 4.

TETRACAINE

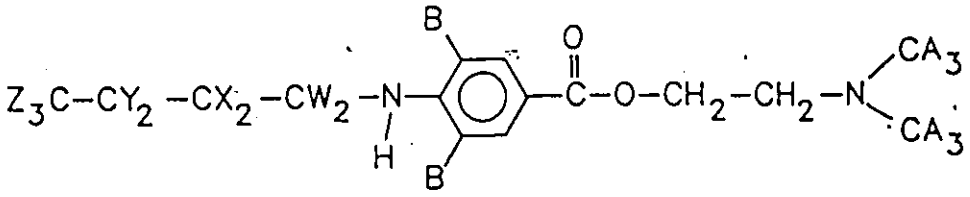

TTC–d_6	A = D	;	B,W,X,Y,Z = H
TTC–d_2	B = D	;	A,W,X,Y,Z = H
TTC–d_3	Z = D	;	A,B,W,X,Y = H
TTC–d_9	W,X,Y,Z = D	;	A,B = H

PROCAINE

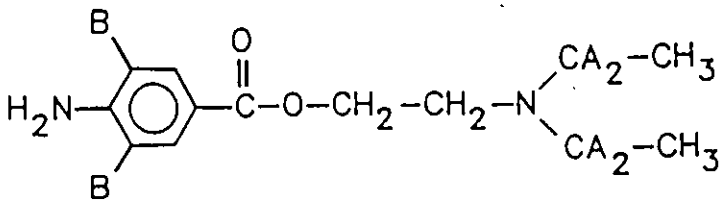

PRC–d_2	B = D	;	A = H
PRC–d_4	A = D	;	B = H

Figure 11. Structures of the specifically deuterated tetracaines and procaines.

Table 4

PARTITION COEFFICIENTS (K_p) FOR TETRACAINE AND PROCAINE IN SEMISYNTHETIC EGG PE[a]

	pH 5.5	9.5
TTC	46	71
PRC	3.3	4.1

a All samples were 100 mg lipid, 5-10 mg of anesthetic and 1 ml of BPC buffer.

The K_P values are considerably larger for TTC relative to PRC, consistent with studies in other lipids (58, 59), and arising as a consequence of the hydrophobic butyl tail on TTC. The K_P values are considerably smaller than those observed for egg PC (59), but are very close to those found for erythrocyte ghosts (90, 116, see Chapter VI of this thesis). Partitioning is also observed to be greater at higher pH, although the differences in K_P at pH 5.5 and 9.5 are smaller than those observed for PC, PS and PC/PS mixtures (58). Because the partition coefficients for positively-charged anesthetics decrease at higher free anesthetic concentrations and at higher ionic strength (116) we have determined K_P on samples as close as possible to the NMR samples. We have confirmed these values by determining the partition coefficients for several of the NMR samples.

^2H NMR of Tetracaine

The ^2H NMR spectra observed for the specifically-deuterated tetracaine species in egg PE are characterized by the presence of a Pake doublet, with quadrupole splitting $\Delta\nu_Q$ and a narrow central resonance. Figure 12 shows the ^2H spectra observed at pH 9.5 and Figure 13 at pH 5.5. The quadrupole splittings observed at pH 5.5, 7.0 and 9.5 are summarized in Table 5.

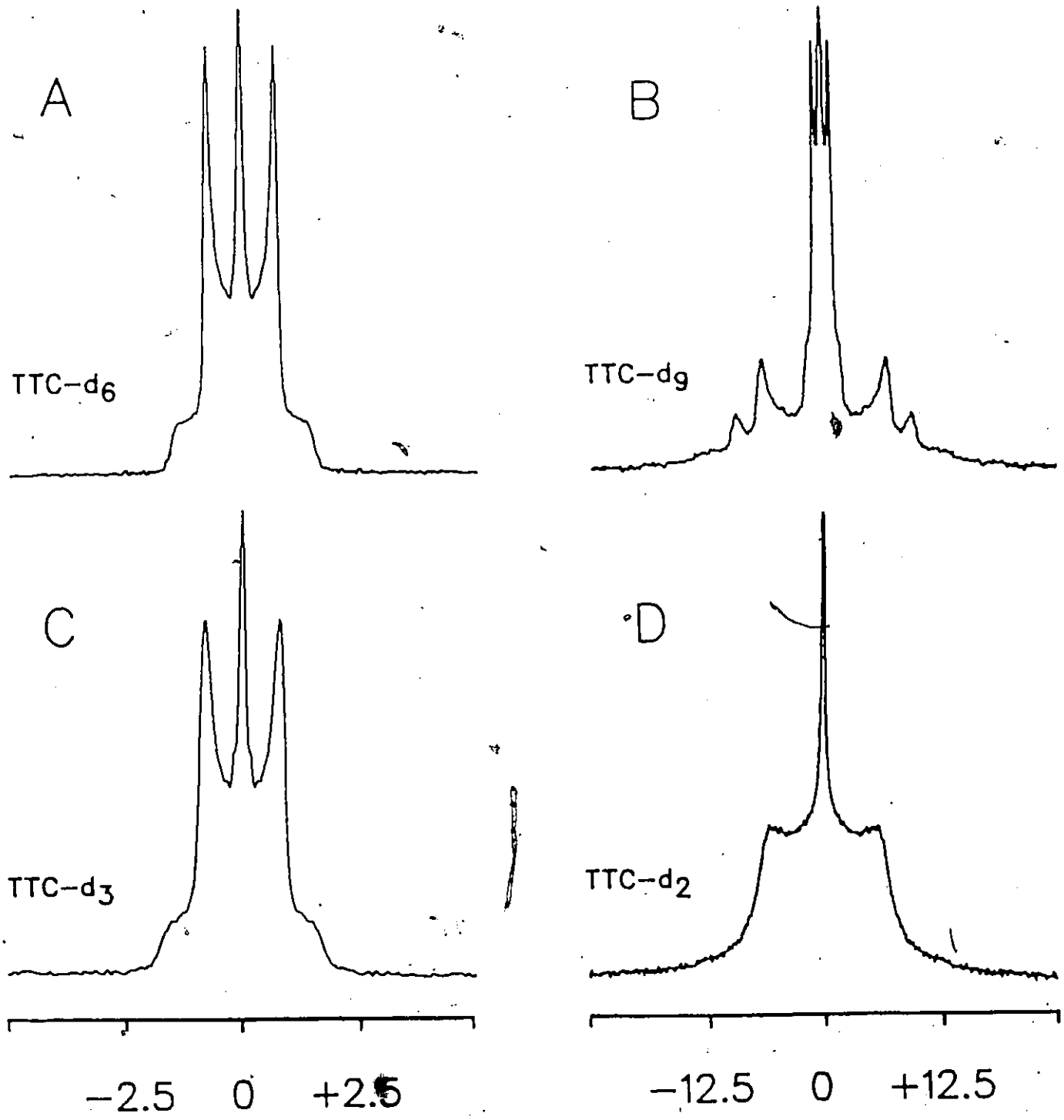

Figure 12. ^2H NMR spectra of the specifically deuterated tetracaines in egg PE at pH 9.5. A) TTC–d_6 (48 mM) and egg PE (184 mM) in 0.75 mL of BPC buffer. B) TTC–d_9 (25 mM) and egg PE (185 mM) in 0.75 mL of buffer. C) TTC–d_3 (50 mM) and egg PE (184 mM) in 0.75 mL of buffer. D) TTC–d_2 (24 mM) and egg PE (370 mM) in 0.4 mL of BPC buffer.

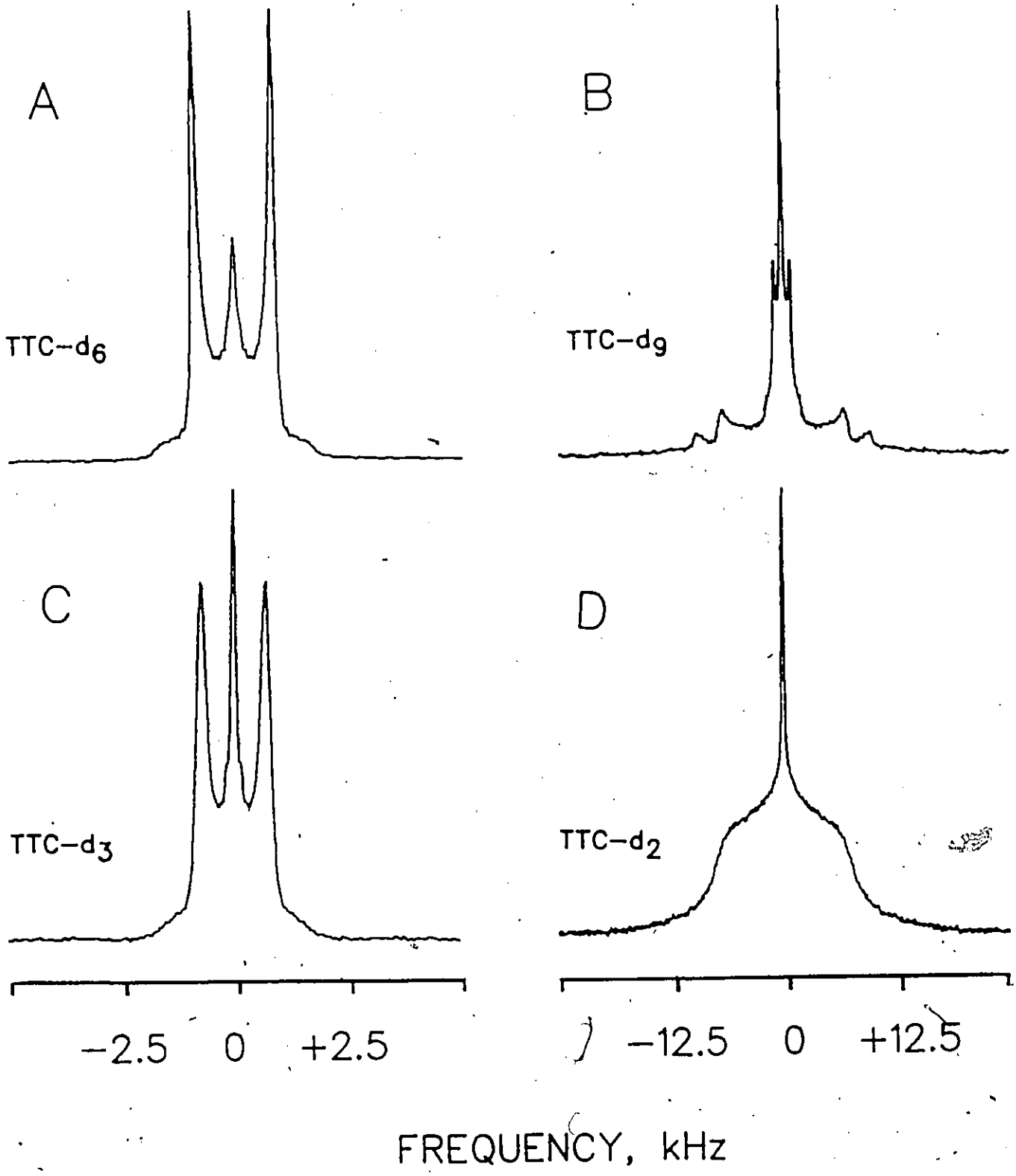

Figure 13. ^2H NMR spectra of the specifically deuterated tetracaines in egg PE at pH 5.5 A) TTC–d_6 (48 mM) and egg PE (184 mM) in 0.75 mL of BPC buffer. B) TTC–d_9 (25 mM) and egg PE (185 mM) in 0.75 mL of buffer. C) TTC–d_3 (50 mM) and egg PE (184 mM) in 0.75 mL of buffer. D) TTC–d_2 (24 mM) and egg PE (370 mM) in 0.4 mL of BPC buffer.

Table 5

QUADRUPOLE SPLITTINGS FOR DEUTERATED TETRACAINES AND PROCAINES IN SEMISYNTHETIC EGG PHOSPHATIDYLETHANOLAMINE (IN kHz)[a]

		pH 5.5	pH 7.0	pH 9.5
TTC-d_6		1.85	1.80	1.55
TTC-d_2		12.5	12.8	13.0
TTC-d_9	α	19.8	20.1	19.9
	β	14.6	14.4	14.6
	γ	13.9	14.0	14.0
	δ	1.60	1.65	1.85
TTC-d_3		1.60	1.65	1.85
PRC-d_4		b		b
PRC-d_2		9.2		11.4

a All spectra show a narrow central resonance.
b No quadrupole splitting was observed, only a narrow resonance.

In all cases, the area of the central resonance correlates well with the TTC solution concentration predicted from the K_p values. This is in contrast to the studies in egg PC, where the area of the central resonance was significantly greater than predicted from the partition coefficients. As a further check, the free TTC concentration of the NMR samples was determined by spinning down these samples on a centrifuge, separating the aqueous layer and measuring the TTC concentration spectrophotometrically. The agreement between the two results was good. The ^2H NMR spectra of the centrifuged sample showed the quadrupole doublet with the narrow line almost completely removed. The narrow signal that remained represents the anesthetic in the residual water.

The observed quadrupole splittings show only a small pH dependence. In fact, it is only at the two end positions of tetracaine, TTC-d_6 and TTC-d_3, that the splittings vary by more than 10%. This is in contrast to the egg PC studies where these positions show a substantial pH dependence (59, 61). However, data for TTC/egg PE at pH 5.5 and 7.0 are almost identical, suggesting that the observed pH dependence of the quadrupole splittings is a function of the charge on tetracaine. The pK_A of the tertiary amino group of tetracaine is 7.5 (59) indicating that the anesthetics are mostly charged at pH 5.5 and 7.0 while almost totally uncharged at pH 9.5.

The splittings for the chain region of tetracaine were obtained by de-Paking the TTC-d_9 spectra. Figure 14 shows the spectrum of TTC-d_9 and the de-Paked result. The central doublet is somewhat distorted, due to the inability to subtract out all the central resonance prior to de-Paking. However, the spectrum does show an approximate 3:4:2 ratio of peak areas, indicating that two of the methylene splittings overlap. We have tentatively assigned the splittings on the basis of a decrease in the quadrupole splitting with position down the butyl chain. The largest splitting (~20 kHz) is assigned to the methylene deuterons adjacent to the nitrogen and the two, almost overlapping, splittings are assigned to the next two methylenes. The narrow splitting, which integrates as three deuterons, is assigned to the methyl group in agreement with the TTC-d_3 spectra. The observed splittings, while large, are less than those observed for specifically deuterated DMPE's in the plateau region (117, 118, see also Chapter V of this thesis). This could result from the presence of the bulky benzoid moiety which has a larger excluded volume than a free chain. The butyl group is thus free to undergo larger amplitude motions than the chains of the PE. A tilt in the butyl group could also reduce the splittings.

For TTC-d_2, where the aromatic ring is deuterated, the spectrum at 30°C is broad, rather featureless and it

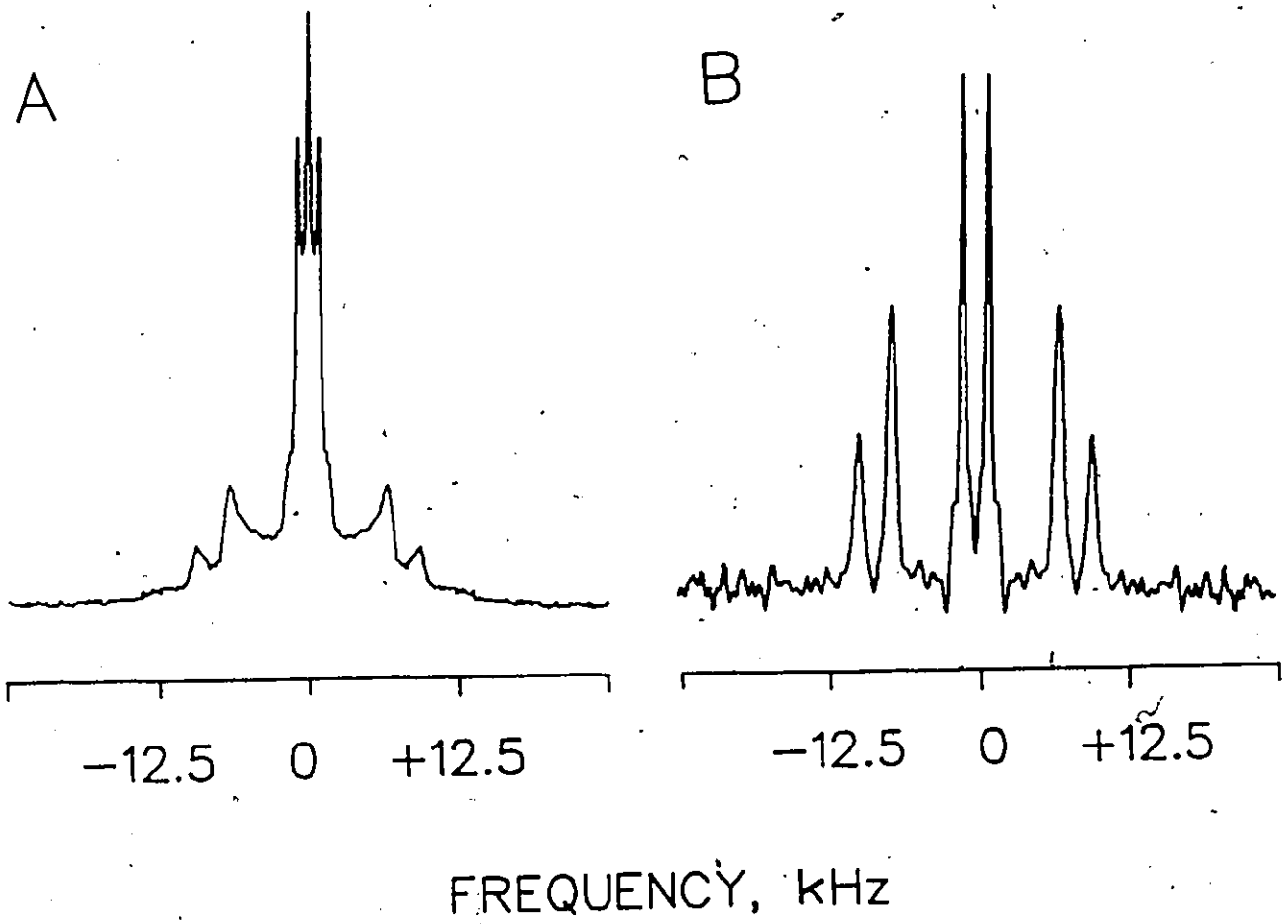

Figure 14. ^{2}H NMR spectra of TTC–d_9 in egg PE at pH 9.5. A) Normal spectrum. B) De–Paked version of A. The narrow doublet is distorted by an inability to remove the central line prior to de–Paking.

has a width of approximately 13 kHz. The broad nature of the spectra is the result of very large component linewidths, corresponding to a short T_{2e}. Attempts to measure T_{2e} were complicated by diffusion and the decay was not a simple exponential; however, T_{2e} appeared to be in the range of 100-150 μsec.

In order to explore the ring motion more fully a temperature study was performed (Figure 15). At 5°C the signal from the quadrupole pattern has almost disappeared, and at -30°C (not shown) *no* wide line spectrum can be seen. This is a consequence of the short T_{2e}, which is reduced further at lower temperatures to the point where the signal is no longer observed after the echo. At higher temperatures the T_{2e} is increased, resulting in a more clearly resolved quadrupole pattern. Also, at higher temperatures, the central resonance is increased relative to the quadrupole pattern. This is a result of a lower K_p and an increased water solubility for TTC. At temperatures above 50°C the spectra are complicated by the presence of non-bilayer structures. These structures, as determined by ^{31}P NMR, give rise to single resonances rather than a bilayer pattern (107, 108) and this is reflected in an increase in the ^2H isotropic component.

The effect of varying the TTC concentration in the bilayer was also studied. Figure 16 shows the ^2H NMR

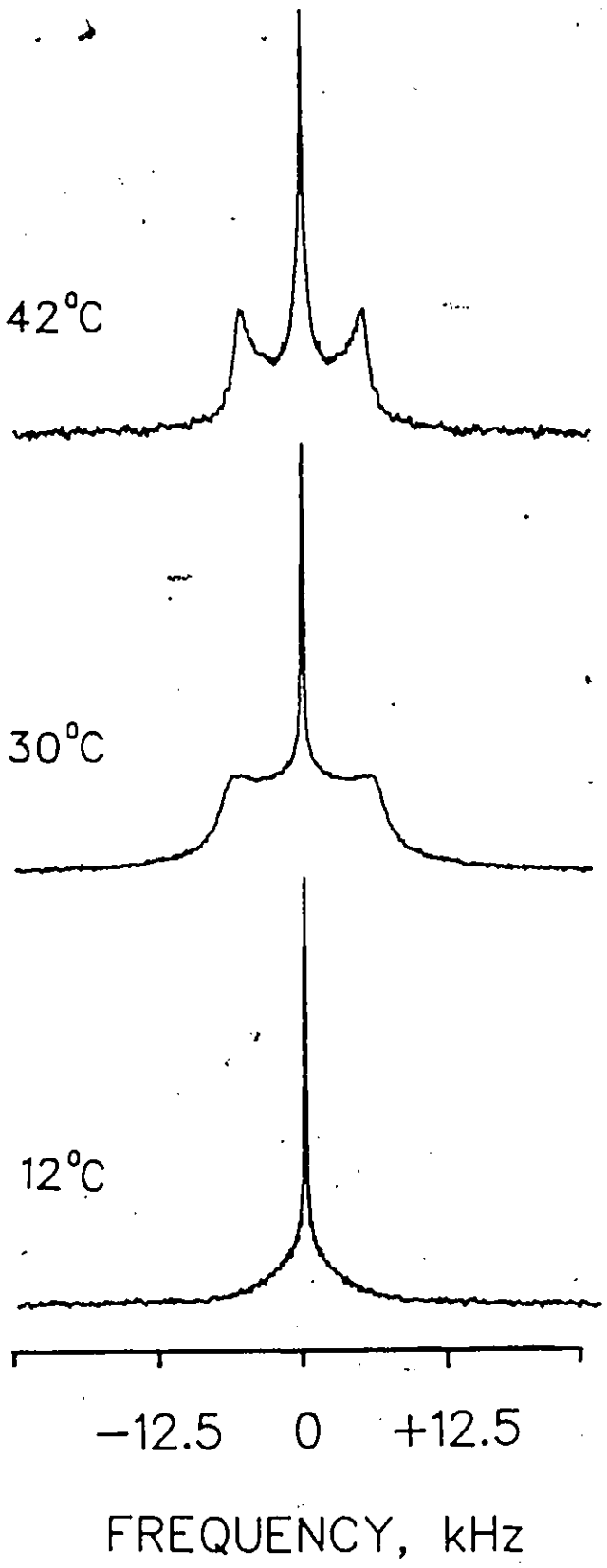

Figure 15. Temperature dependence of the ^2H NMR spectrum of TTC–d_2 in egg PE, at pH 9.5.

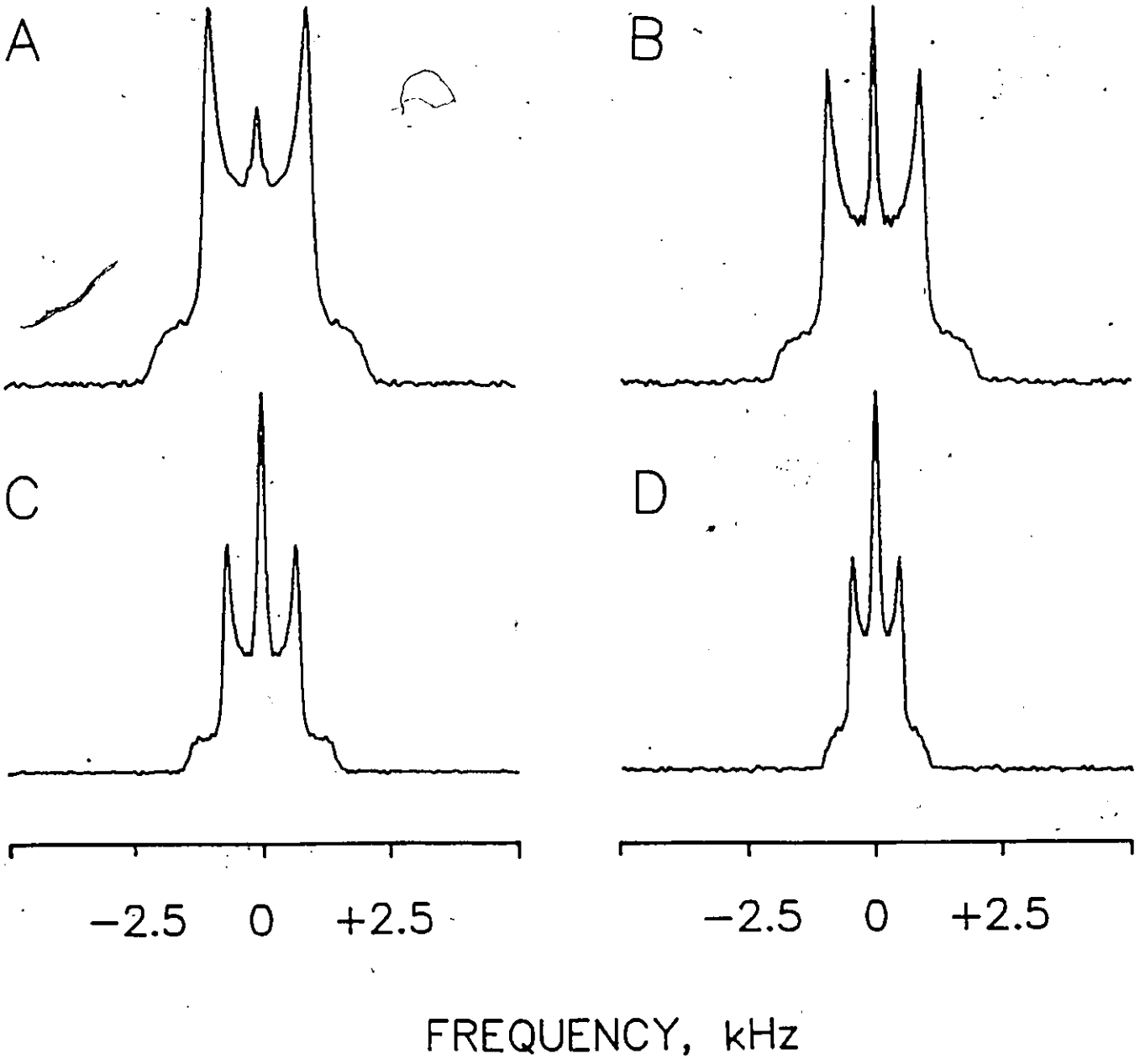

Figure 16. Effect of increasing the TTC-d_6/egg PE ratio at pH 9.5. A) 0.06/1 B) 0.13/1 C) 0.23/1 D) 0.40/1

spectra of varying ratios of TTC-d_6 and egg PE at pH 9.5. Increasing the anesthetic/lipid ratio, by using smaller quantities of egg PE with constant TTC-d_6 and buffer concentrations, results in a decrease in the quadrupole splitting and an increase in the magnitude of the narrow line. The increase in the narrow component merely reflects the greater relative quantity of aqueous tetracaine relative to tetracaine in the lipid phase. Calculation of K_p from the integrated areas of the spectra shows excellent agreement with each other, and with the spectrophotometrically determined partition coefficient. Since the linewidth of the narrow component does not increase with increasing anesthetic concentration, the reduction in the quadrupole splitting is just a reflection of increasing disorder in the bilayer introduced by the tetracaine. The lack of change in the linewidth suggests an exchange rate which is very slow, certainly much less than 10^3 sec^{-1}, between bound and free anesthetic.

Perhaps the most noticeable difference in the spectra at different pH values is the observed angular dependence, of the component linewidths, within the quadrupolar patterns. This indicates that the spin-spin relaxation time (T_{2e}) is angular-dependent at pH 5.5 and angular-independent at pH 9.5. This angular dependence manifests itself with lower spectral intensity in the central portion of the quadrupole

pattern (55^{o} orientation) and at the shoulders (0^{o} orientation). The angular dependence shows quite clearly in an echo pulse-spacing experiment. Figure 17 shows the spectra of TTC-d_6 at pH 9.5 and 5.5, as a function of increasing pulse spacing. The natural logarithms of the intensities of the 0^{o} and 90^{o} orientations are plotted in Figure 18 as a function of pulse spacing. The angular dependence of the pH 5.5 data is very clear; with increasing divergence as the pulse spacing is increased.

It is also interesting to note that the data at both pH 5.5 and 9.5 are clearly not a simple exponential. This indicates that there is a significant modulation of T_{2e} by diffusion at both pH's. Recently, the effect of slow diffusion on the pulse spacing experiment has been modelled by Rance (119). This work showed that slow diffusion alone gave an angular dependence qualitatively very similar to that seen for TTC at pH 5.5. Unfortunately he did not treat the case of faster diffusion, which could be expected to be angular independent.

Further evidence for the difference in lateral diffusion rates comes from studies of TTC in specifically deuterated PE's (reported in detail in Chapter V). At low pH, with TTC:PE ratios less than 0.1/1, two PE signals were observed; one for free PE and one for PE in contact with TTC. As the TTC concentration is increased the free signal

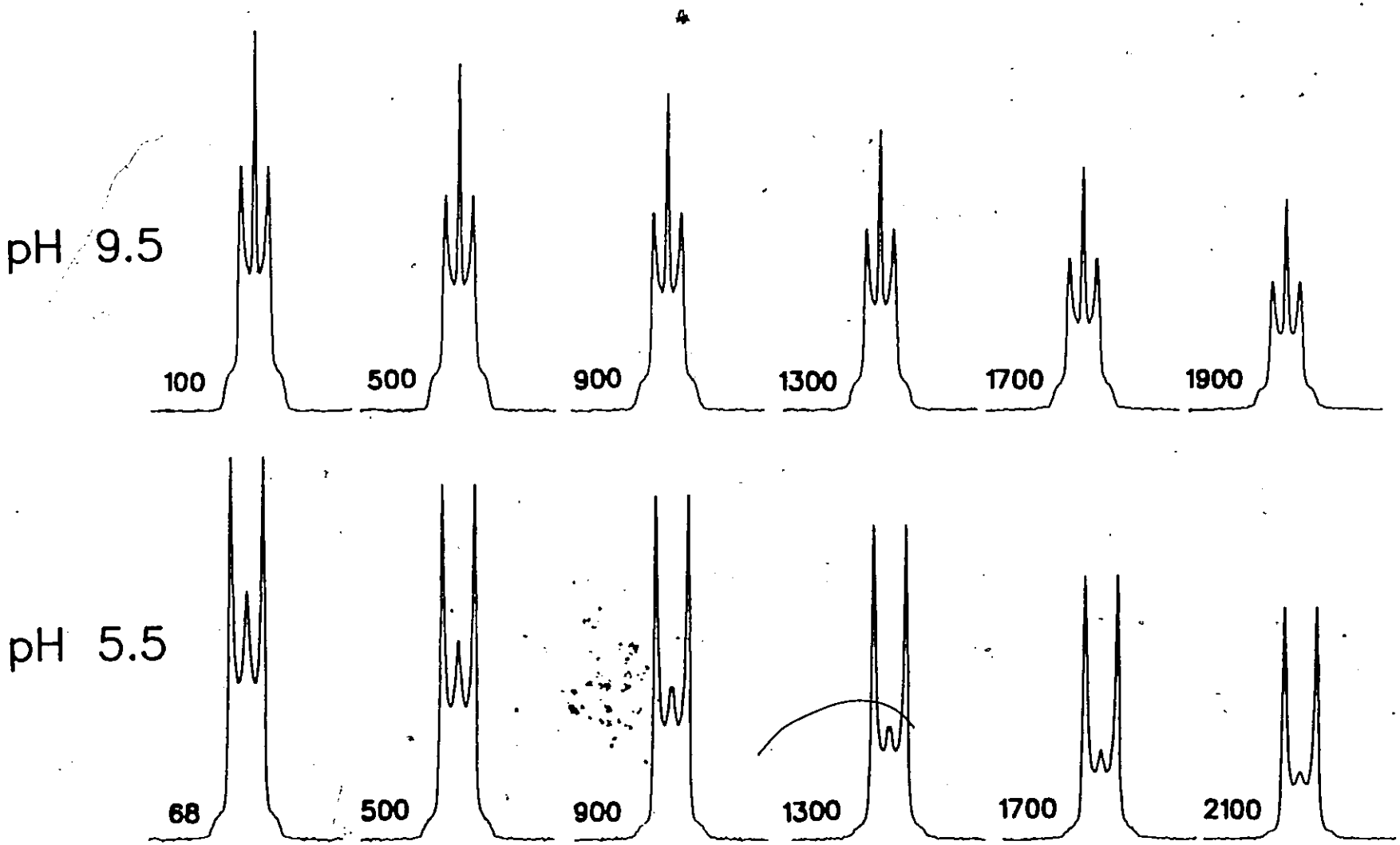

Figure 17. Effect of pulse spacing on the spectra of TTC-d_6 at pH 9.5 (top) and 5.5 (bottom). The total pulse spacing for each spectrum is shown in μsec.

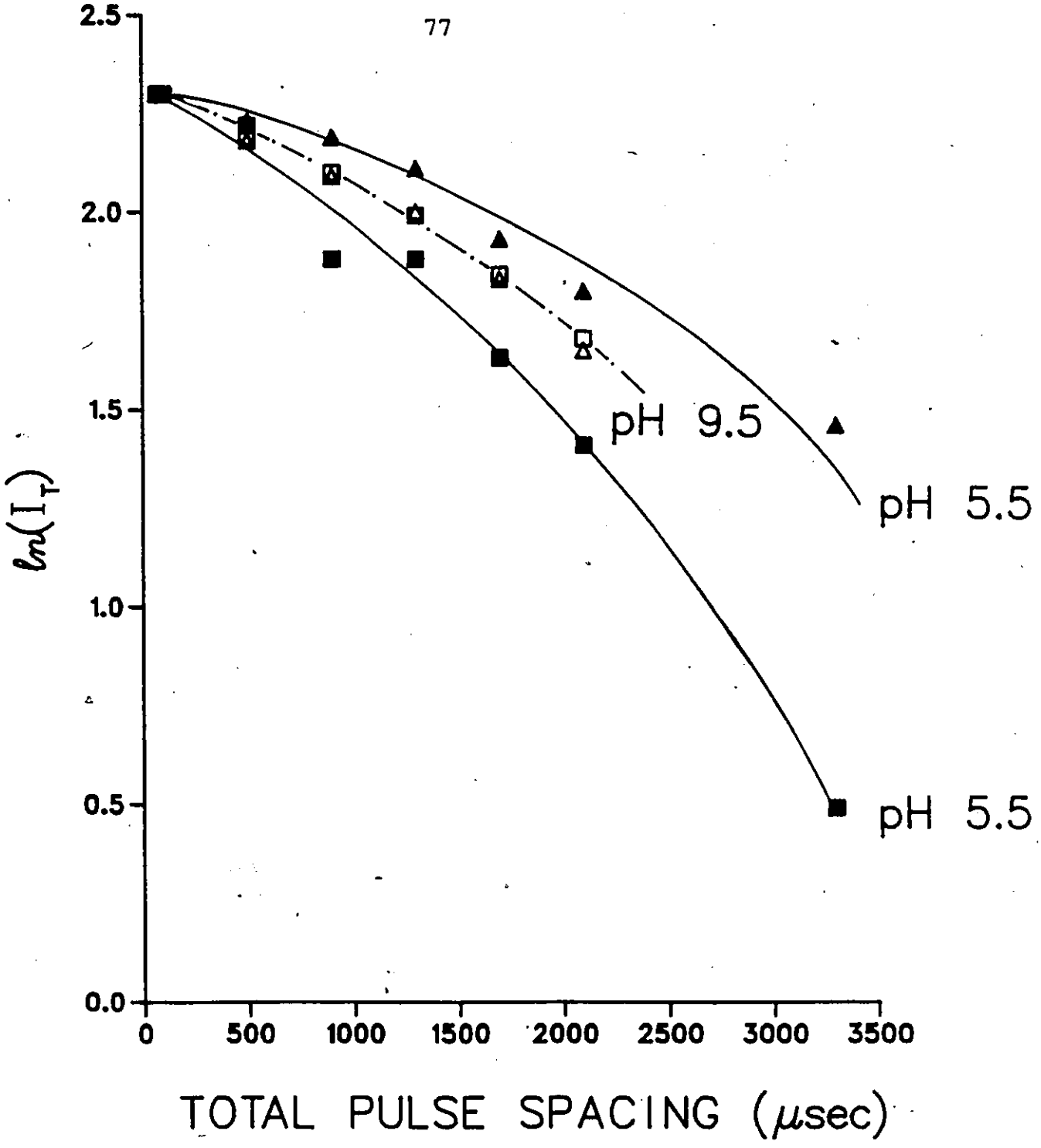

Figure 18. Plot of the *ln* of the spectral intensity as a function of the total pulse spacing for TTC–d_6 at pH 9.5. Intensities are taken at the 0° (■) and 90° (▲) orientations.

disappears and only the signal for PE in contact with TTC remains. This is consistent with TTC diffusing slowly enough that all of the PE does not come in contact with TTC in a time which is less than the ^2H NMR time scale. At pH 9.5 only one PE signal is seen at all TTC concentrations, indicating a faster diffusion.

Finally, it is worth noting that while these diffusion arguments are reasonable, it is possible that a change in the surface morphology may be occurring. Changes in the curvature of the liposomes at different pH's, or the introduction of a wavy surface or small areas of local curvature may radically effect the observed angular dependence.

The TTC-d_6, -d_3 and -d_2 spectra at pH 9.5 were simulated by assuming a two-site exchange model (Figure 19). The exchange, between bound and free TTC is assumed to be slow on the ^2H time scale ($< 1 \times 10^3$ sec^{-1}). This results in spectra which are merely a superposition of the individual free and bound TTC signals, with the populations determined from K_p.

The simulations are of the echo FID, with Lorentzian lineshapes, and take into account pulse spacing distortions. For TTC-d_6 and TTC-d_3 the simulations show good agreement with the experimental spectra. However, for TTC-d_2 there is a small percentage of narrow line which is not accounted for. Its total area is ≈2%, but it requires a much larger

Figure 19. Simulations of A) TTC–d_6; bound $\Delta\nu_Q$ = 1.55 kHz, linewidth = 45 Hz; free linewidth = 50 Hz. B) TTC–d_3; bound $\Delta\nu_Q$ = 1.85 kHz , linewidth = 125 Hz; free linewidth = 75 Hz . C) TTC–d_2; bound $\Delta\nu_Q$ = 13.0 kHz, linewidth = 2500 Hz; free linewidth = 150 Hz. All spectra were simulated with 1024 data points, 150 angles, a total echo delay of 125 μsec and the same spectral width used in the experimental spectra. The experimental spectra are shown in D) TTC–d_6, E) TTC–d_3 and F) TTC–d_2.

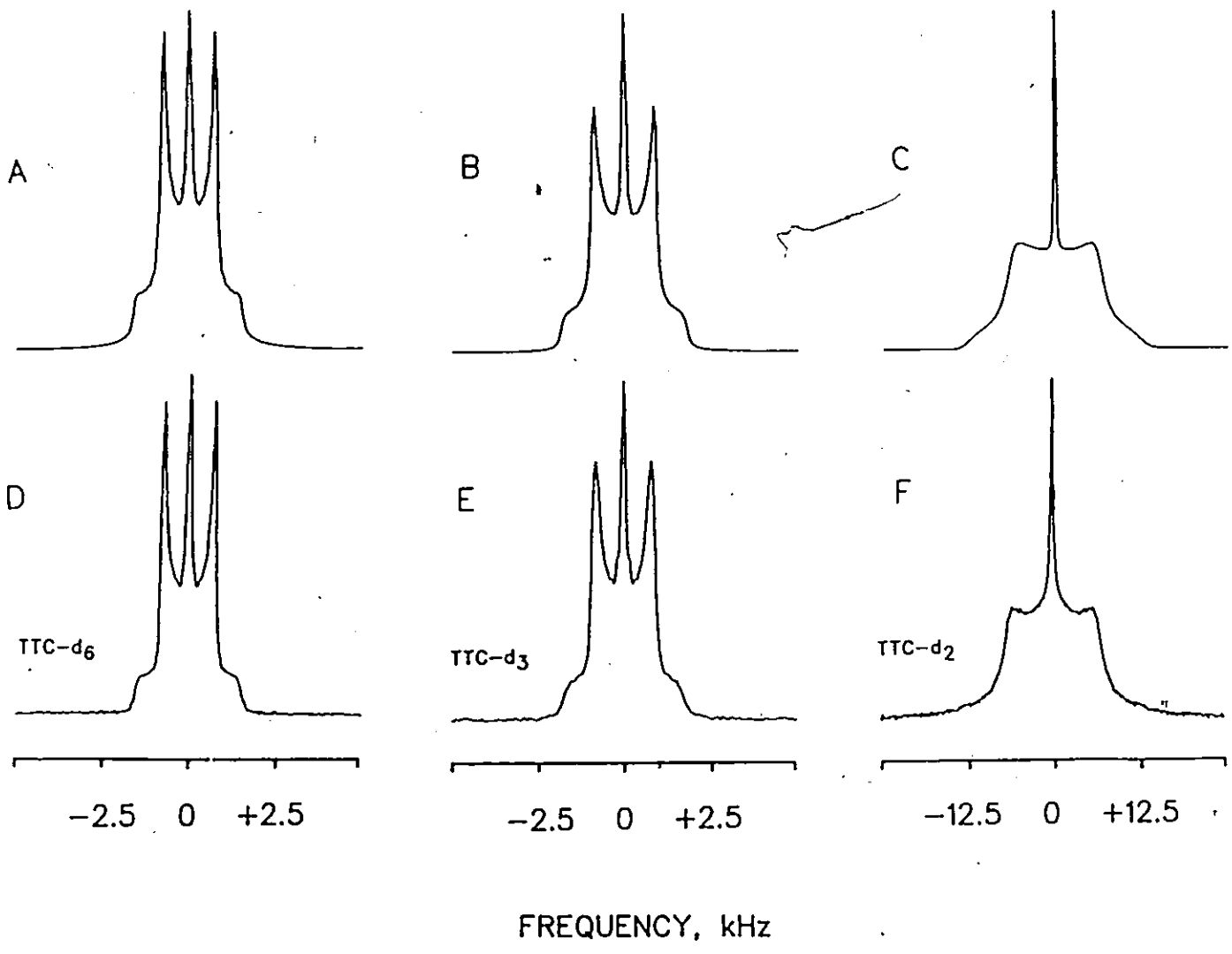
A
B
C
D
E
F
TTC-d6
TTC-d3
TTC-d2
−2.5 0 +2.5
−2.5 0 +2.5
−12.5 0 +12.5
FREQUENCY, kHz

linewidth than is found for TTC-d_2 in solution. This may simply be an artifact of trying to acquire a narrow line with too few data points and a large spectral width. It may be that there is a weak, isotropic association of the free TTC with the PE bilayer surface; however, this should certainly manifest itself in the TTC-d_3 spectrum. Finally it is also possible that it represents a non-bilayer PE structure which binds TTC. There is a small isotropic signal in the ^{31}P NMR of that sample; however, the presence of a phosphate buffer makes an exact determination uncertain.

Determination of Order Parameters

The quadrupole splitting observed for a deuteron attached to a rigid structure is given by Equation 6. The portion of the tetracaine molecule, from the ester carbonyl to the p-amino group is a rigid structure and can be treated with this equation. The deuterons on the aromatic ring give rise to only one quadrupole splitting (Figure 15), confirming that the director passes through the 1,4 position of the aromatic ring (59, 115). The angle γ (of Equation 6) is therefore 120° and if the static quadrupole coupling constant is set at 176 kHz (120), then Equation 6 can be rearranged to give

$$S_{mol} = 0.061\ \Delta\nu_Q \qquad (12)$$

For the aromatic deuterons of tetracaine, a quadrupole splitting of 13 kHz was obtained, giving an S_{mol} of 0.79. This S_{mol} is slightly smaller than the S_{mol} found for TTC-d_2 in egg PC (59) and similar to that observed for specifically deuterated cholesterol in egg PC (53). The value of S_{mol} is much greater than those found for plateau region of the DMPE bilayer (117, 118, see also Chapter V of this work), in part, because of the rigid nature of the ring.

The butyl group of tetracaine will be in the acyl chain region of the PE bilayer and an estimate of the segmental order parameter, S_{mol}, for each position would be of interest. The butyl chain is attached to the rigid aromatic unit through the nitrogen. In x-ray studies of similar structures, like procaine (49), this nitrogen appears to be sp^2 hybridized, making an angle of approximately 120° between the director and the N-C_{α} bond. This imparts to the butyl group a tilt of 24.75° with respect to the director axis (see Figure 20). With this tilt, the values of the chain segment molecular order parameter, S_{mol}, can be calculated according to the convention of Stockton et al. (49).

$$S_{mol} = \frac{S_{CD_2}}{\frac{1}{2}(3\cos^2 90-1) \times \frac{1}{2}(3\cos^2 24.75-1)} = 2.71\, S_{CD_2} \qquad (13)$$

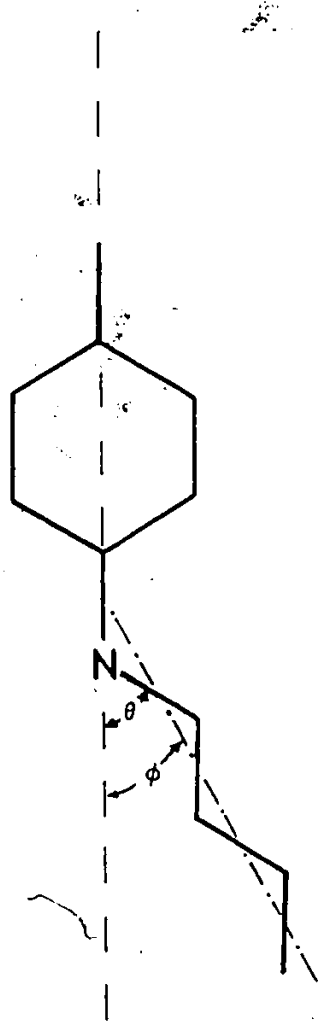

Figure 20. Orientation of the butyl group of TTC with respect to a director passing through the 1,4 position of the aromatic ring. θ = 60° and ϕ = 24.75° (assumes sp^2 nitrogen, ∠CNC = 120° and ∠CCC = 109.5°).

$$S_{mol} = \frac{S_{CD_3}}{\frac{1}{2}(3\cos^2 109.5-1) \times \frac{1}{2}(3\cos^2 35.25-1) \times \frac{1}{2}(3\cos^2 24.75-1)}$$

$$= 8.15\, S_{CD_3} \qquad (14)$$

Values of S_{CD} can be found from Equation 15,

$$\Delta\nu_Q = \frac{3}{4}\frac{e^2qQ}{h} S_{CD} \qquad (15)$$

and used to solve Equations 13 and 14.

The values of S_{mol} calculated for the butyl group, at pH 9.5, are summarized in Table 6. It is important to realize that these values of S_{mol} are based on the chain tilt arising from the sp^2 hybridized nitrogen. Anything more than sp^2 hybridized (i.e., approaching sp^3) will give a large tilt and, hence, a greater S_{mol}. However, because of the aromatic ring adjacent to the nitrogen it is likely to be very close to pure sp^2 hybridized. The proton and the butyl carbon alpha to the nitrogen will therefore be in the plane of the aromatic ring. The values of S_{mol} calculated with a tilt of 24.75^o fall off quite rapidly. This is likely a consequence of the larger cross section of the aromatic ring which allows the butyl group some extra freedom of motion.

Table 6

VALUES OF S_{mol} FOR TTC-d_2 AND TTC-d_9 IN SEMISYNTHETIC EGG PE AT pH 9.5

		S_{mol}
TTC-d_2		0.79
TTC-d_9	α	0.43
	β	0.32
	γ	0.30
	δ	0.12

^{2}H NMR of Procaine

The ^{2}H NMR spectra of PRC-d_2 and PRC-d_4 at pH 9.5 are shown in Figure 21. There is no quadrupole pattern observed for the PRC-d_4 samples, but there is a wide pattern, of low integrated intensity, for PRC-d_2. The low intensity of the quadrupole pattern of PRC-d_2 reflects the very low partition coefficients observed in these systems.

The absence of a quadrupole pattern for the PRC-d_4 samples, at both pH 5.5 and 9.5, suggests that the procaine sits higher in the bilayer than does tetracaine, since the TTC-d_6 samples show quadrupole splittings. The linewidth of the PRC-d_4 is larger than the linewidth of the free anesthetic and of the narrow component of the TTC-d_6 spectra. This suggest a very disordered environment for the procaine 'head-group' region relative to tetracaine.

The quadrupole splitting for PRC-d_2 shows the most pronounced pH dependence. The reduced splitting observed at pH 5.5 suggests that the procaine sits slightly higher in the bilayer. At pH 9.5, where the procaine is primarily uncharged (pK_A = 9.0) (58, 59), it could penetrate more deeply into the bilayer.

^{2}H NMR Spin Lattice Relaxation Times

The quadrupole splittings observed for the deuterated local anesthetics provide information on the amplitude of

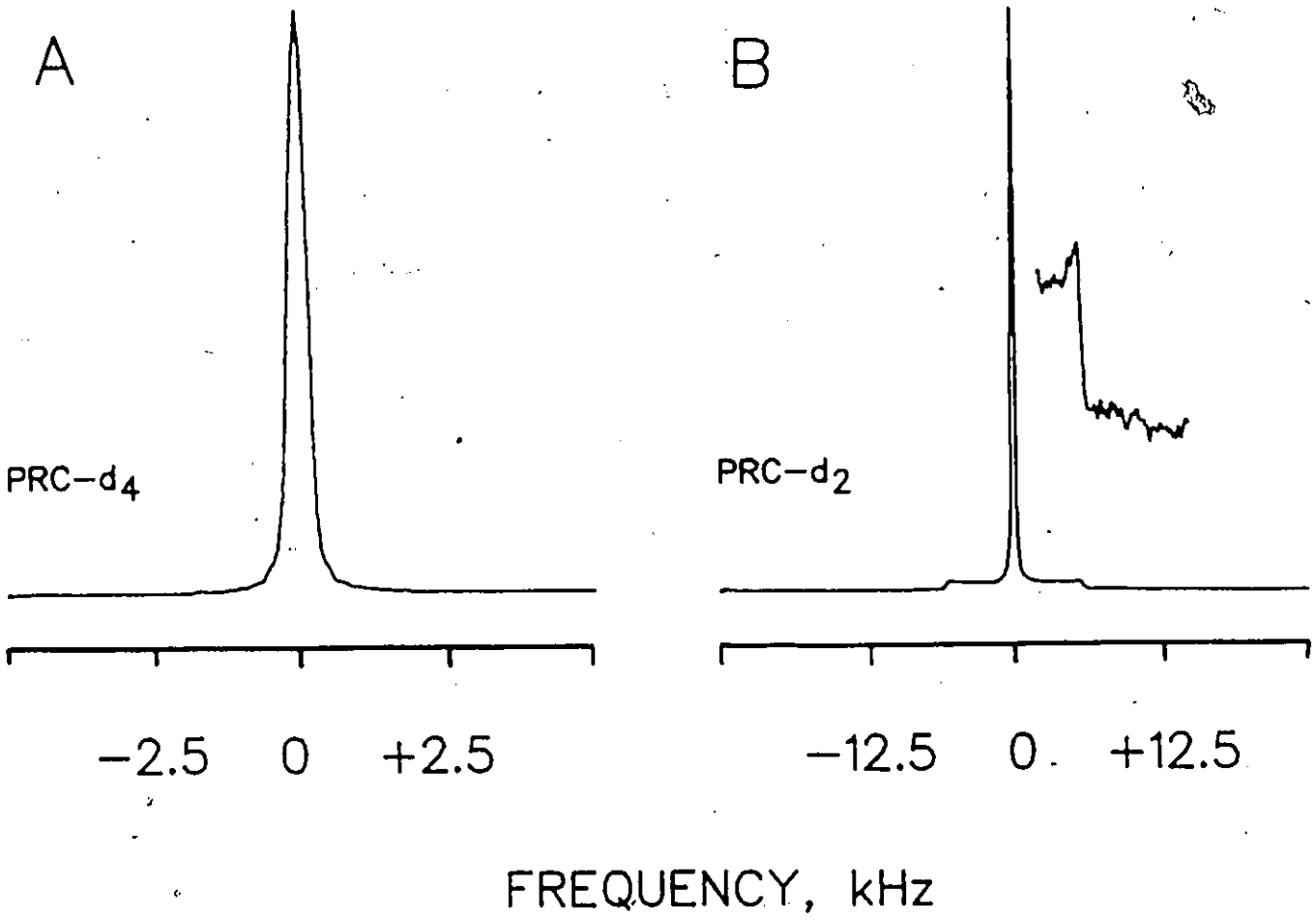

Figure 21. ^2H NMR spectra of specifically deuterated procaines in egg PE at pH 9.5 . A) PRC–d_4 (50 mM) and egg PE (185 mM) in 0.75 mL of BPC buffer. B) PRC–d_2 (50 mM) and egg PE (185 mM) in 0.75 mL of BPC buffer.

the anisotropic motion. The spin-lattice relaxation times (T_1) can give information on the rates of these motions (122, 123). In particular, T_1 is sensitive to rates of motion with frequencies of the order of 46 MHz, the resonance frequency of the NMR experiments. The ^2H T_1 values for TTC-d_6, -d_3 and -d_2 were determined at both pH 5.5 and 9.5; the results are shown in Table 7. Both the T_1's of the narrow line and the quadrupole pattern are reported.

The T_1 values of the narrow lines are slightly smaller than those observed for solutions of TTC alone and this is likely just a reflection of a more viscous solution. The T_1 values are reduced for TTC in the membrane, with the most significant reductions found for TTC-d_2 at both pH 5.5 and 9.5 and for TTC-d_6 at pH 9.5. These smaller T_1 values indicate a generally slower motion in the membrane environment, relative to the free anesthetic.

For TTC-d_2 the reduction in T_1, in the PE bilayer, is quite large. The observed relaxation times are considerably smaller than those found for free TTC-d_2 or for the acyl chains of dipalmitoyl phosphatidylcholine (122). This reflects an increase in the density of ring motions, which have frequencies near the deuterium resonance frequency, on entering the bilayer. As well, the phospholipid acyl chains may exhibit fast trans-gauche isomerisations which are unavailable to the aromatic ring (52). In the PE bilayer the

Table 7

T_1 VALUES FOR SPECIFICALLY DEUTERATED TETRACAINES IN SEMISYNTHETIC EGG PHOSPHATIDYLETHANOLAMINE (msec)

		pH 5.5	pH 9.5
TTC-d_6	narrow line	60	112
	quadrupole splitting	51	44
TTC-d_2	narrow line	40	20
	quadrupole splitting	4.6	4.5
TTC-d_3	narrow line	140	94
	quadrupole splitting	122	105

TTC-d_2 shows a T_1 very similar to the T_1 minimum observed for cholesterol, deuterated in the A ring, in egg PC (52, 53). This indicates similar slow motions for the aromatic ring and the sterol in the bilayer and suggests a correlation time close to the 3.5×10^{-9} $srad^{-1}$ (53) found for cholesterol at 30°C ($\omega_0\tau_c \simeq 1$ at the T_1 minimum).

For TTC-d_3 at both high and low pH the T_1 values are large relative to those of the aromatic deuterons. Furthermore, they change by less than 15% from their solution values on entering the bilayer. This suggests an environment for the terminal methyl group which is deep in the bilayer (124) and which is not greatly influenced by the PE acyl chains. This likely results from the larger cross-sectional area of the aromatic ring, which pushes neighbouring lipids apart, giving considerable freedom to the butyl chain of tetracaine.

For TTC-d_6 and T_1 values at pH 9.5 show a substantial reduction on entering the bilayer, reflecting a more constrained environment for the methyl groups. When free in solution the TTC is unprotonated and will interact less with water than does protonated TTC at pH 5.5. The observed membrane T_1 values are larger than the 20-22 msec observed for the α and β deuterons of the ethanolamine headgroup (see Chapter V of this work), but are not unexpected for methyl groups. The T_1 for the choline methyl groups of DPPC is 85 msec (125).

III.3 Conclusions

We have studied the interaction of deuterated tetracaine and procaine with semisynthetic egg PE. The anesthetics are observed to exist in only two environments, strongly bound in the membrane and free in solution. The former is characterized by a Pake doublet and the latter by a narrow line. The exchange of anesthetic between the two sites is very slow on the ^2H NMR time scale. The evidence indicates that tetracaine penetrates more deeply into the PE bilayer than does procaine.

There is no significant pH dependence of the quadrupole splittings of TTC, indicating a constancy in the depth of bilayer penetration. This is not surprising if one considers the TTC-PE interaction in terms of their molecular shapes (2, 3). Egg PE, because of the small cross-sectional size of the headgroup relative to the chains, has the shape of a cone. Tetracaine, and procaine to a lesser extent, act as wedges when they insert into the bilayer. It is this shape dependence which is suggested to be the cause of the anesthetic's ability to stabilize PE bilayers against a transformation to a hexagonal structure (107). Therefore, it is not the charge, but the general wedge shape of TTC (which is determined by the aromatic ring and the butyl chain) which dictates the depth of penetration, and this will be essentially independent of pH.

In the TTC-PC system (58, 59, 61) the PC molecules have an essentially cylindrical shape, due to their larger headgroup. Therefore, the shape of the anesthetic will have less influence on the depth of penetration. Rather, it is the presence of the TTC charge and its interaction with the PC headgroup which appears to govern the anesthetic location. This gives rise to the strong pH dependence for the TTC quadrupole splittings observed in egg PC.

This molecular shape theory may also account for the apparently slow exchange of TTC from the strong binding site of the PE bilayer to the solution. The PE bilayer is stabilized by the presence of the TTC and thus is likely, for thermodynamic reasons, to bind TTC more strongly than the corresponding PC.

The significant difference found for the interaction of TTC and PRC with PE versus PC or PS, as determined by ^{2}H NMR, is rather interesting. In view of the known preference of PE for the intracellular side of many biological membranes (103, 104) and the observed increase in effectiveness of amine anesthetics applied to the inside surface of the nerve (10, 17, 18), one is tempted to speculate on a TTC-PE interaction as an element in the mechanism of anesthesia. A recent paper on the effect of tetracaine, procaine and dibucaine on the topology of rat brain synaptosomes demonstrated a greater perturbation of PE than PS (126).

This preferential interaction of local anesthetics with phosphatidylethanolamines represents an interesting alternative to the other lipid mechanisms of anesthesia and will be explored further in Chapter VI with studies of labelled PE's.

CHAPTER IV

THE INTERACTION OF SPECIFICALLY DEUTERATED TETRACAINES AND PROCAINES WITH PHOSPHATIDYLCHOLINE

IV.1 Introduction

In the preceding chapter the binding of specifically deuterated procaines and tetracaines to phosphatidylethanolamine was studied by ^2H NMR. The anesthetics were found to be in slow exchange ($< 10^3\ s^{-1}$) between a strongly bound site and free in solution. The bound site was characterized by a Pake doublet while the free anesthetic gave rise to a narrow line. The areas of these two components are in direct proportion to the concentrations predicted from the partition coefficients.

With a clear example of anesthetics in slow exchange, the binding of labelled tetracaine and procaine to egg phosphatidylcholine has been reexamined. In earlier work (58, 59) a three-site model was proposed in which tetracaine was in slow exchange between strongly and weakly bound sites, while there was fast exchange between the weakly bound site and free tetracaine in solution. Later work (61), on the effect of attaining a true equilibrium, showed that repeated freeze-thaw- vortex cycles eliminated the quadrupole patterns observed for PRC-d_4 and TTC-d_6 at most pH values (see Figure 11 for structures of labelled PRC and TTC). It was suggested

that only a two-site, fast exchange model was needed to explain the results and that the observed quadrupole patterns arose from improper equilibration. The quadrupole pattern was thought to arise from anesthetic in fast exchange between a large amount of lipid and a very small amount of water.

In this study we report the results of a ^2H NMR study of the interaction of labelled tetracaines and procaines with egg PC. Spectral line shapes were found to be very dependent on the attainment of a proper equilibrium. However, many of the tetracaine labels still showed a quadrupole pattern after the equilibrium was reached. The tetracaine exchange in egg PC was examined using temperature and dilution studies, and the results confirm the three-site exchange model for tetracaine, proposed earlier (58, 59). An exchange rate of approximately 1.5×10^3 sec^{-1} is predicted for the slow exchange. This is sufficient to average the narrow splittings (< 1 kHz), but is insufficient to average the wider splittings (> 1.8 kHz).

IV.2 Results and Discussion

Effect of Freeze-Thaw Cycles

The ^2H NMR spectra of TTC-d_6, TTC-d_2, TTC-d_3 and PRC-d_2 were studied as a function of the sample preparation. Samples were run after one minute of vortexing and then, again, after

from 5 to 20 freeze-thaw-vortex cycles. Substantial changes were noted for all labels; however, after 7 freeze-thaw-vortex cycles the spectra were insensitive to further manipulation of the sample. For samples containing more than 250 mg of egg PC in 1 mL of BPC buffer, 10 freeze-thaw-vortex cycles were required.

For TTC-d_6 at pH 9.5, a small quadrupole splitting of 885 Hz was observed which disappeared after freeze-thawing (see Figure 22), in agreement with the observation of Westman et al. (61). However, at pH 5.5, freeze-thawing could not remove the quadrupole pattern of TTC-d_6, even after 17 freeze-thaw-vortex cycles. Freeze-thawing did, however, increase the amount of signal giving rise to the quadrupole pattern. The quadrupole splitting of 1.8 kHz is in good agreement with earlier results in egg PC (58, 59, 61) and almost identical to the 1.85 kHz found for TTC-d_6 in egg PE.

Samples of TTC-d_2 showed quadrupole patterns both before and after freeze-thawing, although the general line shape and the ratio of narrow line to quadrupole pattern changed substantially. For TTC-d_2, at pH 9.5 (Figure 23) freeze-thawing causes an increase in the proportion of signal due to the quadrupole pattern and a decrease in the linewidth of the narrow component.

The increase in the intensity of the quadrupole patterns, observed after freeze-thawing, for TTC-d_2 at pH 5.5

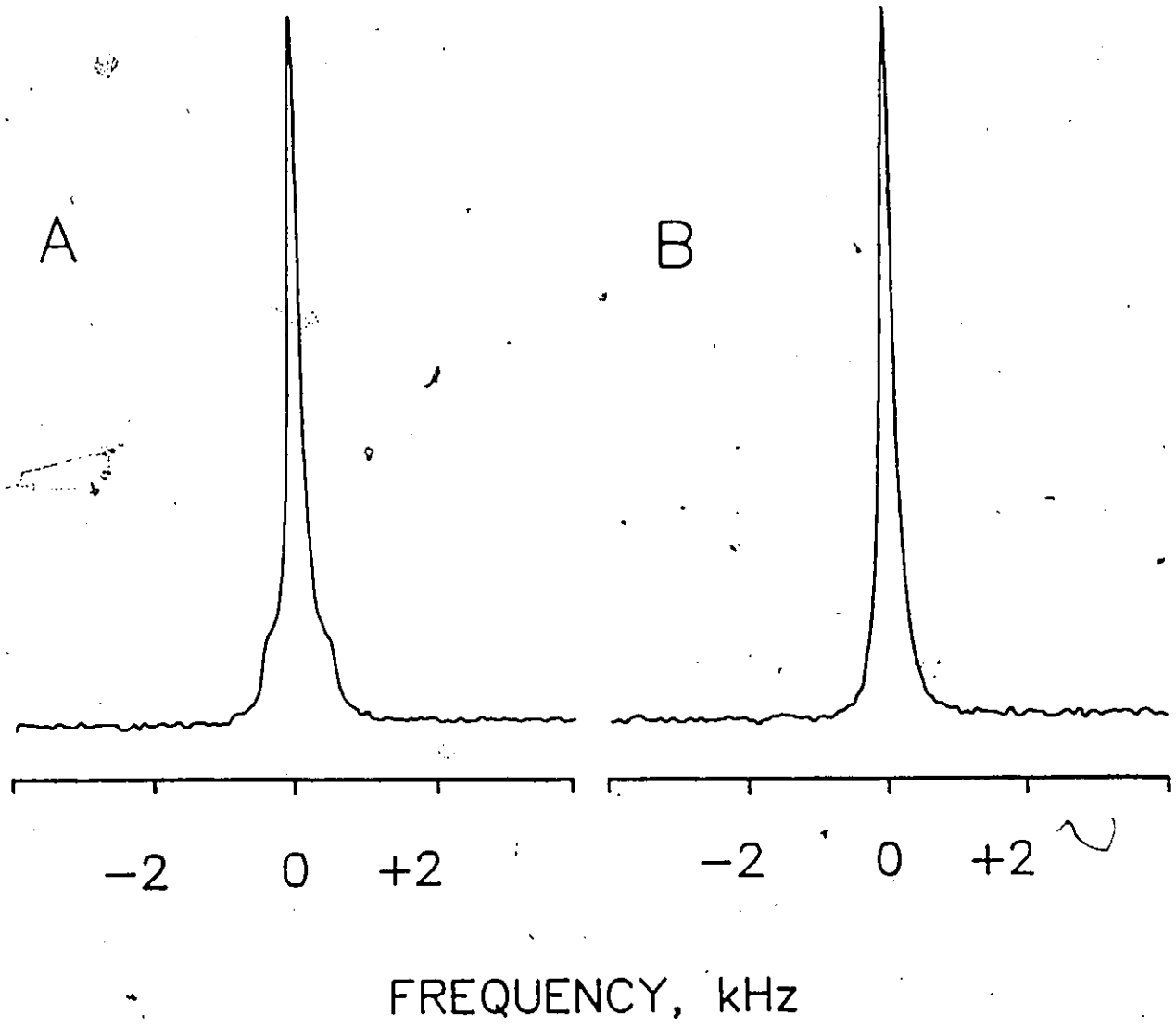

Figure 22. ^{2}H NMR spectra of TTC–d_6 (13 mM) in egg PC (130 mM) and 1.0 mL of BPC buffer (pH 9.5) after A) 1 minute of vortexing and B) 5 freeze–thaw–vortex cycles.

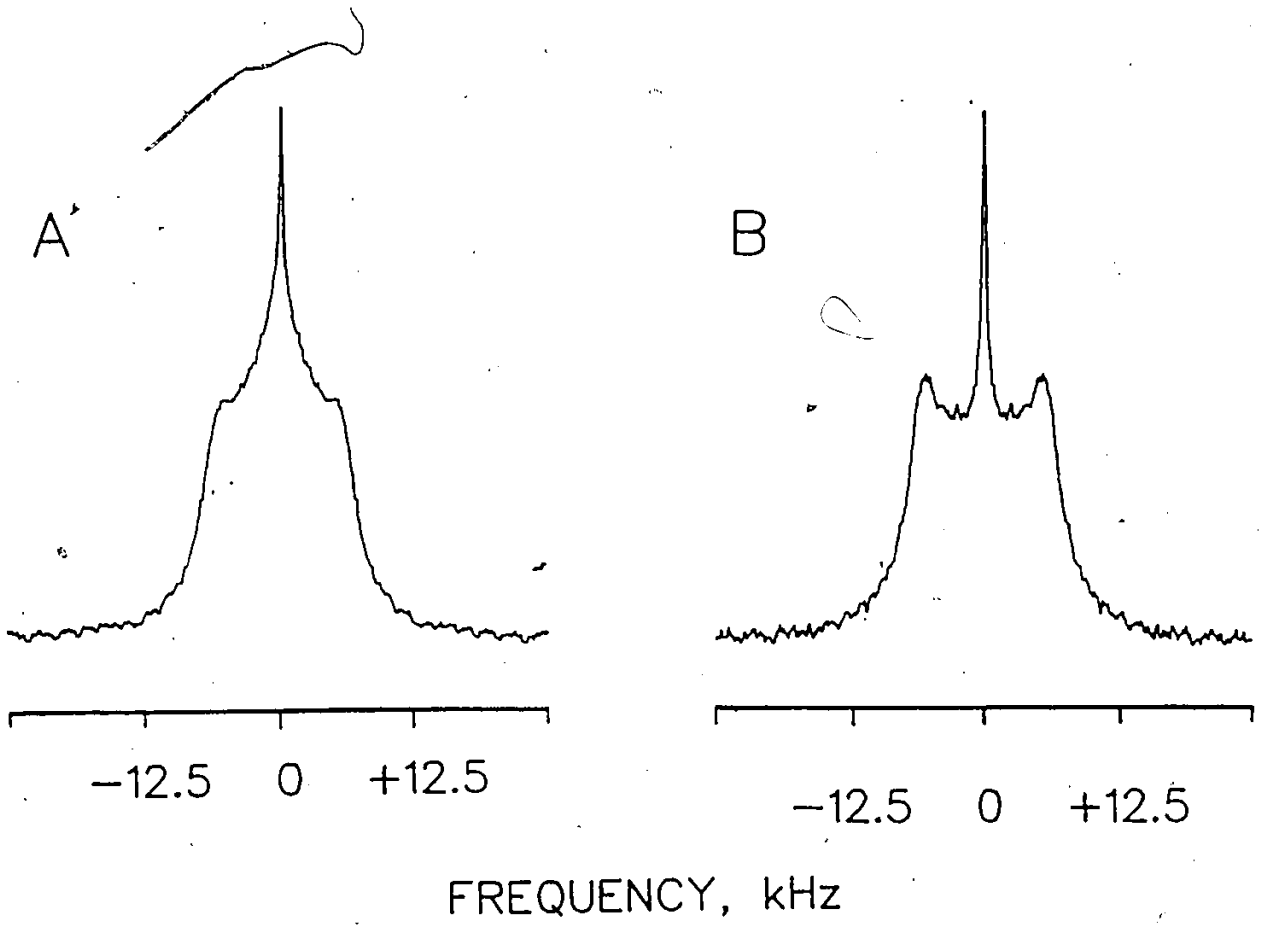

Figure 23. ^{2}H NMR spectra of TTC-d_2 (165 mM) in egg PC (323 mM) and 1.0 mL of BPC buffer (pH 9.5) after A) 1 minute of vortexing and B) 10 freeze–thaw–vortex cycles.

and pH 9.5 and TTC-d_6 at pH 5.5 results from a better equilibrium of tetracaine between lipid and water. Freeze-thawing has been observed to give liposomes of a smaller, more uniform size (61). While these liposomes are not small enough to cause averaging of the quadrupole interaction (49), the smaller size does allow a better equilibrium of anesthetic. Under these conditions, more TTC can partition into the lipid, increasing the intensity of the quadrupole pattern. This increase in the bound proportion of tetracaine, with freeze-thawing, has also been detected by a light absorption study (61).

The quadrupole splittings for TTC-d_2 at pH 5.5 and 9.5 and TTC-d_6 at pH 5.5 are summarized in Table 8. Quadrupole splittings of TTC-d_9, which has the butyl group deuterated, are also reported. The splittings for the α, β and γ positions are visible; however, the exchange rate averages the δ position (TTC-d_3).

For all of the procaine samples, at both pH 5.5 and 9.5, freeze-thawing eliminates the quadrupole patterns and only a narrow resonance remains. This is in contrast to the studies of procaine in egg PE (Chapter III), where PPR-d_2 at pH 5.5 and 9.5 shows quadrupole splittings of 9.2 and 11.4 kHz respectively.

Table 8

QUADRUPOLE SPLITTINGS FOR DEUTERATED TETRACAINE IN EGG PHOSPHATIDYLCHOLINE (IN kHz)[a]

		pH 5.5	pH 9.5
TTC-d_6		1.8	b
TTC-d_2		14.4	15.2
TTC-d_9	α	12.9	13.0
	β	8.8	8.8
	γ	6.8	7.0
	δ	b	b
TTC-d_3		b	b

a All spectra show a narrow central resonance.
b No quadrupole splitting was observed, only a narrow resonance.

Investigation of Anesthetic Exchange

For a deuterated anesthetic exchanging between a bound site, in an oriented phase, and free in solution, the observed ^2H NMR spectrum will depend on two factors. The first is the rate of exchange between the two sites and the second is the extent of partitioning of the anesthetic between the two phases (58, 127, 128). For the exchange rate to be slow on the ^2H NMR time scale, the lifetime of the anesthetic (t) must be

$$t >> \frac{1}{\Delta\nu_Q - \Delta\nu_{1/2}} \simeq \frac{1}{\Delta\nu_Q} \qquad (16)$$

where $\Delta\nu_Q$ is the quadrupole splitting arising from the bound lipid and $\Delta\nu_{1/2}$ is the linewidth of the free anesthetic signal. In this slow exchange regime, two separate resonances will be observed. This is the situation found for tetracaine and procaine in egg PE.

For fast exchange ($t << 1/\Delta\nu_Q$) there will be an averaging of the two signals to give a reduced quadrupole splitting, $\Delta\nu_{QR}$

$$\Delta\nu_{QR} = x_1\Delta\nu_Q + x_2\Delta\nu_{1/2} \qquad (17)$$

where x_1 and x_2 are the mole fractions of anesthetic in the lipid and water phases. For the case of intermediate exchange

($t \cong 1/\Delta\nu_Q$) a very complicated lineshape can be expected (58, 127).

In order to explore more fully the exchange of tetracaine between egg PC and water, we have performed both variable temperature and dilution studies. These studies were done at both pH 5.5 and 9.5 and with both TTC-d_6 and TTC-d_2. Because of the order of magnitude difference in their quadrupole splittings (see Table 8), these two labels will help to provide an estimate of the exchange rates.

Figure 24A shows the spectrum of TTC-d_6, at pH 5.5 and 25°C, after 10 freeze-thaw-vortex cycles. The spectrum shows 2 components; a quadrupole pattern with a width of 1.8 kHz and a central resonance with a linewidth of approximately 600 Hz. This central resonance is considerably broader than the 60-70 Hz noted for TTC-d_6 in egg PE and the quadrupole pattern lacks the well defined line shape found in the egg PE studies. The central resonance is also considerably more intense than would be expected from the partition coefficient of $K_p = 22$.

Dilution of the TTC-d_6 sample with BPC buffer (Figure 24C and D) causes the proportion of the signal due to the quadrupole pattern to decrease, with no decrease in the quadrupole splitting. Concomitantly, the central resonance increases in intensity, but the linewidth of the central

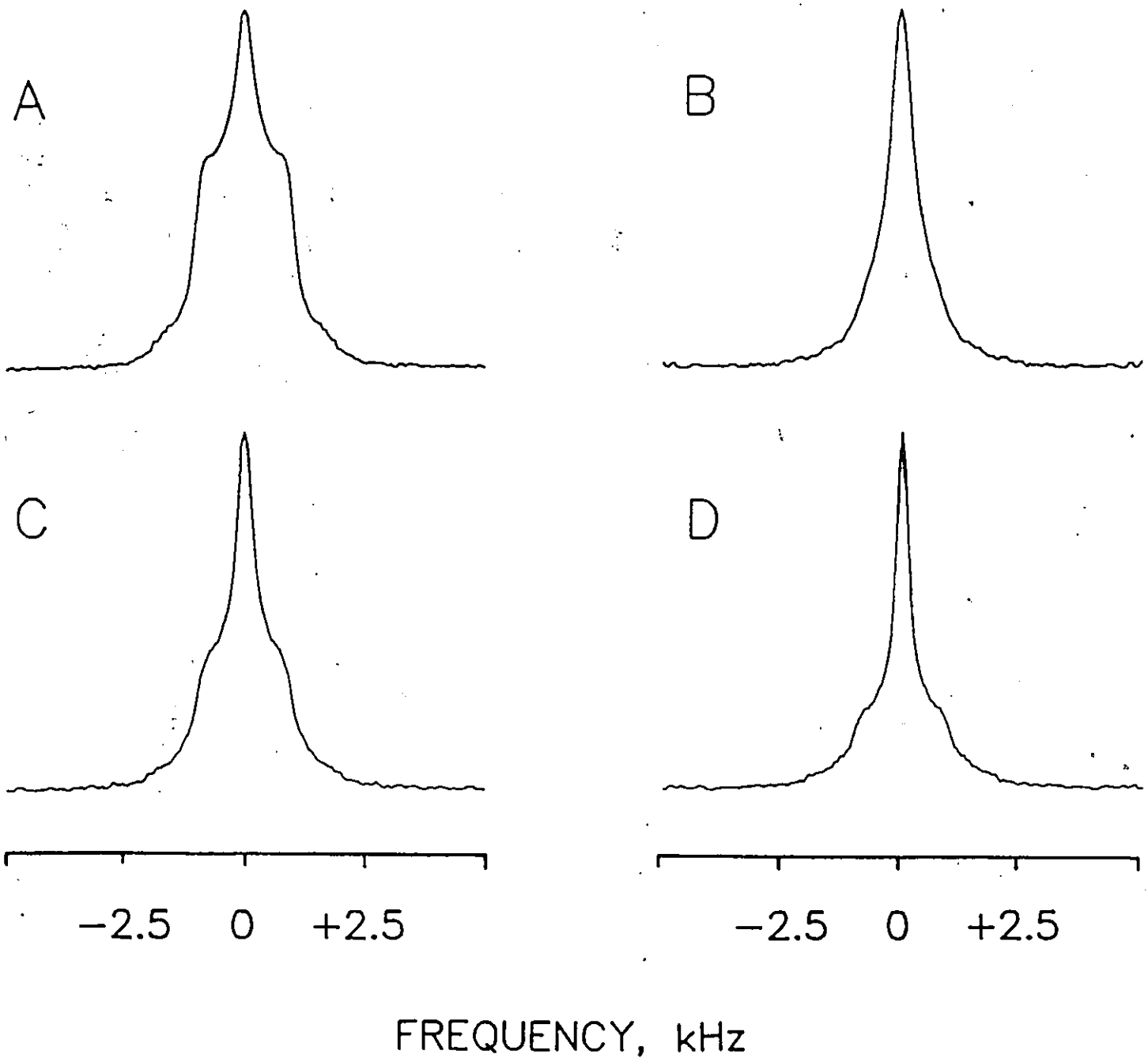

Figure 24. ^{2}H NMR spectra of TTC–d_6 in egg PC at pH 5.5. A) TTC–d_6 (18 mg) in egg PC (250 mg) and 1 mL of BPC buffer after 15 freeze–thaw–vortex cycles. B) same as A, but at 60°C. C) sample A plus 1 mL of BPC buffer. D) sample C plus 1 mL of BPC buffer.

resonance decreases, in complete agreement with earlier work (58, 59).

The original sample of TTC-d_6 (Figure 24A) was also heated to observe the effect of temperature on the anesthetic exchange. On heating to 60°C the quadrupole pattern completely collapsed to a single broad line of approximately 600 Hz in width (Figure 24B). Cooling to 25°C yielded the original spectrum, with the intensities of the components unchanged.

Dilution studies on TTC-d_2, at pH 5.5 and 9.5, gave identical results and the presence of extra signal in the central resonance was very pronounced, especially at high pH. At pH 9.5, and 25°C, the partition coefficient is 660, so that greater than 99% of the tetracaine should be in the lipid. Temperature studies of TTC-d_2 at pH 9.5 (Figure 25) and pH 5.5 (Figure 26) shows that even at 60°C the quadrupole patterns have not completely collapsed. (The patterns do sharpen up slightly because of a longer T_{2e}; see Figure 15.) The quadrupole patterns are narrower; however, this is primarily a result of increasing disorder. This is analogous to the effect of temperature on the quadrupole splittings of specifically deuterated stearic acid in egg PC (49).

At low temperatures, the line shape of the TTC-d_2 samples is extremely distorted (Figure 25A). This is not

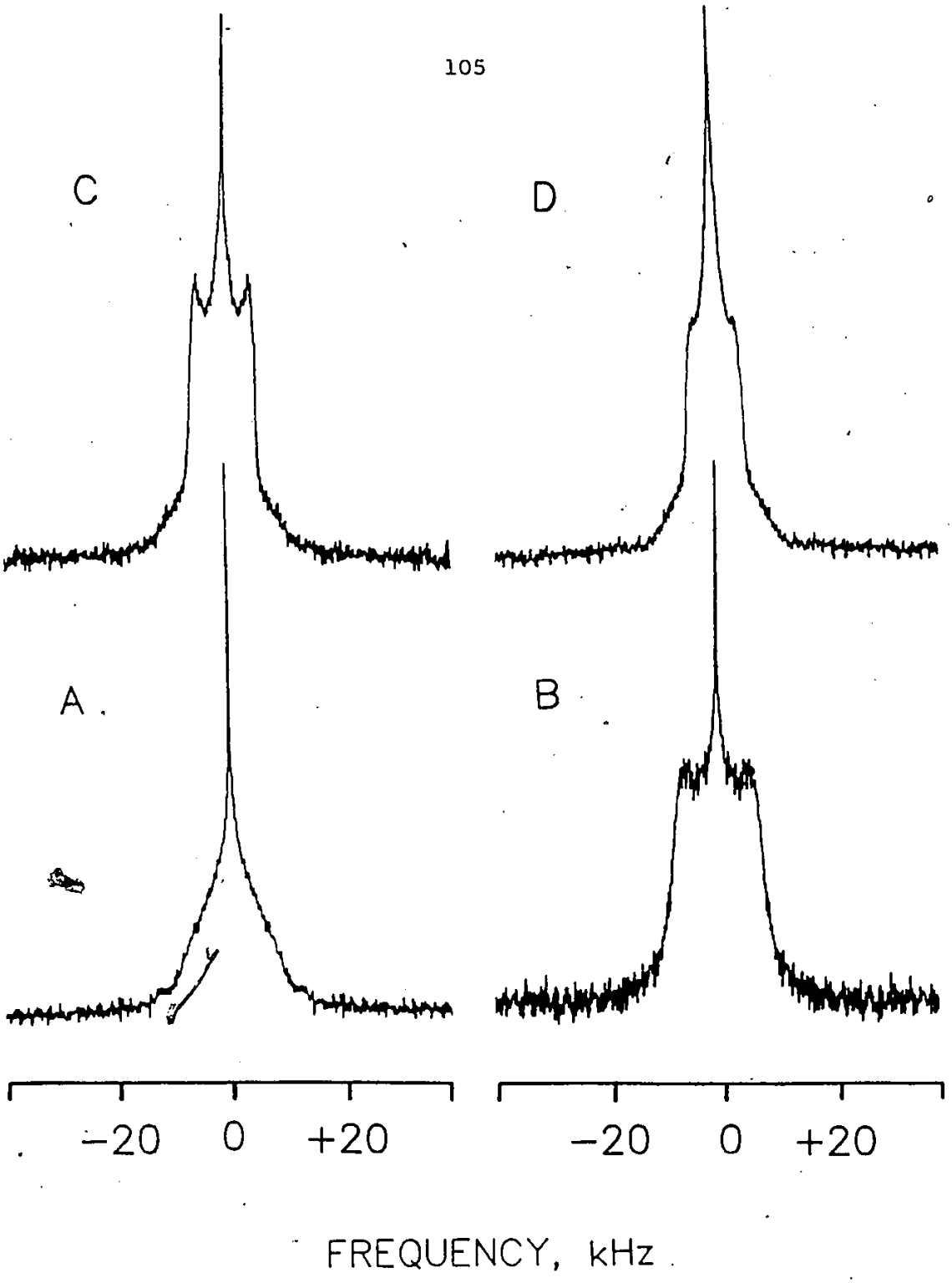

Figure 25. ^{2}H NMR spectra of TTC-d_2 (143 mM) in egg PC (320 mM), at pH 9.5 and A) 4°C , B) 24°C , C) 52°C , D) 67°C.

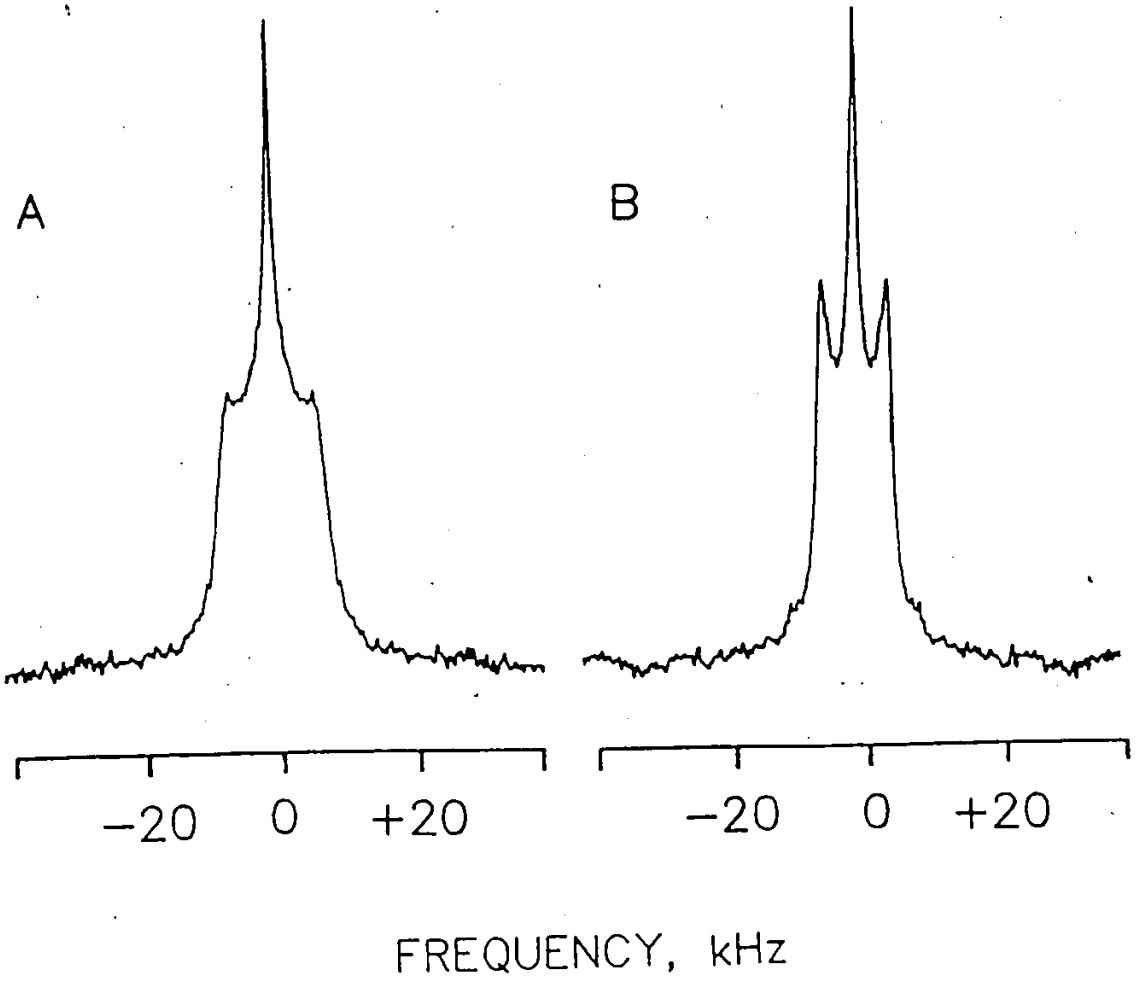

Figure 26. ^{2}H NMR spectra of TTC-d_2 (160 mM) in egg PC (315 mM) at pH 5.5 and A) 25°C , B) 60°C .

an effect of exchange, but rather a result of the short T_{2e} of the aromatic deuterons (100-150 μsec for TTC-d_2 in egg PE). As the temperature is lowered to 4°C, the T_{2e} will become shorter than the total echo pulse spacing of 120 μsec and this results in a substantial line shape distortion (119, 120, Chapter III of this work).

These experiments all serve to confirm the three-site model for tetracaine exchange, in egg PC, proposed earlier (58, 59). Tetracaine exchanges slowly between a strongly bound site and a weakly bound site, and quickly between the weakly bound site and free in solution. The need for two lipid bound sites arises from the lack of correspondence between the area calculated by ^2H NMR and those predicted from the partition coefficients. The partition coefficients predict much higher percentages of bound TTC than are found in the ^2H NMR spectra. In particular, at pH 9.5, the K_p is 660 which would result in greater than 99% of the tetracaine being bound. The narrow lines in the spectra are too intense to arise from only free TTC. The very low solubility of TTC in BPC buffer at pH 9.5 (58) also rules against the intensities. Clearly, the narrow line must arise from an exchange between a second, weakly bound site and free tetracaine in solution.

The slow exchange between a strongly bound site and a weakly bound site is confirmed by the dilution studies.

These studies change only the intensity of the quadrupole pattern, and not the magnitude of the quadrupole splitting. This behaviour is in agreement with the slow exchange requirements of Equation 16. The weakly bound site may only be a loose association at the lipid/water interface which would give rise to a narrow line, although broader than free tetracaine. Alternatively, the weak site may be in the bilayer, but have a low degree of order and, hence, a small quadrupole splitting. The fast exchange between the weakly bound site and free tetracaine manifests itself in the narrowing of the central resonance with increases in the amount of water added (Equation 17). The linewidth of the weakly bound species has been estimated to be 600 Hz from the dilution studies of Boulanger et al. (58, 59).

The magnitude of the slow exchange rate can be estimated from the temperature studies of TTC-d_2 and TTC-d_6. At room temperature, and pH 5.5, TTC-d_2 shows a more well resolved quadrupole pattern than does TTC-d_6 suggesting an exchange rate of $\simeq 1.5 \times 10^3$ sec^{-1}. This means that TTC-d_6 experiences an intermediate exchange rate while for TTC-d_2, with its larger quadrupole splitting, the exchange rate only qualifies as slow (Equation 16). Increasing the temperature of the samples confirms this assignment. At 60°C the TTC-d_6 sample now shows only a broad line, indicative of a faster exchange regime, while TTC-d_2 still shows a

spectrum consistent with a slow to intermediate exchange rate (Figure 26B). Thus, at 60°C, the exchange rate must increase to between 1.8×10^3 s^{-1} and 10×10^3 s^{-1}.

At pH 9.5 the spectra are consistent with a slightly faster exchange rate for tetracaine. The TTC-d_6 sample shows only a narrow line, which even on cooling to 1°C fails to resolve a quadrupole pattern. For TTC-d_2 at 52°C and 67°C the spectra show more averaging than the corresponding pH 5.5 spectra, suggesting a slightly faster exchange rate at pH 9.5.

In the earlier work, where freeze-thawing was not always performed, local domains existed where some anesthetic was in exchange between a large amount of lipid and a small amount of water (61). This biased the exchange in favour of the strongly bound site, resulting in quadrupole patterns being observed for all labels, even those which are normally averaged by exchange. Clearly, many portions of the tetracaine molecule, in egg PC, exist in areas of very low order and have splittings less than 1 kHz (TTC-d_3 at pH 5.5 and 9.5 and TTC-d_6 at pH 9.5). The slow exchange rate of 1.5×10^3 sec^{-1} is thus sufficiently fast to cause averaging of these splittings once a proper equilibrium is restored. These small quadrupole splittings, observed with incomplete equilibration in earlier work represent the signal from the strongly bound site.

For all of the procaine labels, freeze-thawing eliminated the quadrupole splittings resulting in only narrow lines. This is partly the result of the small partition coefficients for procaine in egg PC which biases the exchange in favour of water. It is also a result of a much faster exchange rate between bound PRC and free PRC. (There is probably only one bound site.) The bound procaine is in a site of much lower order in egg PC than in the corresponding PE. Quadrupole splittings for labelled procaine are less than 2 kHz in the poorly equilibrated PC samples (these splittings would correspond to bound PRC), while PRC-d_2 gives large (~10 kHz) splittings in egg PE.

Characterization of the Strong Binding Site

With the attainment of a proper equilibrium the quadrupole splittings still show a much greater dependence on pH than was observed in the PE studies. In particular, the TTC-d_6 samples show a strong pH dependence with egg PC, indicating that the tetracaine adjusts its position in the PC bilayer to accommodate the charge (58, 59). At pH 9.5, when uncharged, the tetracaine probably sinks lower into the bilayer, while at pH 5.5 the charged dimethylamino group is level with the trimethylamino moiety of PC. This tetracaine location in PC bilayers appears to be confirmed by the effect of tetracaine on deuterium labelled phosphatidylcholines (60).

The absence of quadrupole splittings of greater than 1 kHz for TTC-d_3 and the reduced splittings observed for TTC-d_9 in egg PC, relative to egg PE is quite interesting, and can be rationalized in terms of molecular shapes (2, 3). Egg PC has an approximately cylindrical shape because the cross sectional area at the headgroup is similar to that of the chains. When tetracaine is inserted into the bilayer it pushes neighbouring PC molecules apart. The large cross section of the aromatic ring results in there being substantial room for the butyl group of tetracaine. This results in chain motions which reduce the splittings for the deuterons on the butyl group. These splittings are considerably smaller than those of the PC chains in the plateau region (60). The TTC-d_9 splittings, in PC, are also smaller than those observed in the corresponding PE (Chapter III). Phosphatidylethanolamine has a cone shape due to its smaller headgroup and the TTC molecule acts as a wedge in this PE bilayer. When tetracaine acts as a wedge, the butyl chain is in a much more constrained environment and the resulting quadrupole splittings are larger. Since both this study and the PE work in Chapter III were done on lipids with the same fatty acid distributions, the observed differences are due to the effect of the headgroup on the molecular shape.

Finally, since the PC molecules have a cylindrical shape, the aromatic moiety of tetracaine should experience

greater order in PC than in PE, where the wedge shape is important. This is, in fact, what is observed to occur. TTC-d_2 in egg PC at both pH 5.5 and 9.5 has quadrupole splitting 10% to 15% greater than in PE, even though the PE bilayer is more ordered in the plateau region (117, 118).

IV.3 Conclusions

We have studied the interaction of several specifically deuterated tetracaines and procaines with egg PC. The ^2H NMR line shapes were found to be very dependent on the attainment of a true equilibrium. The tetracaine is observed to follow the three-site model proposed earlier (58, 59). Tetracaine is in slow exchange between a strongly and a weakly bound site and in fast exchange between the weakly bound site and free in solution. At pH 5.5 the slow exchange rate is approximately 1.5×10^3 s^{-1}, while at pH 9.5 this rate is slightly faster.

The quadrupole splittings observed for labelled TTC appear to be dependent on the anesthetic charge. Since the molecular shape of PC is cylindrical, the depth of penetration of the tetracaine is dependent on the TTC charge. This is in contrast of studies in PE where the anesthetic acts as a wedge, and it is this wedge shape, not the charge, which governs the anesthetic location in PE.

CHAPTER V

THE INFLUENCE OF TETRACAINE AND PROCAINE ON PHOSPHATIDYLETHANOLAMINE BILAYERS

V.1 Introduction

The studies of specifically deuterated tetracaine and procaine in egg PE, reported in Chapter III, provide a clear example of an anesthetic in slow exchange between a bound and a free site. The experiments also indicate a depth of anesthetic penetration into the bilayer which is independent of the charge on the anesthetic. The only apparent dependence on anesthetic charge is in the observation of a strong angular-dependent linewidth, when TTC is in its charged form, while uncharged TTC shows an angular independent linewidth. This strong angular dependence can be correlated with a slow diffusion of TTC over a surface of finite curvature, while the angular independent linewidth, found at high pH, suggests a faster lateral diffusion.

The results in PE are in sharp contrast to the work on labelled TTC in egg PC, reported in Chapter IV and in earlier studies by Boulanger et al. (58, 59). Tetracaine is observed to exist in three sites; strongly bound in the membrane, weakly bound in a site of low order and free in solution. The location of the strong binding site for TTC

in the PC bilayer has also been studied, by observing the effect of TTC on the ^{2}H NMR spectra of specifically labelled DPPC's (60). This work showed a strong pH dependence to the anesthetic location. At low pH, when TTC is charged it sits high in the bilayer with the charge interacting with the PC headgroup. However, at high pH, when TTC is uncharged it is able to intercalate more deeply into the bilayer. A similar location for procaine, in egg PC/cholesterol bilayers, has been suggested from x-ray diffraction results (114). The local anesthetic benzyl alcohol has also been observed to disorder the acyl chains of specifically deuterated DMPC. This indicates a hydrocarbon environment for the benzyl alcohol binding location (130).

In order to explore more fully the interaction of TTC with PE bilayers, specifically labelled DMPE's were prepared. The DMPE's were specifically deuterated in the ethanolamine headgroup (3-[1', 2'-$^{2}H_{4}$]DMPE), on the 1 chain (1-[2'-$^{2}H_{2}$] DMPE) and on the 2 chain (2-[2'-$^{2}H_{2}$]DMPE, (2-[4', 14'-$^{2}H_{5}$] DMPE). These DMPE's were mixed 1:1 with the semisynthetic egg PE or bovine PS and the influence of TTC and PRC on the ^{2}H and ^{31}P NMR spectra were studied. The addition of a natural lipid ensured a fatty acid distribution more comparable with the work on labelled TTC and PRC in PE (Chapter III). It also results in a lower gel-liquid crystal phase transition, enabling the experiments to be performed at a

lower temperature, where the exchange rate is slower. As in the earlier work, experiments were performed at both pH 5.5, when TTC and PRC are primarily charged, and at pH 9.5 when they are uncharged.

V.2 Results

Headgroup

The ^2H NMR spectrum of a multilamellar dispersion of 3-[1', 2'-$^2H_4$]DMPE, above its phase transition of 53°C, shows two quadrupole splittings of 10.4 and 4.3 kHz. These quadrupole splittings are similar to those observed for specifically labelled DPPE and are assigned to the deuterons adjacent to the oxygen (α) and the deuterons adjacent to the nigrogen (β) respectively (131). When mixed 1:1 with the semisynthetic egg PE the phase transition temperature is lowered to approximately 35°C. The ^2H NMR spectrum of this mixture, at 40°C, showed only liquid crystal phase and quadrupole splittings of 10.5 and 4.4 kHz at pH 5.5 and 10.6 and 4.3 kHz at pH 9.5 (see Figure 27 for the location of the deuterium labels and the ^2H NMR spectrum). The consistent nature of these quadrupole splittings with variations in the pH and the type of fatty acid indicates that the orientation of the headgroup is essentially unchanged over the pH range and fatty acid mixtures used.

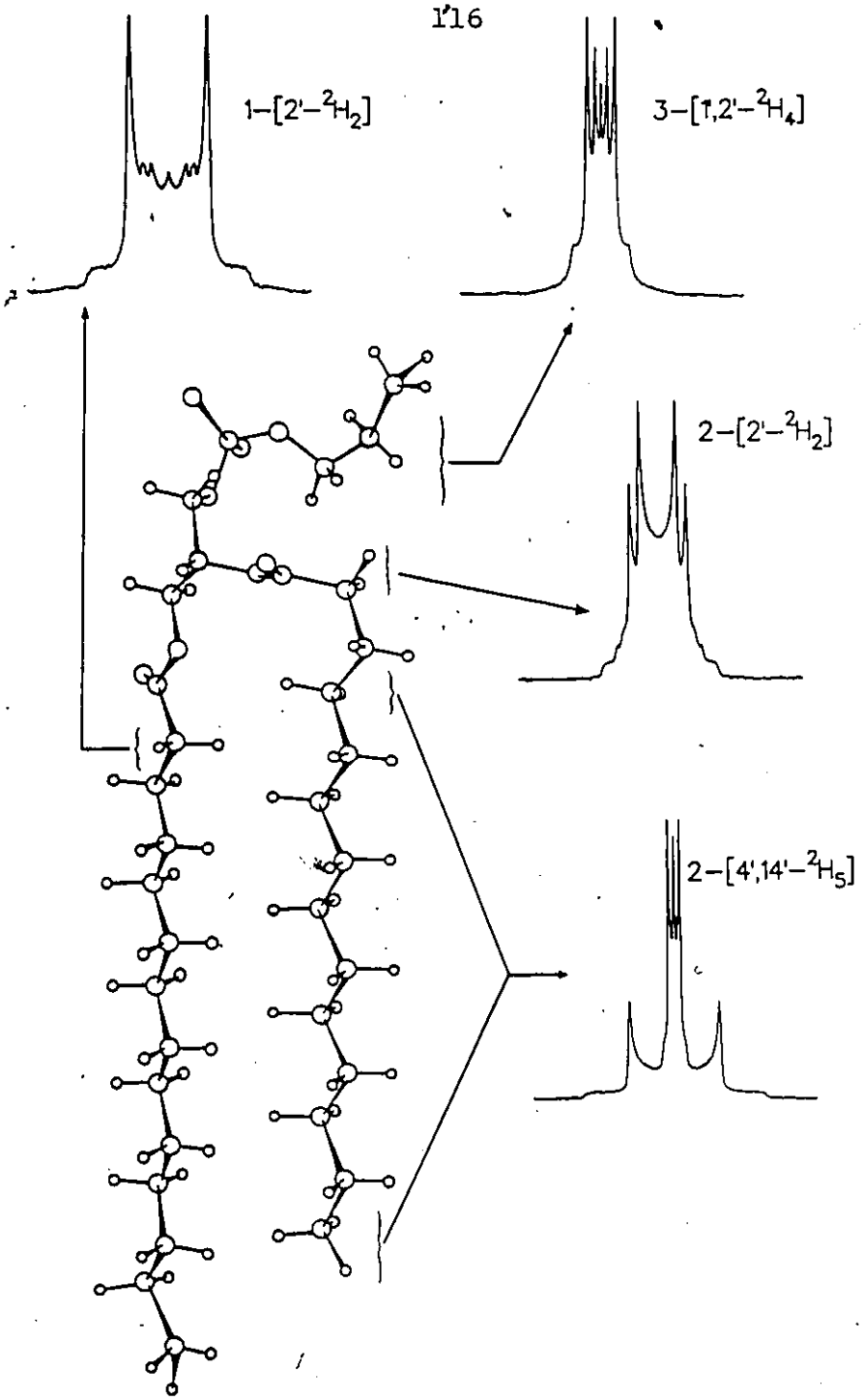

Figure 27. Spectra of labelled DMPE's, at pH 5.5 and 40°C, in a 1:1 mixture with egg PE. Each spectrum is 100 kHz in width.

The addition of tetracaine and procaine to the PE dispersion causes a decrease in the splitting of the α deuterons and an increase in the quadrupole splittings of the β deuterons. This suggests that a conformational change of the headgroup is occurring. Figure 28 shows the variation in quadrupole splittings, at pH 9.5 when TTC and PRC are added. The ratio of $[\text{Anesthetic}]_{\text{BOUND}}/[\text{Lipid}]$ is calculated from the amount of anesthetic, water, and lipid and the known partition coefficients (see Table 4). Therefore, the effect of equal amounts of TTC and PRC, bound in the lipid, can be compared directly.

Figure 29 shows the effect of TTC and PRC on the headgroup labelled, PE mixture at pH 5.5. At this low pH, TTC and PRC are primarily in their charged forms (59), but they show only a slightly greater effect on the PE bilayer than at pH 9.5, when the anesthetics are uncharged. At low TTC concentrations the ^2H NMR spectrum shows three superimposed quadrupole patterns: one from the β deuterons and two from the α deuterons (see Figure 30). Of the two splittings arising from the α deuterons, one is essentially unchanged from the neat PE sample, while the other has a substantially reduced quadrupole splitting. The assignment of the quadrupole splittings can be made from the integrated areas of the de-Paked spectra. With increased concentrations of TTC it is clear that the outer splitting, from the α deuterons,

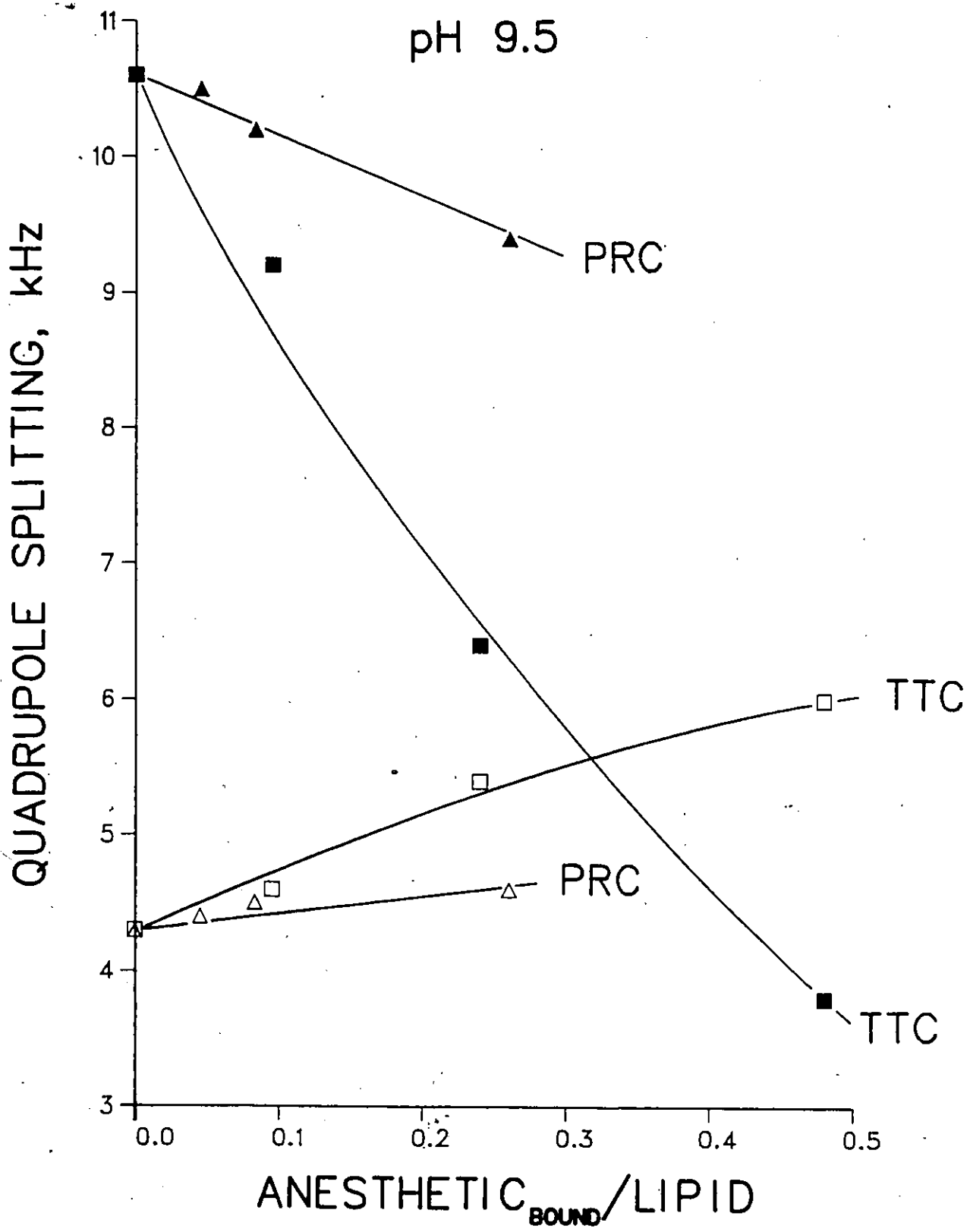

Figure 28. Variation of the quadrupole splittings of the headgroup labelled PE with the addition of TTC and PRC at pH 9.5. (▲) α deuterons with PRC,(△) β deuterons with PRC,(■) α deuterons with TTC,(□) β deuterons with TTC.

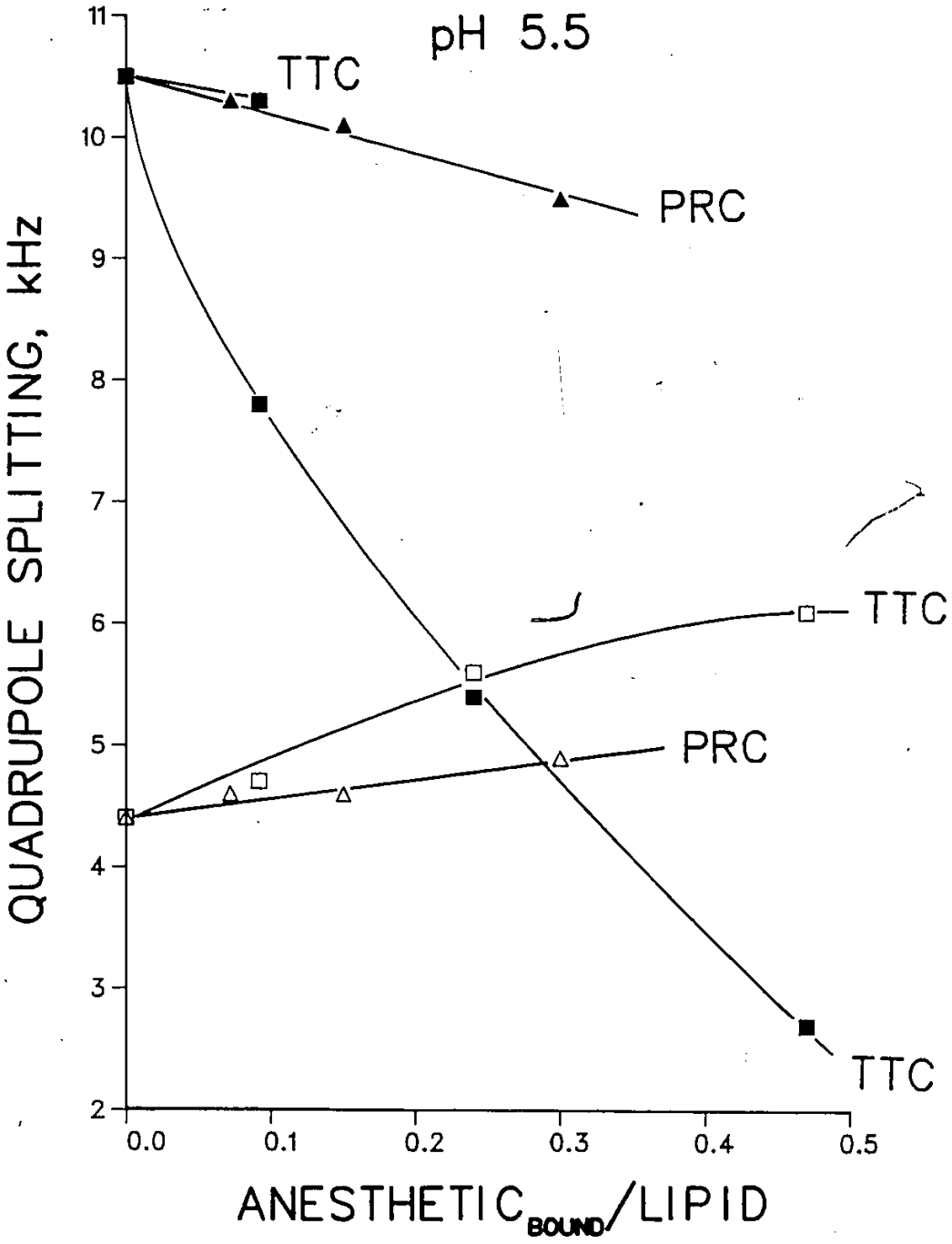

Figure 29. Variation of the quadrupole splittings of the headgroup labelled PE with the addition of TTC and PRC at pH 5.5. (▲) ∝ deuterons with PRC, (△) β deuterons with PRC, (■) ∝ deuterons with TTC, (□) β deuterons with TTC.

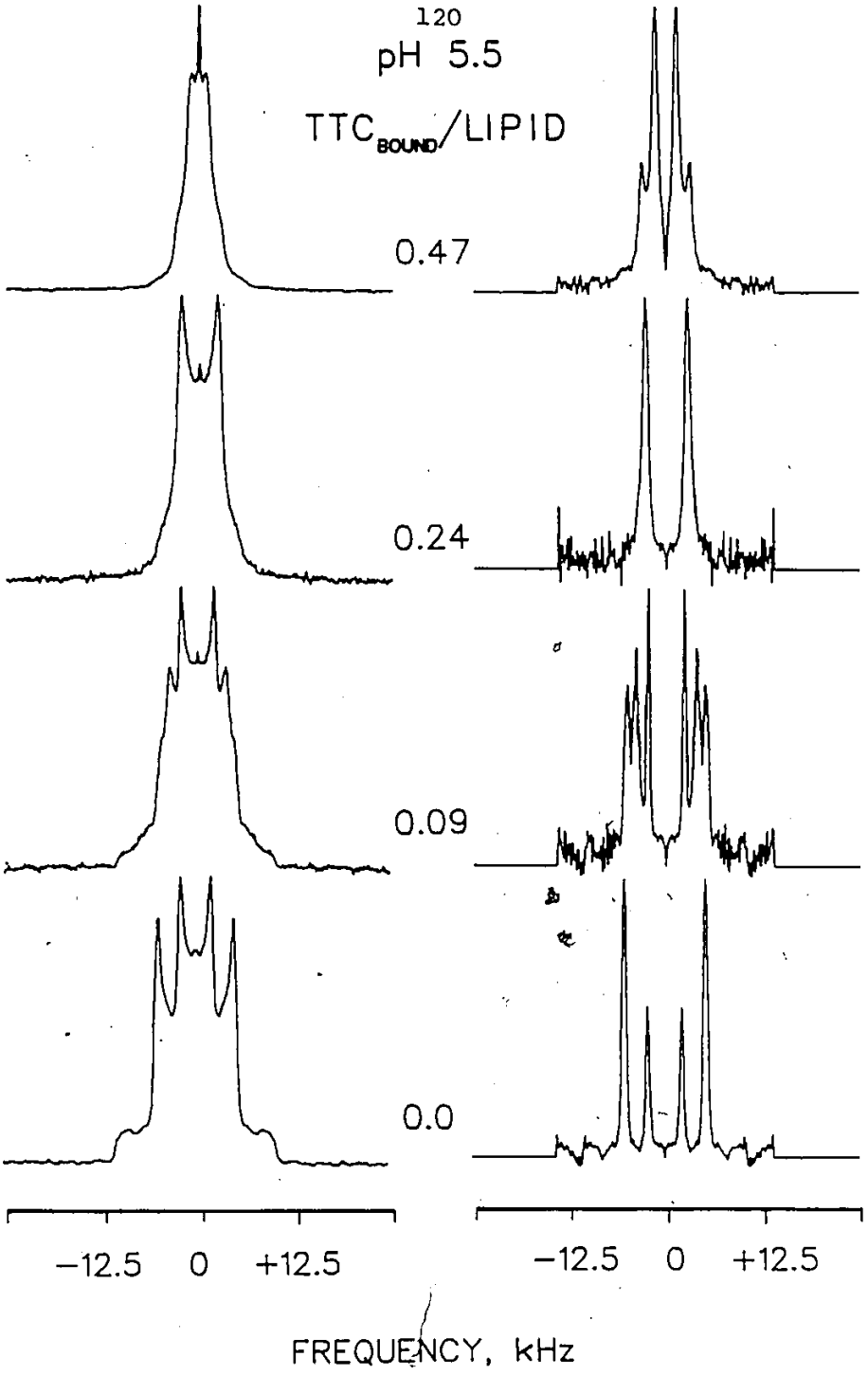

Figure 30. ^{2}H NMR spectra of a 1:1 mixture of 3-[1',2'-$^{2}H_4$] DMPE and egg PE, at pH 5.5 with varying amounts of TTC. The TTC$_{BOUND}$/LIPID ratio is indicated on the spectrum and the de-Paked spectra are shown on the right.

eventually disappears while the inner α-splitting experiences an increase in its intensity and a decrease in its quadrupole splitting. Concomitantly, the β deuterons show a more gradual increase in their quadrupole splitting, with added TTC. For the α deuterons, additions of very high concentrations of TTC (≈1/1) will ultimately cause the quadrupole pattern to reduce to a narrow line and then increase again, indicating a change in the sign of the quadrupole splitting.

Similar experiments were also performed on equimolar mixtures of the 3-[1', 2'-$^2H_4$]DMPE and bovine PS. Figures 31 and 32 show the effect of TTC and PRC on the quadrupole splittings of the labelled DMPE at pH 9.5 and 5.5 respectively. As in the PE experiments TTC showed a much more pronounced effect than PRC, and this effect was, again, only slightly greater at pH 5.5 than at 9.5. Also, there was no evidence for a third quadrupole splitting, as was observed in the neat PE experiments. The effect of the local anesthetics on DMPE/bovine PS mixtures is quantitatively similar to the reduction in quadrupole splittings observed in the DMPE/egg PE mixtures.

The spin lattice relaxation times of the α and β deuterons of the DMPE headgroup, at pH 9.5, were also measured. While the quadrupole splittings provide information on the amplitude of the anisotropic motion the spin-lattice relaxation times (T_1) can give information on the rates of these motions (122, 123). Addition of TTC (.1/1) resulted

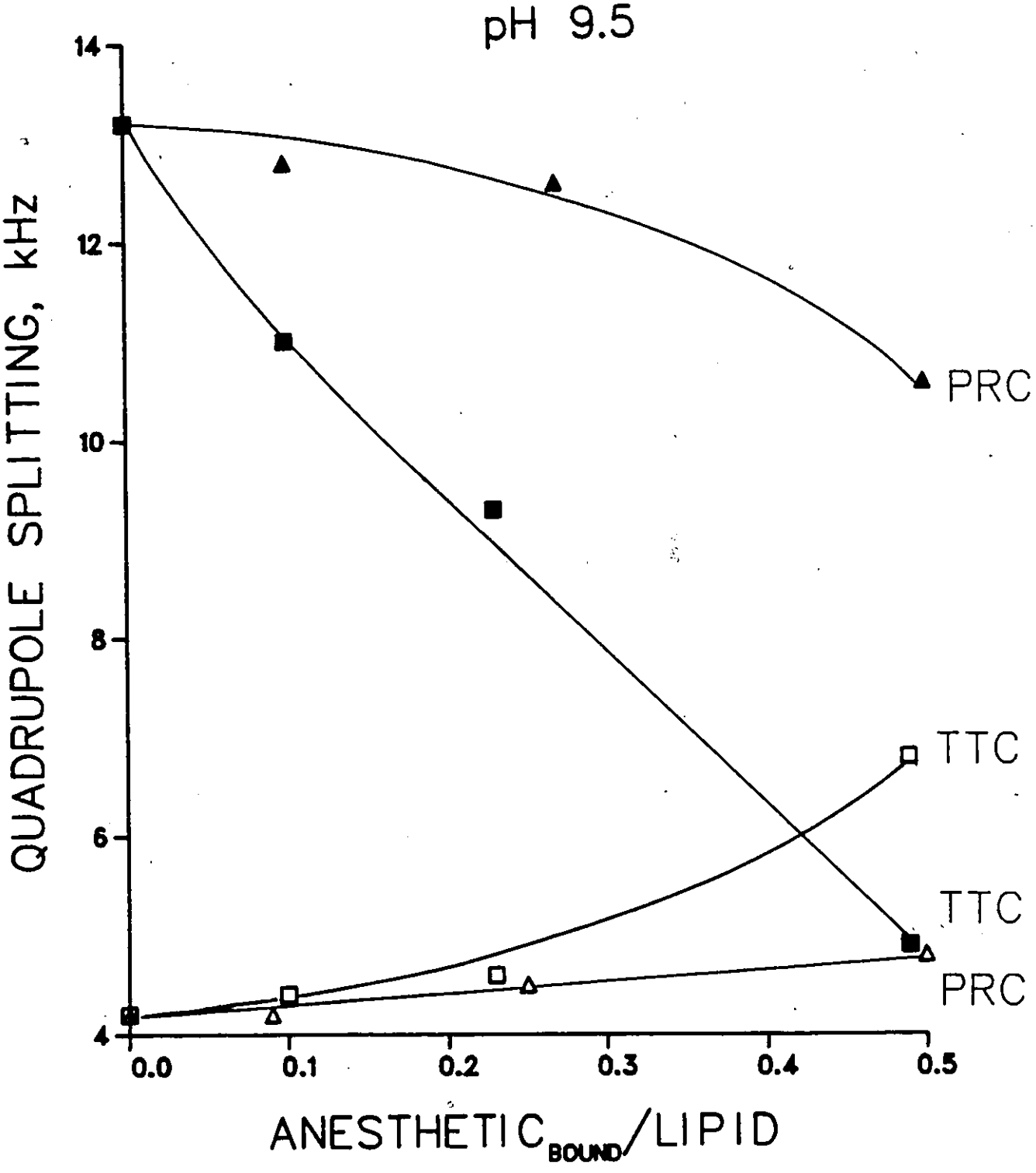

Figure 31. Variation of the quadrupole splittings of the headgroup labelled DMPE, in a 1:1 mixture with PS (at pH 9.5), as TTC and PRC are added. (▲) ∝ deuterons with PRC, (△) β deuterons with PRC, (■) ∝ deuterons with TTC, (□) β deuterons with TTC.

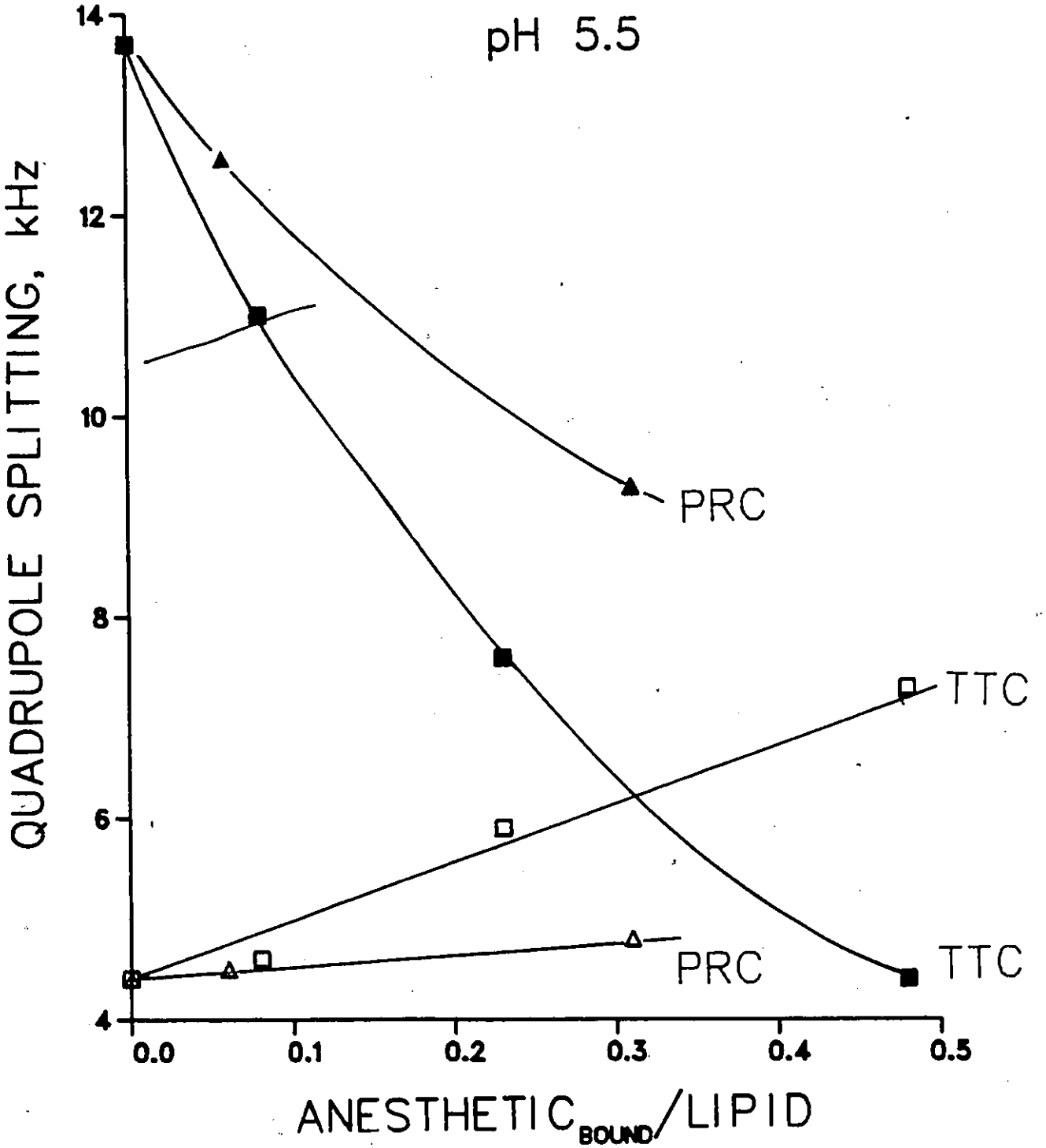

Figure 32. Variation of the quadrupole splittings of the headgroup labelled DMPE, in a 1:1 mixture with PS (at pH 5.5), as TTC and PRC are added. (▲) α deuterons with PRC, (△) β deuterons with PRC, (■) α deuterons with TTC, (□) β deuterons with TTC.

in only a small reduction (≈10%) of the T_1's (see Table 9), while PRC, at a .05/1 ratio, showed no significant effect. At PRC/PE ratios of .25/1 the T_1's were reduced, but by less than 10%. Clearly then, the rates of motion of the headgroup are not significantly effected by the addition of anesthetics.

The ^{31}P NMR of the semisynthetic egg PE, with and without anesthetics were also recorded. The spectra at both pH's, and at all concentrations studied, showed only ^{31}P patterns characteristic of bilayer structures. Addition of anesthetic results in an increase in the absolute magnitude of the ^{31}P chemical shielding anisotropy (see Table 10). This increase in the CSA is much more pronounced for TTC than PRC. Figure 33 shows the ^{31}P NMR spectra of egg PE at pH 5.5, with and without TTC. The small signal at the centre of the pattern is due primarily to the BPC buffer, but at high anesthetic concentrations this signal grows slightly in intensity. This is likely a consequence of the formation of a small percentage of small vesicles. The formation of a small isotropic component is also evident in the ^{2}H spectra at high anesthetic concentrations.

Hydrocarbon Region

The effect of anesthetics on the hydrocarbon region of the PE bilayer has been studied using several specifically

Table 9

SPIN LATTICE RELAXATION TIMES (T_1) OF A 1:1 MIXTURE OF 3-[1',2'-$^2H_4$]DMPE AND EGG PE (IN msec)[a]

	No Anesthetic	$\frac{TTC}{PE} \simeq 0.1$	$\frac{PRC}{PE} \simeq .05$	$\frac{PRC}{PE} \simeq .25$
α deuterons	23.5	19.7	22.8	21.4
β deuterons	22.5	20.8	22.7	20.9

a Anesthetic/PE ratios are based on the bound anesthetic, calculated from the partition coefficients.

Table 10

^{31}P CSA FOR EGG PE WITH ADDED ANESTHETIC

		Anesth/Lipid[a]	CSA
pH 5.5			-39.5
	TTC	0.05	-40.5
		0.24	-42.4
		0.34	-43.7
	PRC	0.14	-40.0
pH 9.5			-37.2
	TTC	0.05	-39.9
		0.08	-40.5
		0.23	-43.0
		0.47	-44.7
	PRC	0.14	-40.1

a Anesthetic/lipid ratio is based on bound anesthetic.

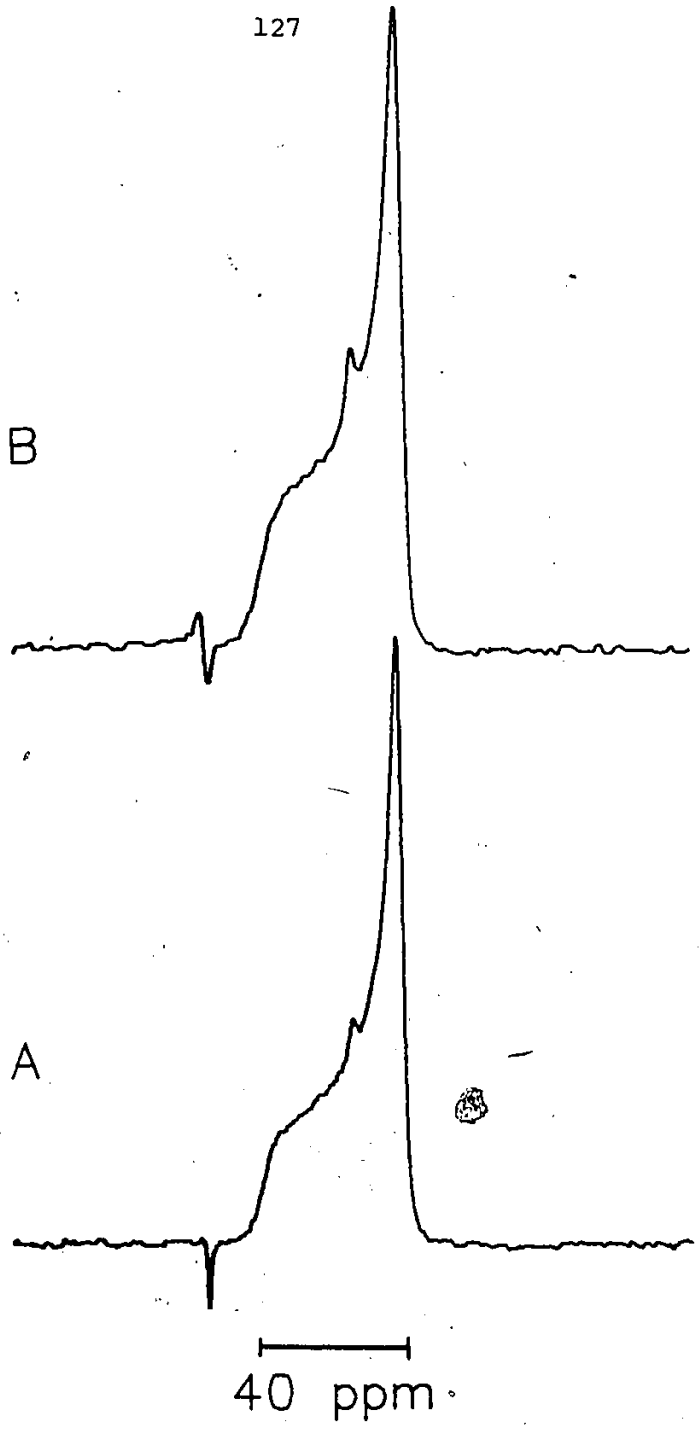

Figure 33. ^{31}P NMR spectra of egg PE (200 mg), at pH 5.5, with A) no TTC , B) TTC/PE = 0.24 .

deuterated DMPE's. The DMPE's were deuterated at the 2 position of the 1 chain (1-[2'-$^2H_2$]DMPE), at the 2 position of the 2 chain (2-[2'——$^2H_2$]DMPE), and simultaneously at the 4 and 14 positions of the 2 chain (2-[4', 14'——$^2H_5$] DMPE). These DMPE's were mixed 1:1 with the semisynthetic egg PE and the ^2H NMR spectra were recorded at both pH 5.5 and 9.5 with the addition of PRC and TTC. Figure 27 shows the location of the deuterium labels and the pH 5.5, ^2H NMR spectra of the 1:1 DMPE/egg PE mixtures.

In the 1:1 mixtures of labelled DMPE and egg PE, with no anesthetic added, the labels on the 2 chain show no pH dependence to their quadrupole splittings; changing by less than 0.3 kHz between pH 9.5 and 5.5. However, for the deuterons at the 2 position on the 1 chain the quadrupole splitting goes from 30.2 kHz at pH 9.5, to 28.7 kHz at pH 5.5. Since the 2 position of the 1 chain is just slightly lower in the bilayer than the 4 position of the two chain (132), the 3.3 kHz difference in quadrupole splittings between them (the quadrupole splitting of the 4 position is 32.0 kHz) is somewhat surprising and may suggest a slight conformational change of the 1 chain at low pH.

The quadrupole splitting of 32.0 kHz for the 4 position gives an S_{mol} of approximately 0.5 for the plateau region, which is higher than that observed for DMPC or DPPC (133), but similar to recent studies on labelled DPPE's (117).

DPPE, labelled at the 4 position, gave a quadrupole splitting of 31.5 kHz at 68°C, which is just above the phase transition. This indicates that the DPPE and DMPE/egg PE bilayers exprience greater conformational constraints than the corresponding phosphatidylcholines.

The addition of PRC, at pH 9.5 to the DMPE/egg PE mixtures caused no measureable change at the 2 positions. However, the 4 and 14 quadrupole splittings were reduced slightly (≈6%). At pH 5.5 a similar effect was noted, with the exception that the 2 position on the 1 chain showed a very slight (3%) reduction in the splittings. The variation of quadrupole splittings with PRC addition is shown for pH 9.5 data in Figure 34 and for the pH 5.5 results in Figure 35.

The influence of TTC on the PE hydrocarbon region is much more pronounced than that of PRC at similar bound concentrations. At pH 9.5 the quadrupole splittings for all chain positions are reduced, with the most pronounced reductions occurring at positions 4 and 14 (Figure 36). At pH 5.5 (Figure 37) the 2 positions experience reductions in quadrupole splittings which are almost identical to those observed at pH 9.5. However, positions 4 and 14 each show two quadrupole patterns at low TTC concentrations. This is entirely analogous to the effect of TTC on the α deuterons of the headgroup at pH 5.5. For each of the 4 and 14 positions, one of the quadrupole patterns shows only a very small reduction in the splitting, but a large decrease

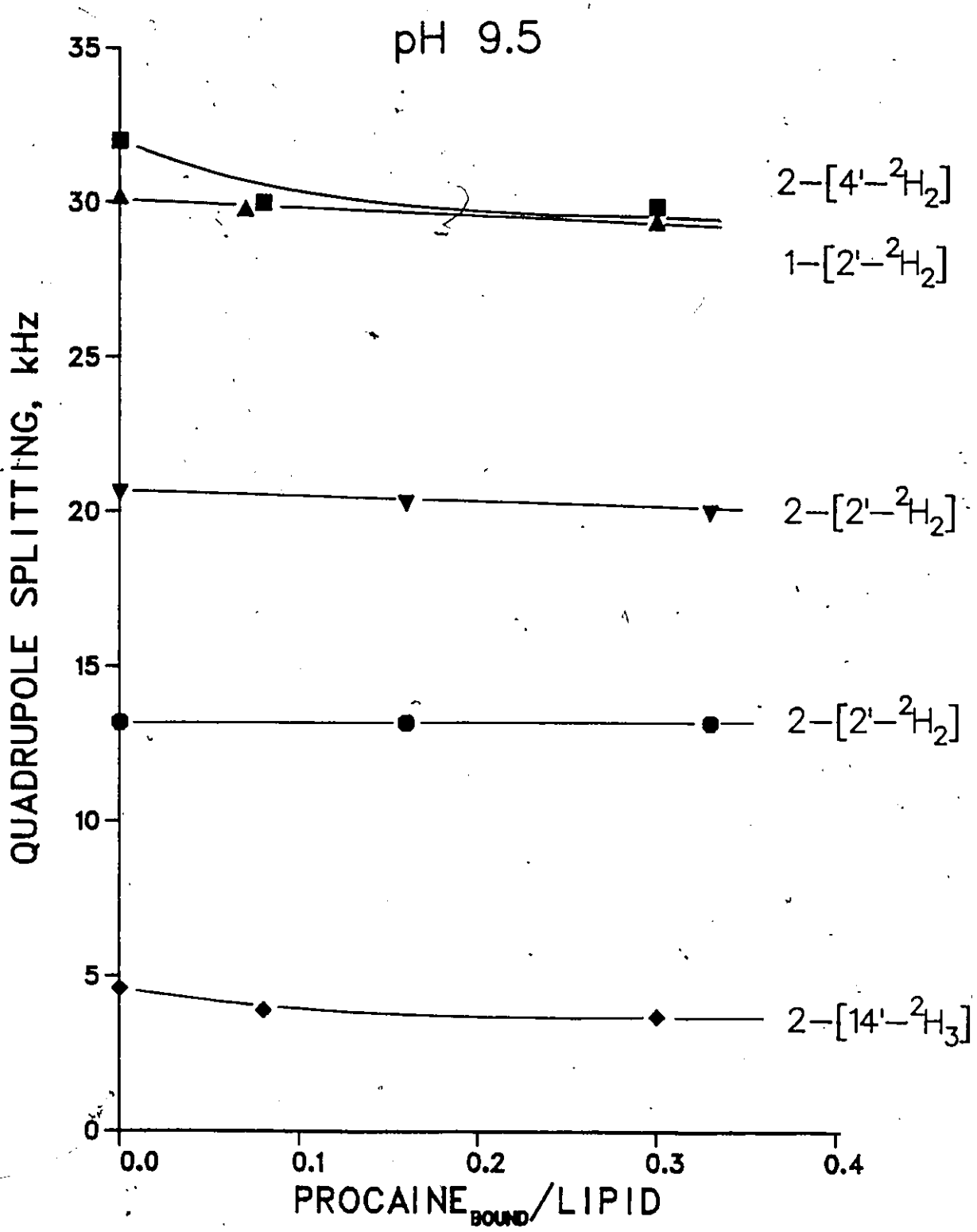

Figure 34. The influence of PRC on the PE hydrocarbon region at pH 9.5 .

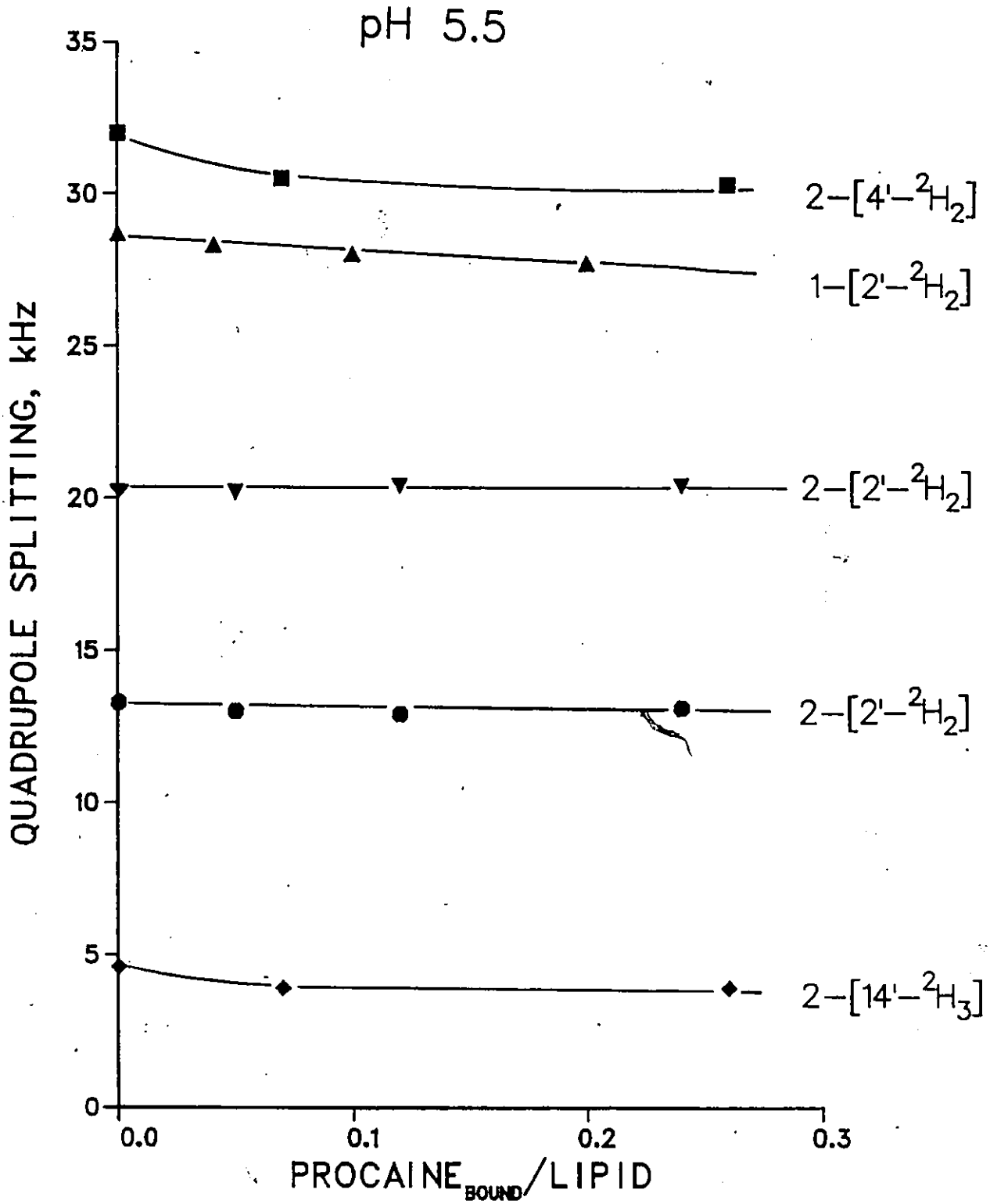

Figure 35. The influence of PRC on the PE hydrocarbon region at pH 5.5 .

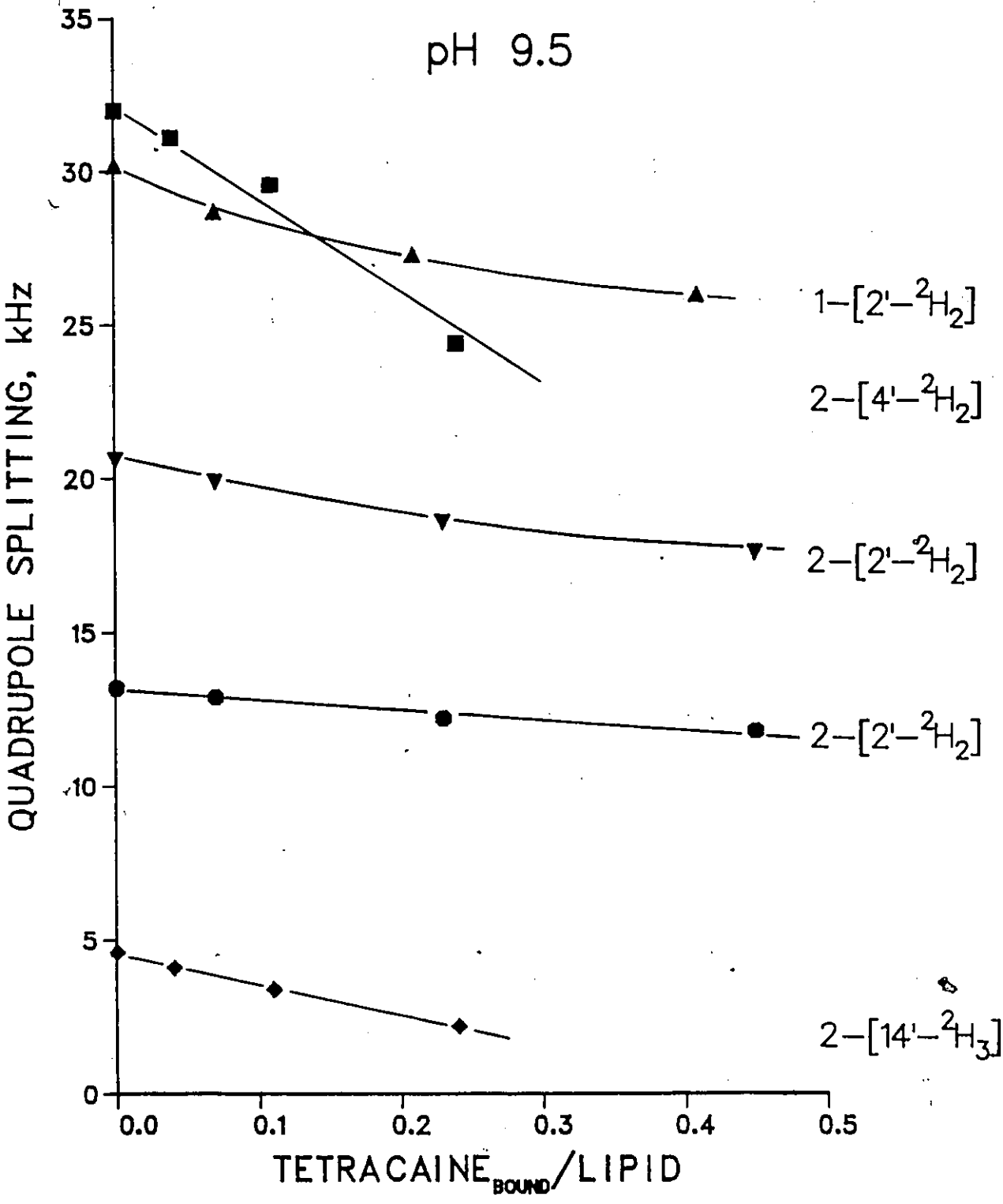

Figure 36. The influence of TTC on the PE hydrocarbon region at pH 9.5 .

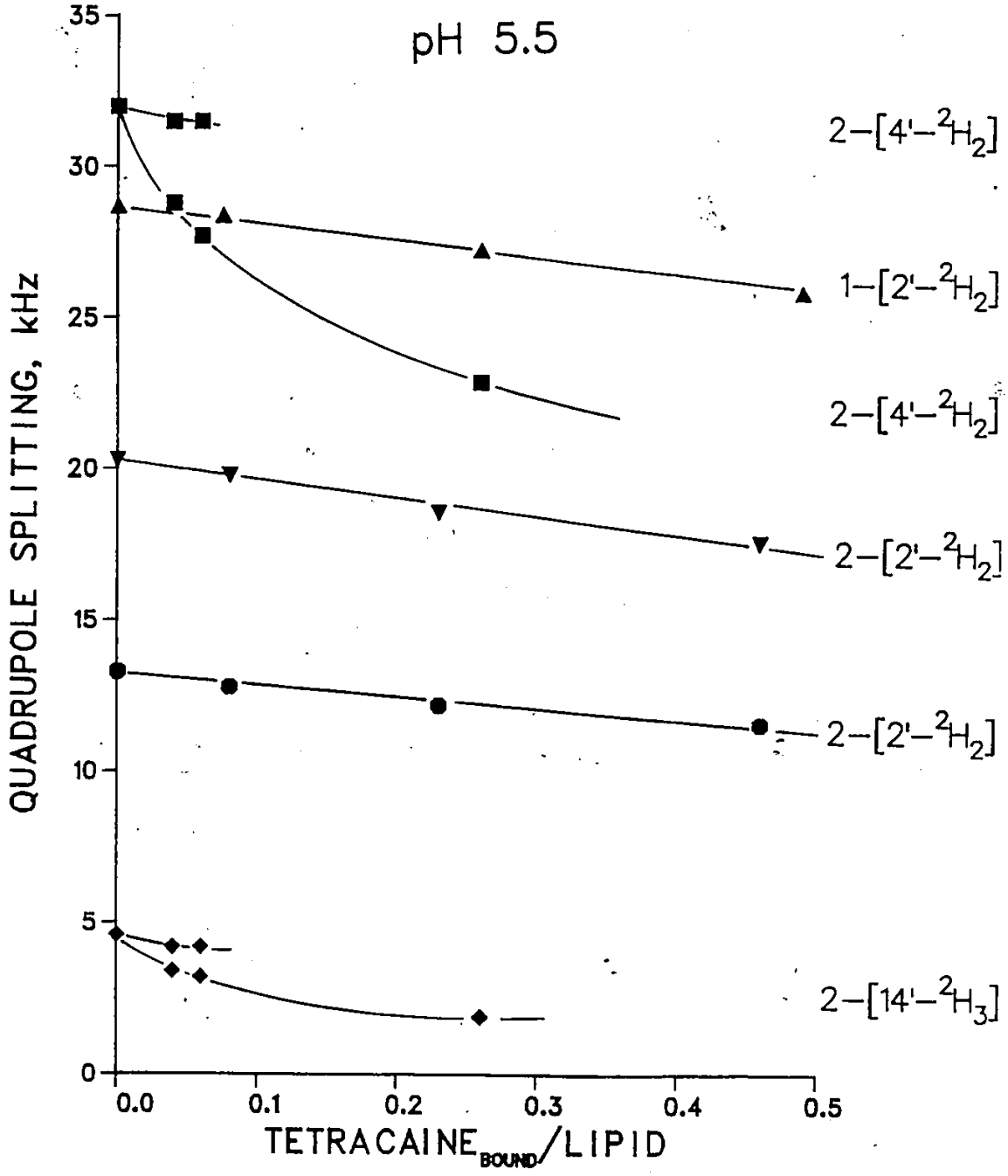

Figure 37. The influence of TTC on the PE hydrocarbon region at pH 5.5 .

in intensity as TTC is added. At concentrations greater than .1/1 (TTC_{BOUND}/LIPID) this pattern completely disappears. The other pattern shows a substantial reduction in the splitting with added TTC and an increase in intensity until it is the only signal observed. Figure 38 shows the ^2H NMR spectra of a 1:1 mixture of 2-[4', 14'-$^2H_5$]DMPE and egg PE, at pH 5.5 with added TTC. The de-Paked spectra clearly show the two components for each position and the changes in intensity.

V.3 Discussion

Headgroup Conformation

Studies of the headgroup orientation in model and biological membranes, by a number of techniques, have led to a picture of the phosphatidylethanolamine headgroup which has its dipole (the C_α-N vector) aligned parallel to the surface of the bilayer (131, 134, 135). Figure 39 shows this arrangement and indicates the respective torsion angles, α_i (angles are measured from the cis-planar configuration). From ^2H and ^{31}P NMR studies of labelled DPPE's, Seelig and his coworkers (131, 134) have shown that the conformation of the headgroup, in the liquid crystal phase, is very close to the conformation in the crystal structure (136). Solution NMR studies of PE have confirmed the presence of the gauche

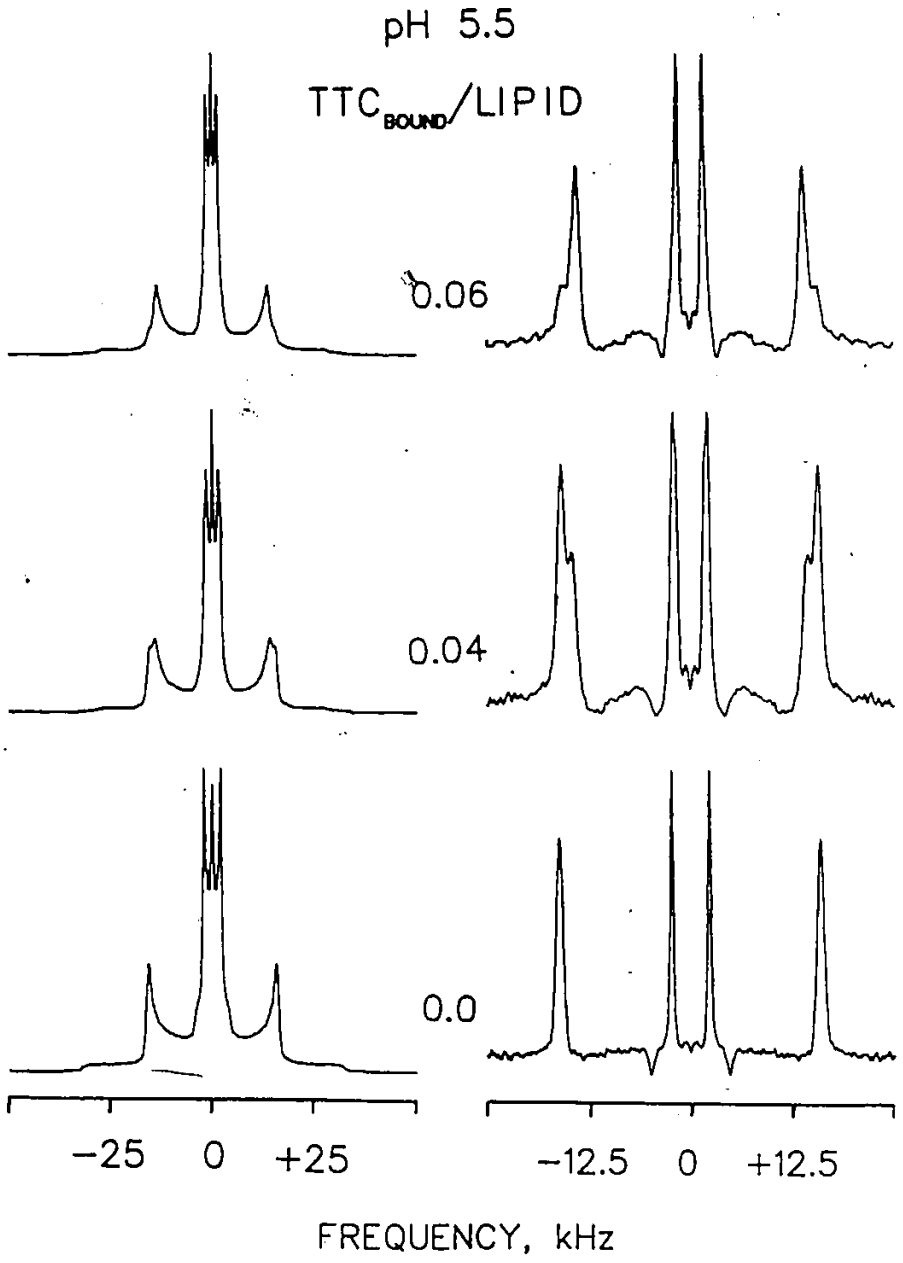

Figure 38. ^{2}H NMR spectra of a 1:1 mixture of egg PE and 2—[4',14'-$^{2}H_{5}$] DMPE, at pH 5.5, with varying amounts of TTC. The TTC_{BOUND}/LIPID ratio is indicated on the spectrum and the de-Paked spectra are shown on the right.

conformation of the O-C-C-NH_3 system, which is present in the crystal structure (137).

It has recently been suggested (117) that the strong hydrogen bonds occurring between the headgroups in the crystal structure of DLPE (136), and proposed for the PE headgroups in the gel state (138, 139), are also present, albeit reduced in strength, in the liqiud crystal phase. These interactions, which are not present in comparable PC systems, could account for the increased quadrupole splittings of the acyl chain region of PE bilayers, compared to the corresponding PC (this work and references 117 and 118). Further evidence for the increased headgroup interactions comes from the observation of the specific volumes of PE and PC (140). In the gel state, dilatometry shows very similar results for the specific volume of PE and PC, but in the liquid crystal phase the PC volume is larger than PE's, suggesting stronger PE interactions. Studies of PE and PC monolayers also indicate similar conclusions (141, 142).

The effect of TTC on the headgroup of PE is very pronounced, while PRC exerts only a very small effect. Since the size of the ^2H quadrupole splitting is determined by both an average conformation and the amplitude of the fluctuations about the average conformation, the TTC results must be explained by a change in the average conformation.

A change in the amplitude of the fluctuations alone, should change both of the quadrupole splittings in the same direction. The decrease in the α quadrupole splittings and the increase in the magnitude of the β splittings, when TTC is added, are indicative of a conformation change which alters the α_4 and α_5 torsional angles (Figure 39). Similar effects have been noted for the addition of the local anesthetic dibucaine, and the ions Eu(III) and La(III) to headgroup deuterated DPPE (109).

The actual conformational change, necessary to cause the observed changes in quadrupole splittings, need not be large. Brown and Seelig (134) have shown that even subtle modifications of the ethanolamine torsional angles ($\approx 5^{\circ}$) can produce substantial changes in the observed quadrupole splittings.

The change in headgroup conformation is also manifested in the ^{31}P NMR spectra. Tetracaine, at both high and low pH, results in the absolute magnitude of the chemical shielding anisotropy becoming larger while PRC induces a similar, but much smaller effect. This suggests that the conformational change includes changes in the α_1 and α_2 torsional angles. A change in one of the torsional angles might account for the observed ^{2}H and ^{31}P NMR results, however, it is likely that a complex interplay of several changes, is occurring.

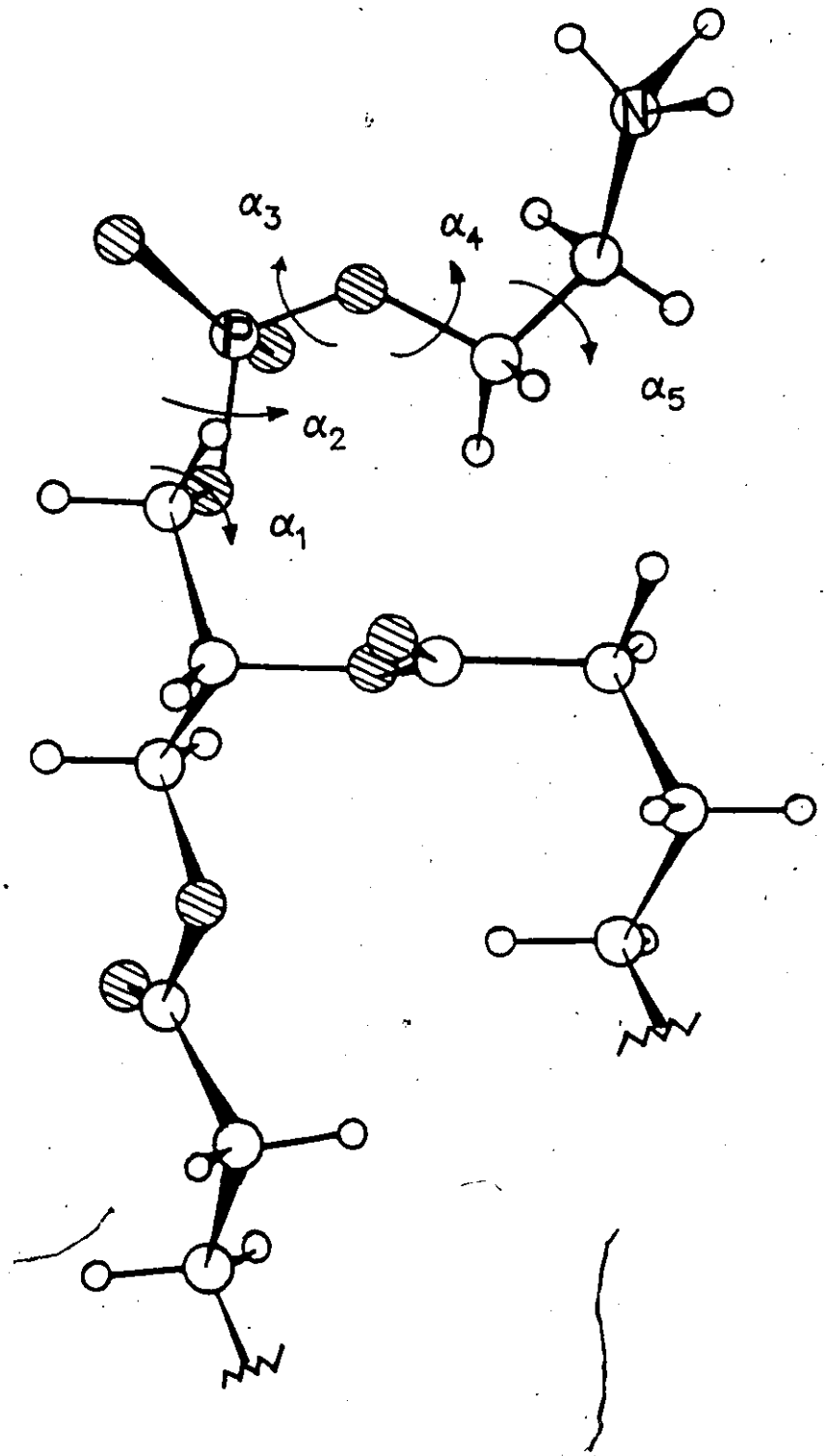

Figure 39. Torsional angles for the PE headgroup (134).

Similar behaviour has also been observed in the interaction of several local anesthetics with PE and PC model membranes. Chlorpromazine, dibucaine, tetracaine and procaine were observed to increase the CSA of natural egg PE (as opposed to the semisynthetic egg PE used in this work) at pH 7.0 (107). Diethazene and chlorpromazine, at neutral pH, also cause a similar effect on DPPC (143). Tetracaine (60) and dibucaine (109) were observed to increase the CSA, at pH <7.0 in DPPC bilayers, while at high pH the TTC induced only a small change.

The effect of TTC on the PE headgroup is in sharp contrast to the effect of cholesterol. Cholesterol causes a reduction in the magnitude of the quadrupole splittings of the α and β deuterons and induces only a small change in the ^{31}P CSA (134, 70, 144). While cholesterol increases the order of the hydrocarbon region (144, 145), it merely acts as a spacer between adjacent headgroups (134).

In the DMPE/PS mixtures the quadrupole splittings for the α and β deuterons are greater than in the DMPE/egg PE systems. This is indicative of a more rigid headgroup, due presumably to PE:PS headgroup interactions. The anesthetics, TTC and PRC, induce changes in the ^{2}H NMR spectra which are quantitatively similar to those seen in the neat PE systems. This indicates that for the PE/PS bilayer the actions of TTC and PRC are similar to those in the pure PE bilayers.

Hydrocarbon Region

At both high and low pH, TTC causes a disordering of the 4 and 14 positions while the 2 positions are almost unaffected. The extent of disordering by TTC, when corrected for the partition coefficients, appears to be same at both high and low pH. For PRC, the effect on the hydrocarbon region is very small and suggests that PRC does not intercalate into the hydrocarbon region at all.

Similar effects have been observed for the interaction of TTC with specifically deuterated DPPC, however, the effects were more pronounced at low pH. This was taken to indicate a greater depth of penetration for TTC, in PC bilayers, when it is uncharged (60).

Comparison of Tetracaine and Procaine

It is quite clear that for all of the experiments performed, the effect of tetracaine on labelled PE is dramatically greater than that observed for procaine. Even when the effect is compared for equal amounts of bound anesthetic (corrected for partition coefficients), the effect of TTC is still substantially larger. Since at these pH levels tetracaine and procaine experience similar degrees of protonation (pH 5.5) or non-protonation (pH 9.5) and since from the tertiary amine to the aromatic amine the two anesthetics are structurally very similar, then the substantial

differences observed must arise as a consequence of the presence of the butyl tail on TTC.

Although the butyl group substantially increases the partition coefficient of TTC, relative to PRC (see Table 4), this has been taken into account in Figures 28, 29, 31, 32, 34-37. Clearly, therefore, the TTC molecule must penetrate much more deeply into the bilayer than PRC does. Further, the tetracaine must interupt the headgroup interactions between neighbouring PE's in such a way as to allow a conformational change in the headgroup of PE. The inability of PRC to induce similar effects suggests that PRC is interacting only with the bilayer surface or intercalating into spaces already present in the polar regions of the bilayer.

Influence of pH

All of the ^{2}H and ^{31}P NMR experiments show a surprising similarity between the results at high and low pH. With the exception of the observation of a portion of the PE which is unaffected by low concentrations of TTC at pH 5.5 (which will be discussed later) the high and low pH results show variations in the magnitudes of the quadrupole splittings which are quantitatively very similar. This similarity extends to the DMPE/PS mixtures where only a slightly larger effect at pH 5.5 is noted.

The results of these experiments are in sharp contrast to work on the interaction of TTC with labelled phosphatidylcholines where larger reductions in the quadrupole splittings of the acyl chains were observed at pH 5.5 than at pH 9.5 (60). It has been postulated that when TTC is charged it sits higher in the bilayer and interacts more strongly with the headgroup. At pH 9.5 TTC is uncharged and penetrates more deeply into the hydrocarbon region. The deeper penetration of TTC results in the bulky benzoid moiety being in contact with the PC acyl chains. Under these conditions the acyl chains will remain in a more motionally restricted environment. At pH 5.5 when TTC sits higher in the PC bilayer the acyl chains have more motional freedom and an increased probability of gauche conformers at positions further along the chain. These conditions lead to a greater reduction in the quadrupole splittings of the acyl chains at pH 5.5 (60).

In these current PE studies the similarity between high and low pH results indicates a similar depth of penetration for the charged and uncharged forms of the anesthetics. This is in agreement with the results of the labelled anesthetic studies in Chapter III, which were also supportive of a charge — independent location for TTC and PRC in the bilayer.

Tetracaine Lateral Diffusion

The presence of two signals for the 4, 14 and α positions, at pH 5.5 and low TTC concentration, can be interpreted as a manifestation of slow lateral diffusion of TTC through the bilayer. If the diffusion is slow on the ^2H NMR time scale, then with small TTC/PE ratios not all of the PE molecules will experience the influence of the anesthetic. As the TTC concentration is increased, the proportion of PE unaffected by TTC decreases and, finally, disappears (Figures 29 and 37). For the 2 positions and the β deuterons of the headgroup, TTC does not sufficiently alter the quadrupole splittings to allow resolution of two signals. However, careful examination of the de-Paked spectra does show a slight asymmetry to the lineshape, suggesting the presence of two lines.

This slow diffusion could arise as a result of two factors. Firstly, since TTC is charged at pH 5.5 there could be an electrostatic interaction between TTC and the zwitterionic PE. This would act to prevent an easy lateral diffusion of TTC. This seems a plausible explanation, since at pH 9.5, when TTC is uncharged, the diffusion is faster and only one lipid signal is observed. A second cause for the slow diffusion could be increased interactions between neighbouring PE headgroups at the low pH. This would result

in a "tighter" lipid matrix which would act to prevent lateral diffusion.

An increased PE-PE interaction would also act to slow the diffusion of the PE molecule itself. Since TTC and PE are of an approximately similar size and both are present in the samples in similar concentrations (i.e., neither is in a large excess) then the actual requirement of a "slow diffusion of TTC" will be a complex interplay of the diffusion of both TTC and the lipid. A more exact description is that in the lipid - TTC matrix the *net* diffusion must be such that on the ^{2}H NMR time scale, discrete areas of free lipid must exist.

This slow diffusion could also account for the observation of two quadrupole patterns for each of the α and β deuterons of headgroup labelled DPPE in the presence of dibucaine (109). In the experiments with dibucaine, performed at pH <7.0, the second signal persisted to much higher dibucaine concentrations (≈0.4/1.0 dibucaine/DPPE). This indicates an even slower *net* diffusion for dibucaine in PE. This is consistent with the bulkier hydrophobic group of dibucaine which would make lateral diffusion even more difficult. Also, dibucaine was shown to induce a similar effect in labelled DPPC bilayers at low pH. This is not observed for TTC or PRC in labelled DPPC bilayers at high or low pH (60).

The difference in diffusion rates of TTC with pH also manifests itself in the lineshapes of labelled TTC in PE bilayers (see Chapter III). At pH 5.5 labelled TTC samples show a strong angular dependence to the linewidth, while at pH 9.5 the linewidth is angular independent. This strong angular dependence at low pH can be correlated with slow lateral diffusion over a surface of finite curvature (119).

Membrane Location of Tetracaine and Procaine

The influence of TTC and PRC on the ^{2}H NMR and ^{31}P NMR spectra of labelled PE's can be used to ascertain the location of the anesthetic in the bilayer. As well, the results of the labelled anesthetic studies can be correlated with the location of the anesthetic in the PE bilayer.

The similarity of the ^{2}H NMR results, regardless of whether TTC is charged or uncharged (ignoring the diffusion effects) indicates that the depth of intercalation of TTC into the bilayer must be the same at high and low pH. The very small effects noted for the 2 position of the 2 chain suggests that the bulky aromatic ring is located at, or near that level (Figure 40). Since this pushes neighbouring lipids apart, the acyl chains now have more room and less motional constraints. The decreased quadrupole splittings at the 4 and 14 positions would appear to confirm this. Also, with the aromatic ring at the level of the glycerol

backbone, the amine headgroup of TTC is still able to interact with the PE headgroup.

The similarity of the high and low pH results supports the molecular shape model of TTC interaction with PE which was discussed in Chapter III. It is clear that it is the shape and volume considerations which appear to govern the interaction of TTC with PE and not the effect of anesthetic charge. This model contrasts with the model for the interaction of TTC with egg PC (60). In egg PC, TTC sits higher in the bilayer when it is charged and it penetrates more deeply when it is uncharged. For TTC interacting with PC it is clear that the anesthetic charge is the dominant factor in determining the anesthetic location, and not the molecular shapes.

Although PRC induces only minor changes in the ^{2}H and ^{31}P. NMR spectra of the labelled PE, the anesthetic is intercalating into the bilayer. The observation of a quadrupole pattern for PRC, labelled in the aromatic ring (Figure 21), in the presence of egg PE indicates an ordered environment for bound PRC and not just a loose surface effect. This quadrupole splitting is, however, almost 40% less than that observed for the corresponding label on TTC. This would be consistent with a PRC molecule whose aromatic ring sits higher in the PE bilayer than does tetracaines (Figure 40). This higher position for PRC also explains the lack of a

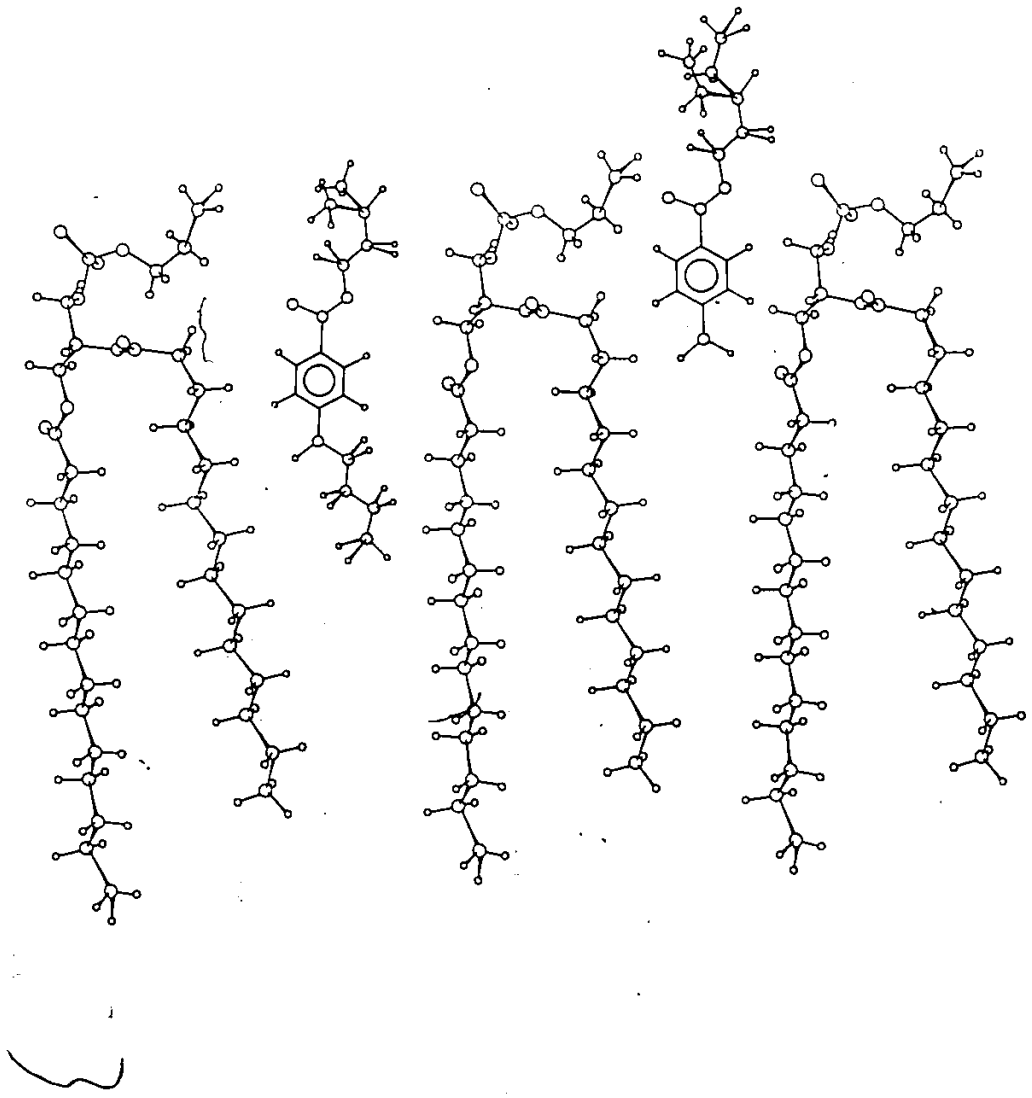

Figure 40. Locations of PRC and TTC in the PE bilayer.

quadrupole splitting for PRC-d_4. The N-ethyl groups of PRC are probably sticking out into the water and are therefore subject to substantial motional averaging. It would appear, therefore, that PRC does not penetrate into the hydrocarbon region at all, preferring instead to locate only in the hydrophilic, headgroup region.

V.4 Conclusions

The studies of the effect of TTC and PRC on PE bilayers have demonstrated the importance of the butyl group to TTC. While otherwise very similar, only TTC is able to penetrate into the bilayer. Tetracaine also induces changes in the ethanolamine headgroup. It would appear that both the charged and uncharged forms of TTC penetrate to the same depth in the PE bilayer and that this depth is governed by the molecular shapes of TTC and PE, not the charge. This is in agreement with the studies of labelled TTC reported in Chapter III.

The one substantial difference induced by pH changes is in the lateral diffusion rates. At pH 5.5 the *net* diffusion rate (a combination of the TTC and PE rates) is slower than the ^2H NMR time scale and two regimes of PE can be detected. This slower diffusion likely arises from increased headgroup interactions between neighbouring PE's. This is the first example of such a slow lateral diffusion and suggests that studies on other systems, such as lipid-protein

interactions might be more successful with PE than with the currently popular PC.

Finally, because of the known preference of PE to occupy the inside of a membrane, and the propensity for amine anesthetics to be more effective when applied to the intracellular side of the membrane, these results are quite interesting. It may well be that for a heterogeneous site of anesthesia, of the type described by Trudell (22), PE might be localized near the sodium channels. In such a case, the interactions observed might modulate the ability of the sodium channel to function and thus prevent the propagation of a nerve signal.

CHAPTER VI

THE INTERACTION OF TETRACAINE AND PROCAINE WITH MEMBRANES OF ERYTHROCYTES AND *ACHOLEPLASMA LAIDLAWII* B

VI.1 Introduction

With experience in a number of model systems, the techniques used in the earlier chapters have been extended to a study of the interaction of TTC and PRC with two biological membranes. If the model systems reported on in this work, and in earlier studies (58, 59, 60), are to have relevance to the biological experience, then it is necessary to demonstrate similar interactions of anesthetics with natural membranes. For this purpose, the membranes of human erythrocytes (ghosts) and *Acholeplasma laidlawii* B were chosen.

The red cell membrane is a widely studied biological membrane (146) whose lipid composition is similar in type and quantity to some of the nerve membranes (30, 104, 147). It is now well established that the red cell membrane has an asymmetric distribution of lipids, with PC and sphingomyelin preferentially distributed on the outside and PE and PS on the inside (104, 148). Cholesterol, which is also a significant component of the membrane, is found on both sides of the membrane.

The organization of the lipids and their phase behaviour have been studied by a number of techniques including ESR (149), fluorescence (150) and ^{31}P NMR (151), but with questionable success. Ghosts, incubated with a perdeuterated palmitic acid probe, were studied by ^{2}H NMR (152). The ^{2}H NMR spectra of the ghosts, with the probe present at low concentrations, indicated no phase transition in the temperature range of 0^{o}-$45^{o}C$. This was confirmed by a ^{2}H NMR study of ghosts containing DPPC-d_{62} (153). The labelled DPPC was incorporated using a PC transfer protein, and therefore, it represents the least perturbing probe yet used to study the hydrocarbon region. The ^{2}H NMR of the ghosts containing DPPC-d_{62} did, however, show a phase transition between -5^{o} and $-15^{o}C$, consistent with a change from the liquid crystal to the gel phase. This temperature is somewhat misleading since natural, unsaturated PC's were replaced by DPPC and this results in a higher phase transition temperature than would occur in the natural membrane.

Erythrocyte ghosts have been used as model biological membranes in several studies of anesthetic action. Seeman and his coworkers have studied the binding of many amphipathic molecules, like anesthetics, using centrifugation techniques (90). ESR (110) studies of spin labelled compounds, very similar in structure to tetracaine, have shown binding of the anesthetic at pH 9.5. A fluorescence study

of the same anesthetics, interacting with ghosts, has indicated that there are both protein and lipid binding sites (154). Finally, a recent series of studies by Conrad and Singer (155, 156), using a hygroscopic desorption technique, have cast doubt on this earlier work. They indicated that amphipathic molecules, including several local anesthetics, do not enter the bilayer in any substantial concentration. They further propose that the biological membrane has a large 'internal pressure' which acts to keep amphipathic molecules out. This 'internal pressure' is suggested to arise from strong lateral interactions between lipids and proteins.

The membrane of *Acholeplasma laidlawii* B was chosen for study because it readily incorporates exogeneous ^{2}H-labelled fatty acids. Unfortunately, because the major lipids in *Acholeplasma aidlawii* B are monoglucosyldiacylglycerols and diglucosyldiacylglycerols they have less relevence to the nerve membrane. However, the already extensive studies made of the hydrocarbon region of *Acholeplasma laidlawii* B (88, 119, 157-159) make it a useful membrane in which to observe anesthetic interactions. It also provides a good test of Conrad and Singer's new vision of the membrane.

The interaction of TTC and PRC with the membranes of human erythrocytes and *Acholeplasma laidlawii* B has been studied by first obtaining the ^{2}H NMR spectra of the labelled

anesthetics. Also, the effect of TTC and PRC on ghosts doped with perdeuterated palmitic acid has been studied by ^2H NMR. The influence of TTC and PRC on *Acholeplasma laidlawii* B was studied by using membranes grown on oleic acid deuterated at the 5 and 18 positions. A comparison of the charged and uncharged forms of the anesthetics was made by performing the experiments at both pH 5.5 and 9.5.

VI.2 Results and Discussion

Studies with Labelled Anesthetics

The partition coefficients for TTC in ghosts were determined by the centrifugation technique (89). The values of K_p are reported in Table 11 along with the values for PRC determined by Roth and Seeman (90). The partition coefficients are found to be lower in ghosts than in model membranes of PC (58, 59), but similar to the partitioning in PE (see Table 4). Partition coefficients for *Acholeplasma laidlawii* B were not determined because the highly coloured lipids in the membrane interferred with the spectrophotometric determination of TTC and PRC. However, none of the ^2H NMR spectra showed a signal from solid TTC. Since the solubility of TTC in the buffer is low (58), the remaining TTC must be in the membrane, or it would appear as the solid ^2H NMR signal. The K_p values for TTC and PRC in *Acholeplasma laidlawii* B must, therefore, be at least as large as those for ghosts.

Table 11

PARTITION COEFFICIENTS FOR TTC AND PRC IN GHOSTS

	pH 5.5	pH 7.0	pH 9.5
TTC	10	12	65
PRC[a]		3.1	

a From reference 90.

The ^2H NMR spectra of TTC-d_6, TTC-d_3 and TTC-d_2 in ghosts and in *Acholeplasma laidlawii* B membranes, at pH 9.5, are shown in Figure 41. From the K_p values for TTC in ghosts, the bulk of the TTC should be in the membrane. Clearly however, there is no obvious quadrupole pattern as was observed for all TTC samples in PE and most of the TTC samples in PC.

The ^2H NMR spectra of TTC-d_2 are reminiscent of the spectra of TTC-d_2 in egg PC (Figure 25) or PE (Figure 15) at low temperatures. In order to check if the line shapes are due to the effects of a short T_{2e}, the TTC-d_2 spectra were run again at higher temperatures. The spectra of TTC-d_2 in *Acholeplasma laidlawii* B at 27°C and 50°C (Figure 42) show a pronounced broadening at higher temperatures. This is opposite to the effect expected for a simple exchanging system and suggests that for TTC-d_2 a quadrupole pattern is present, but cannot be detected due to a very short T_{2e} (<100 μsec). Since the T_{2e} is of the order of 100-150 μsec in egg PE, it would not be unreasonable to expect an even smaller T_{2e} in the natural membranes (119). These line shapes are also present for TTC-d_2 in the extracted lipids alone. Figure 43 shows the spectra of TTC-d_2 in ghosts and in extracted lipids. It is clear that the absence of proteins does have an influence on the spectrum of TTC-d_2. This result would appear to agree with a fluorescence study

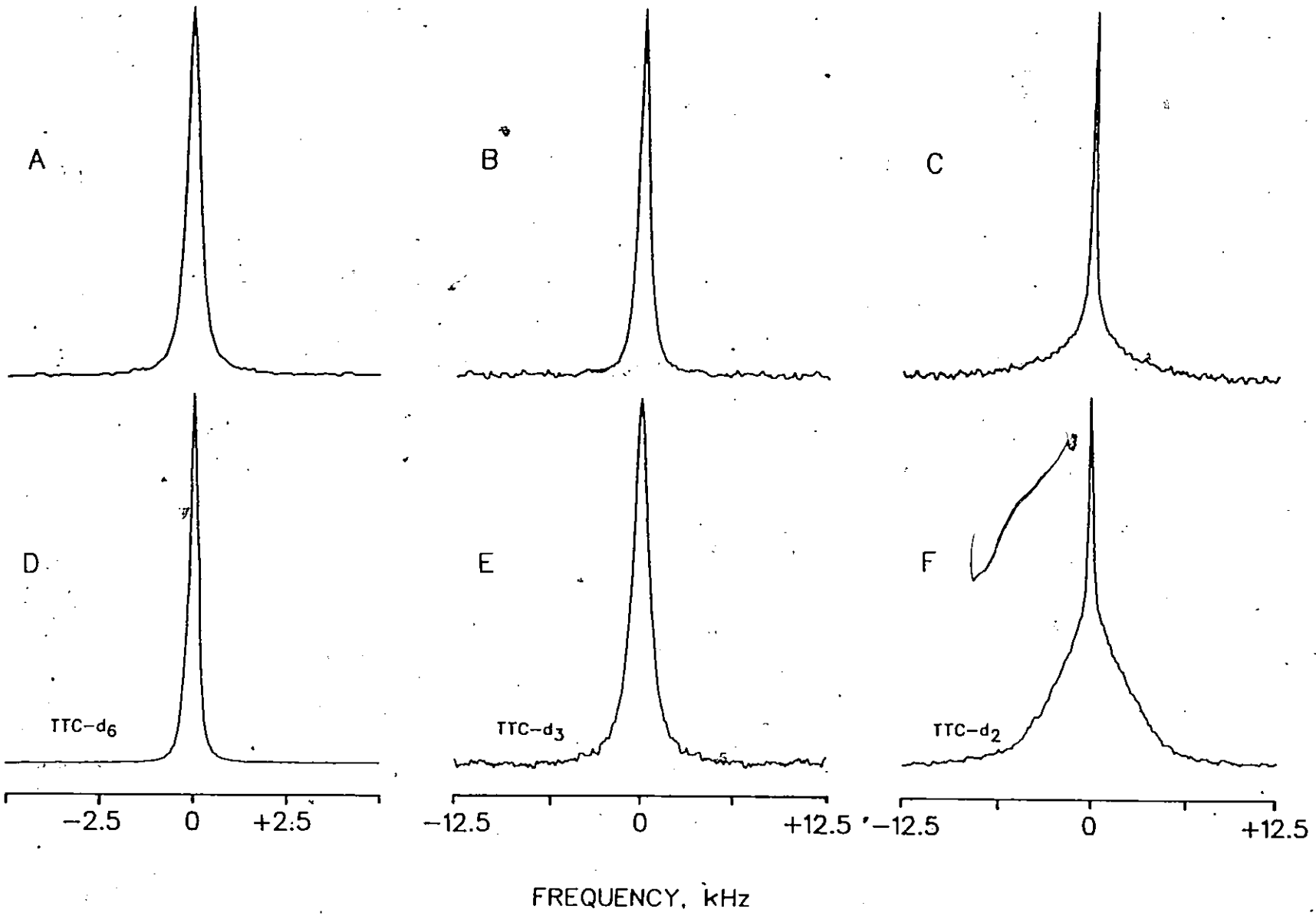

Figure 41. ^2H NMR spectra of labelled tetracaines in *A. Laidlawii* B (A–C) and human erythrocytes (D–F) at pH 9.5 . All samples contained 5–10 mg of TTC, 200 mg of membrane and 1.0 mL of BPC buffer.

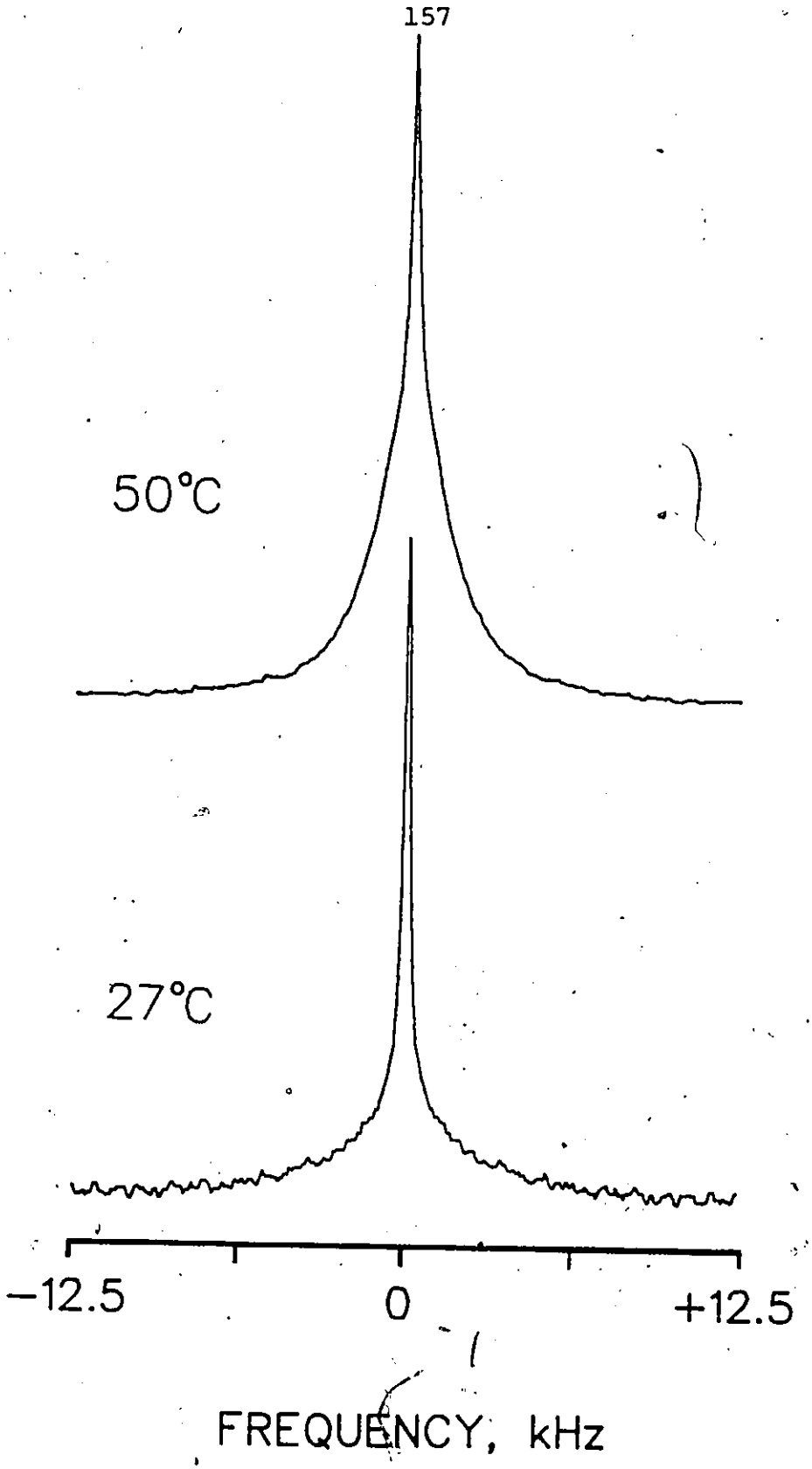

Figure 42. ^{2}H NMR spectra of TTC-d_2 in *A. Laidlawii* B, at pH 9.5. Spectra are at 27°C and 50°C.

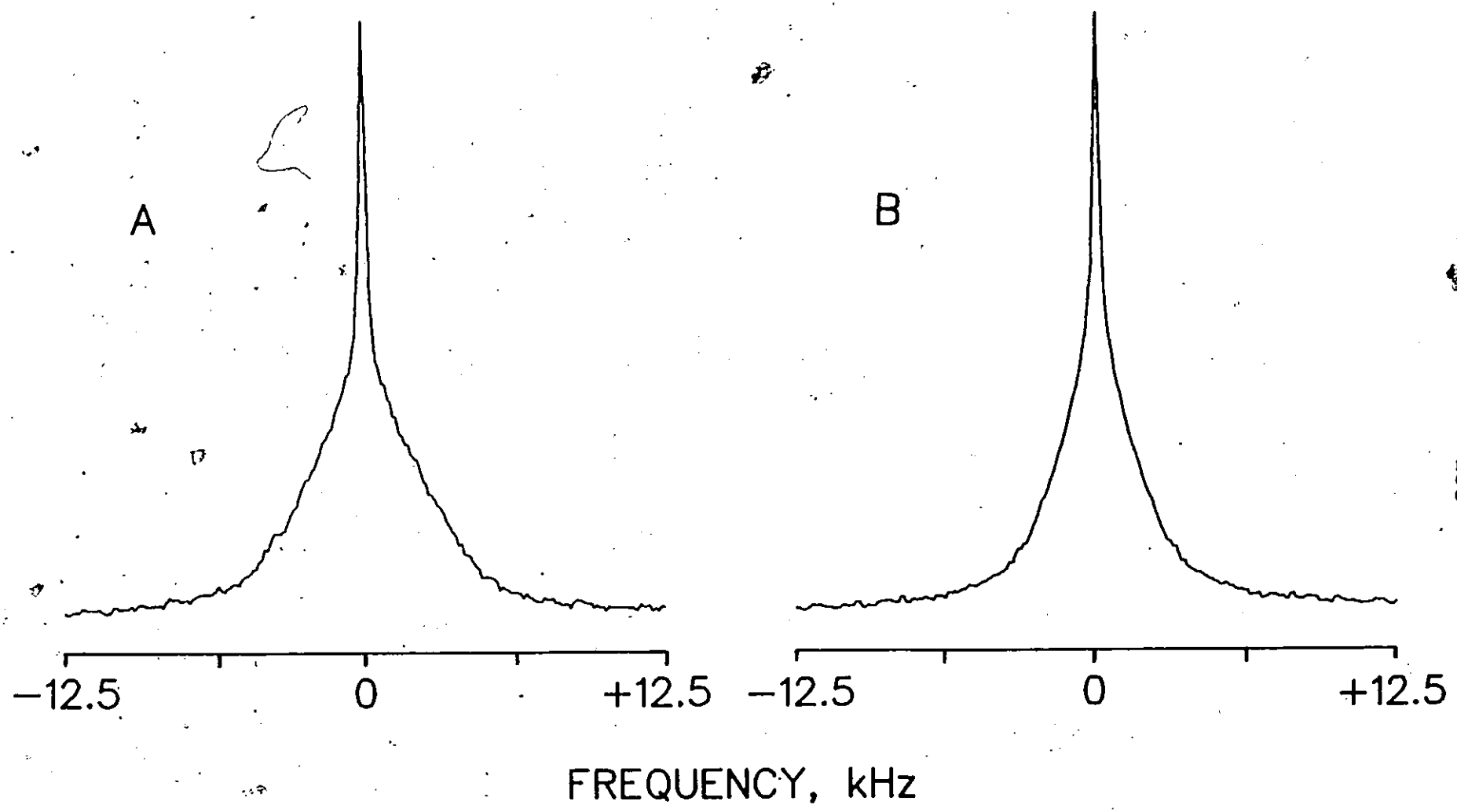

Figure 43. ^{2}H NMR spectra of TTC-d_2 (10 mg) in A) 200 mg of ghosts and B) 150 mg of lipids extracted from ghosts. Both samples were hydrated with 1.0 mL of BPC buffer at pH 9.5 .

of a spin labelled analog to tetracaine, which showed binding to both lipid and protein (154).

The spectra of the other labels, TTC-d_3 and TTC-d_6, all show only a single line at both pH 5.5 and 9.5. The spectra of TTC-d_3 in natural membranes are generally broader than those for TTC-d_6, and are up to 1000 Hz in width for TTC-d_3 in ghosts at pH 9.5. The spectra are consistent with a more rapid exchange which averages the quadrupole patterns to a narrow line. This is analogous to the spectrum of TTC-d_6 in egg PC, at high temperatures (Figure 24B), which shows only a narrow resonance. The larger linewidths for the TTC-d_3 samples suggests that, in the bound site, the butyl group is in a more rigid environment, most likely the hydrocarbon region. Since rapid exchange obeys Equation 17, the linewidth observed is an average of the free TTC linewidth and the quadrupole splitting for the bound site, weighted by the populations in each site. The populations, derived from the partition coefficients, indicate that approximately 95% of the anesthetic is in the membrane and this suggests that the averaged linewidth must be close to the quadrupole splitting of the bound site. A quadrupole splitting of from 1 to 1.5 kHz would be similar to the model studies of PE and PC reported in the earlier chapters. For TTC-d_6 the narrow lines observed indicate that in the bound site the dimethylamino moiety of TTC is in a very disordered environment.

The spectra of labelled PRC all show only a single narrow line which is only very slightly broader than that for PRC in water. This suggests a very rapid exchange rate and/or only a small portion of PRC bound in a site of low order. This is consistent with the results of the model studies reported in Chapters III and IV and the small K_p values for PRC in ghosts found by Roth and Seeman (90).

Influence of Anesthetics on Labelled Membranes

Erythrocyte ghosts, incubated with perdeuterated palmitic acid, were studied by ^2H NMR at pH 9.5. The addition of TTC causes a substantial reduction in the quadrupole splittings, especially in the plateau region (Figure 44), while PRC, at similar concentrations has no detectable effect. These results are entirely analogous to those seen for labelled PE (Chapter V) and labelled PC (60) and they indicate that while PRC might interact only slightly at the headgroup, TTC must penetrate into the hydrocarbon region.

The influence of TTC and PRC on *Acholeplasma laidlawii* B labelled at the 5 and 18 positions was studied at both pH 5.5 and 9.5 and the results are reported in Figures 45 and 46. Figure 47 shows the ^2H NMR spectra of *Acholeplasma laidlawii* membranes specifically labelled at the 5 and 18 positions, in the presence of TTC. Since K_p values are not known, the effects of equal amounts of anesthetic bound

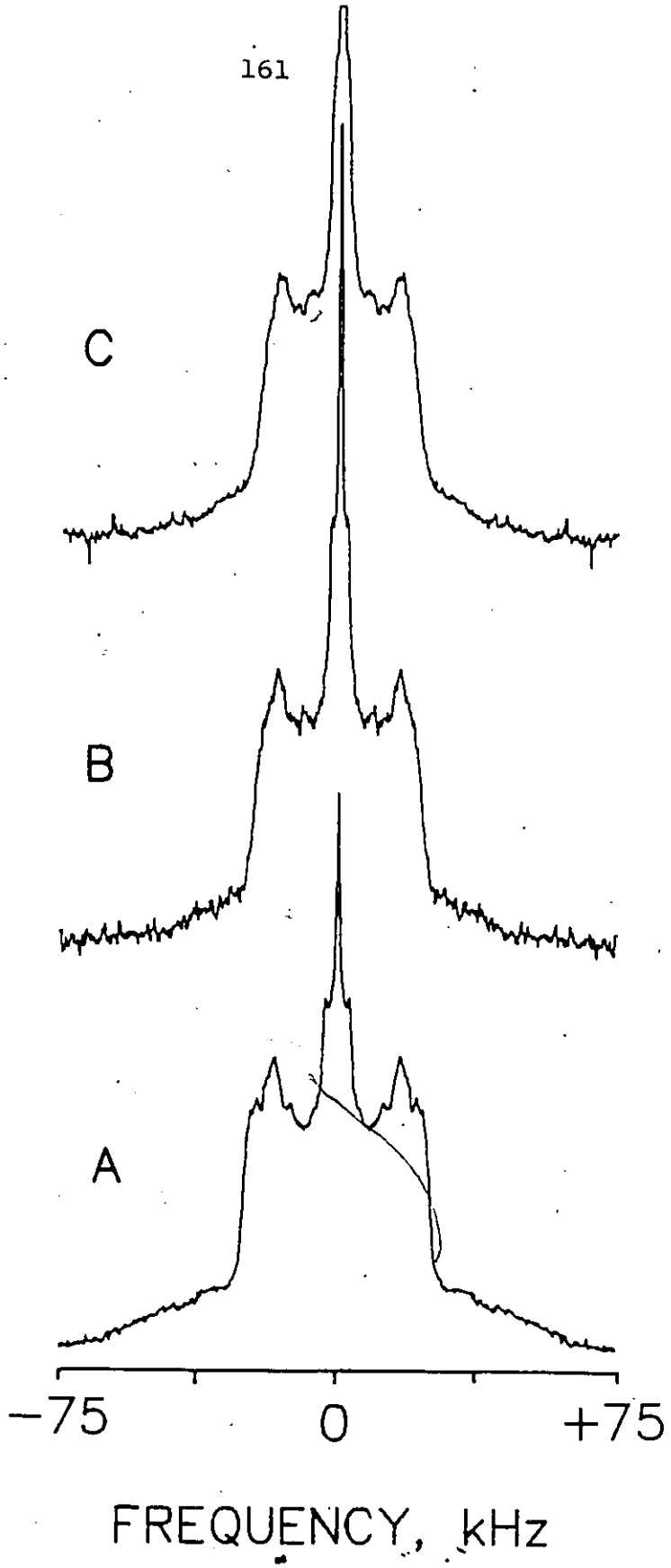

Figure 44. The influence of TTC on the ^{2}H NMR spectra of ghosts incubated with perdeuterated palmitic acid. A) 150 mg of ghosts and 1.0 mL of BPC buffer, pH 9.5. B) Sample A with 5.0 mg of TTC·HCl added. C) Sample A with 10.9 mg of TTC·HCl added.

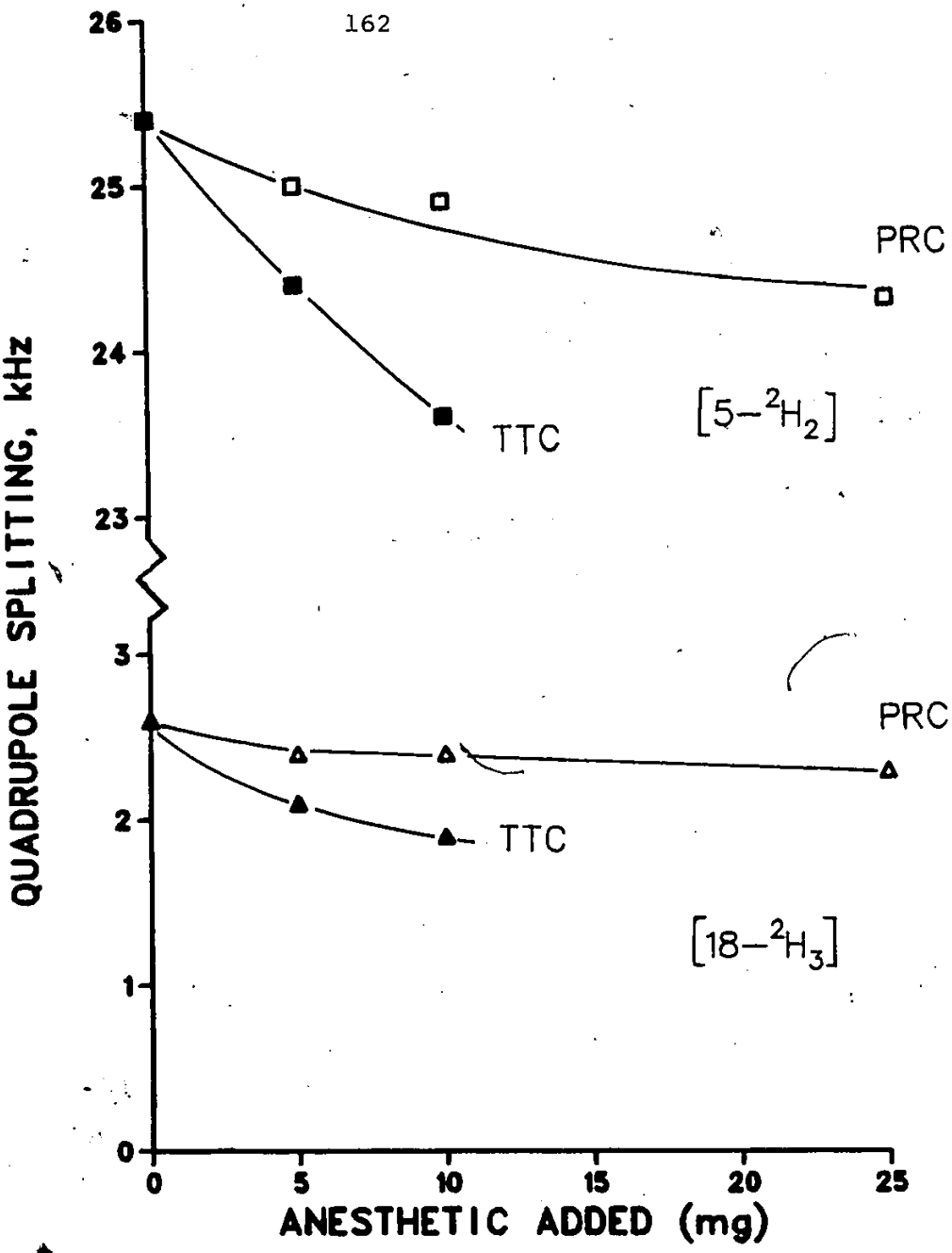

Figure 45. The influence of TTC and PRC on *A. Laidlawii* B membranes (200 mg) grown on $[5-^2H_2]$ (■) or $[18-^2H_3]$ (▲) oleic acid, in BPC buffer (0.75 mL) at pH 5.5.

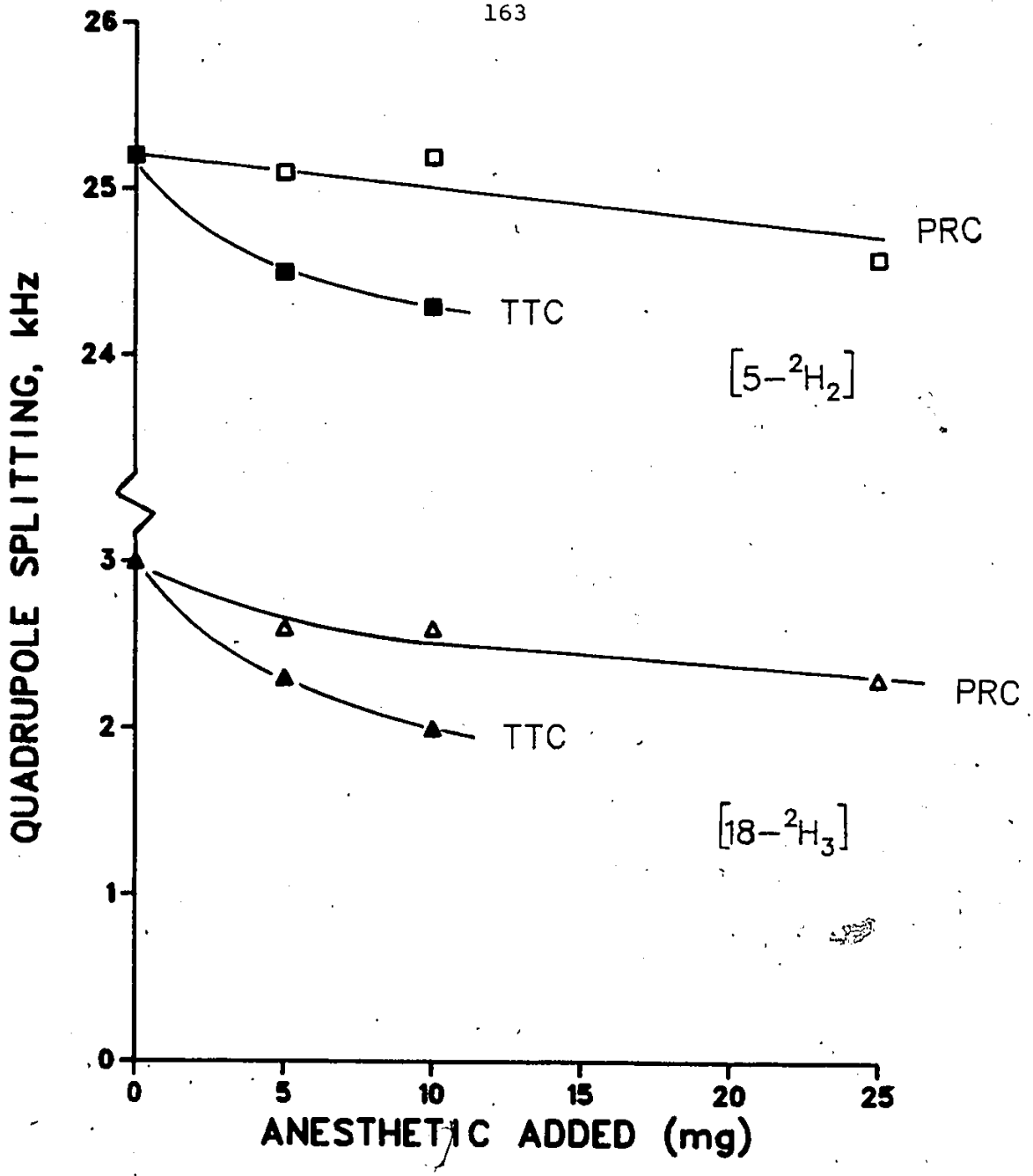

Figure 46. The influence of TTC and PRC on *A. Laidlawii* B membranes (200 mg) grown on [5-$^2H_2$] (■) or [18-$^2H_3$] (▲) oleic acid, in BPC buffer (0.75 mL) at pH 9.5.

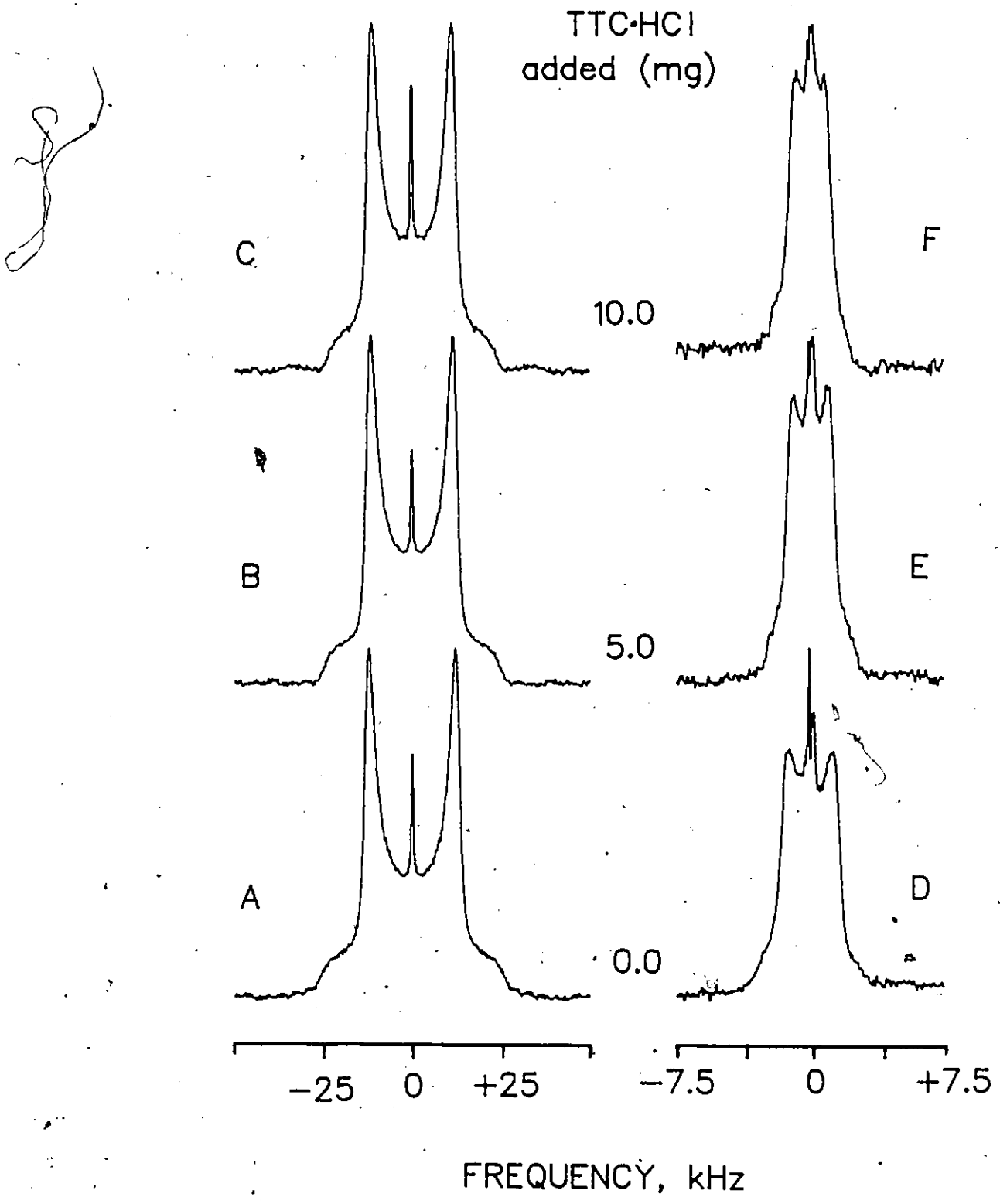

Figure 47. The influence of TTC on the ^2H NMR spectra of *A. Laidlawii* B grown on [5-$^2H_2$] oleic acid (A-C) and [18-$^2H_3$] oleic acid (D-F) Spectra are of 200 mg of membrane in 0.75 mL of BPC buffer. Spectra of the 5 position are at pH 5.5, while the 18 position spectra were run at pH 9.5. The amounts of TTC·HCl added are indicated on the spectra.

cannot be compared. However, it is clear that TTC exerts a much more substantial influence than does PRC. It is also clear that there is no significant difference between the high and low pH results. These results indicate that, despite the very different lipid compositions of erythrocytes and *Acholeplasma laidlawii* B, the influence of a local anesthetic like TTC is very similar.

Comparison of the Natural Membranes with Model Membranes

The results of the labelled anesthetic studies are, in some respects, discouraging. It would appear that the combination of a short T_{2e} and a more rapid exchange rate has eliminated the most useful information which could be obtained, that is, the quadrupole splittings of the labelled anesthetic at its binding site in the membrane. Despite this, we can still deduce a great deal of information about the anesthetic interaction. The first and most obvious observation is that the exchange rate of TTC and PRC is fast. From a comparison with the studies in PE and PC it would appear that the rate for TTC exchanging between a bound site and a free site is certainly greater than 1.5×10^3 sec^{-1}, since TTC-d_3 does not show a quadrupolar pattern. This assumes, of course, that the exchange is a simple two-site exchange model and not something more complex. Since a three-site model is required to explain the TTC/PC results, we cannot rule it out for the natural membranes.

Secondly, the increased broadening noted for TTC-d_3 relative to TTC-d_6 suggests a much more constrained environment for the butyl group. This differs from the behaviour in model systems (59, Chapter III and V) where the quadrupole splittings for TTC-d_3 are less than or equal to those for TTC-d_6. This could well indicate that TTC sits somewhat higher in the bilayer in natural membranes than in model membranes. This would place the dimethylamino group of TTC further out, possibly into the water, enabling a greater degree of motional averaging to occur. The butyl chain would still be in the hydrocarbon region, and experience an ordered environment. Unfortunately, the rapid exchange averages out the quadrupole patterns, and this cannot be confirmed.

Finally, the studies on labelled natural membranes show effects whose magnitudes are very similar to those of the model systems. Tetracaine causes a disordering of the chain region while PRC does not. All of this suggests that, as in the model systems, TTC penetrates into the hydrocarbon region while PRC does not.

Relationship of this Work to Conrad and Singer's Model

The model of Conrad and Singer marks a subtle, but substantial departure from the currently-held view of the membrane (155, 156). It proposes an internal pressure which

acts to prevent amphipathic molecules from intercalating into the bilayer. Conrad and Singer base this conclusion on studies using a hygroscopic desorption technique. This technique makes use of a series of filters which should allow small amphipathic molecules through, but retain the biological membrane. Determination of the concentration of the amphipath at the start of the experiment and in the filtrate allows a calculation of K_p. Although the technique gives values of K_p for model lipids very close to those found by the centrifugation technique, the results indicate a $K_p << 1$ for real membranes. The discrepancy between the two techniques is suggested to result from the formation of mixed micelles between the amphipaths and lipids removed from the membrane. These micelles adhere to the membrane surface and are centrifuged down with the membrane. In the desorption technique, the filters separate these micelles from the bilayer.

Since the technique appears reasonable (although no other group has attempted to repeat it) it is necessary to discuss the NMR results in light of Conrad and Singer's work. For the experiments conducted in this work, TTC was always present in amounts at least 10 times greater than the solubility in the buffer. If this labelled TTC was present as a solid, a rigid limit ^2H NMR spectrum would be expected. Since in no case was the solid spectrum observed,

we must conclude that the bulk of the anesthetic is in the membrane (tests showed that the solid would have been detected). If the TTC forms mixed micelles, as Conrad and Singer postulate, then the reductions in the quadrupole splittings observed for the labelled ghosts and *Acholeplasma Laidlawii* B would not be expected.

Several other studies of the interaction of shape changing molecules with red cells also rule against Conrad and Singer's model. The pyrene derivatives 1-pyrenebutyrylcholine (PBC) and 1-pyrenebutyric acid (PBA) convert normal biconcave erythrocytes into echinocytes (160). If only a very small quantity of PBC or PBA goes into the cell it is difficult to rationalize how it can induce a shape change. Further, the inability of lipid-insoluble collisional quenchers like Mn^{2+} to quench the fluorescent PBC and PBA, indicates that the pyrene must be in the hydrophobic region of the membrane.

Although there is no obvious error in the hygroscopic desorption technique, the very small values of K_p found for amphipaths in real membranes is disturbing. Both fluorescence and ^2H NMR studies present evidence against it, yet there is no apparent reason why Conrad and Singer's technique should not be providing a correct answer.

VI.6 Conclusions

The studies of the interaction of TTC and PRC with the membranes of *Acholeplasma laidlawii* B and human erythrocytes have shown that anesthetics exchange much more rapidly between natural membranes and water than between model systems and water. As in the model systems, PRC does not appear to penetrate the hydrocarbon region while TTC does. Unlike model systems, however, it appears that TTC sits somewhat higher in the bilayer in real membranes, giving rise to the narrow lines observed for TTC-d_6 samples.

Finally the results of this work indicate that the model for the membrane proposed by Conrad and Singer is questionable. It is clear that the amphipath TTC intercalates into the membrane in concentrations for in excess of those predicted by the Conrad and Singer model.

CHAPTER VII

A ^{2}H NMR STUDY OF THE SOLID-PHASE BEHAVIOUR OF NONADECANE

VII.1 Introduction

Nonadecane (n-C_{19}) forms two solid phases prior to melting at 32.2°C (37, 161). The low temperature form (phase I) is composed of molecules in an all-trans conformation, arranged in layers and packed in an orthorhombic unit cell. The chain long axes are parallel to each other and perpendicular to the surface of the layer. The high temperature form (phase II) appears at 22.8°C. This phase conserves the layered arrangement found in phase I, with greatly altered unit cell dimensions (40). In particular, there is lateral expansion within the layers which would allow orientational disorder around the molecular axes. Much experimental and theoretical work supports the idea that hindered rotation is the predominant chain motion in phase II (38, 42, 43, 162), with other molecular motions such as self diffusion (42) and longitudinal fluctuations (38) occurring to a lesser extent.

Recently, however, the presence of non-planer molecules in phase II n-alkanes has been demonstrated (38, 39, 46, 163). In the case of n-C_{19} the gauche bond concentration in phase II is <5% at the ends of the chains and much less at central chain positions (46, 163).

This chapter reports the ^2H NMR spectra of perdeuterononadecane (C_{19}-d_{40}) and nonadecanes specifically labelled at positions two (C_{19}-2-d_2), ten (C_{19}-10-d_2) and at the methyl groups (C_{19}-1,19-d_6). The phase I and phase II spectra indicate very different motions for the chains. The phase II spectra indicate hindered rotation for the chains with a positional dependence to the rotation.

VII.2 Results

Figure 48 A-D, shows the ^2H NMR spectra of C_{19}-d_{40}, C_{19}-10-d_2, C_{19}-2-d_2 and C_{19}-1,19-d_6, at 20°C, in phase I (orthorhombic). The spectrum of C_{19}-d_{40} consists of two Pake doublets, from the methylene and methyl deuterons (164), while the spectra of C_{19}-10-d_2, C_{19}-2-d_2 and C_{19}-1,19-d_6 each consist of a doublet from either the C^2H_2 or C^2H_3 groups.

The bottom part of Figure 48(E-H) shows the ^2H NMR spectra of the four alkanes in phase II (25°C). The quadrupole splittings are substantially reduced, relative to those in the phase I spectra. Also, the spectra exhibit line shapes consistent with an intrinsic or a motionally induced non-equivalence of the principal components of the electric field gradient tensor (47). The values of the quadrupole splittings in phase I, and the phase II spectral features corresponding to the inner splitting and to the separation between the two sets of observed shoulders, are listed in Table 12. In all of the spectra we note the

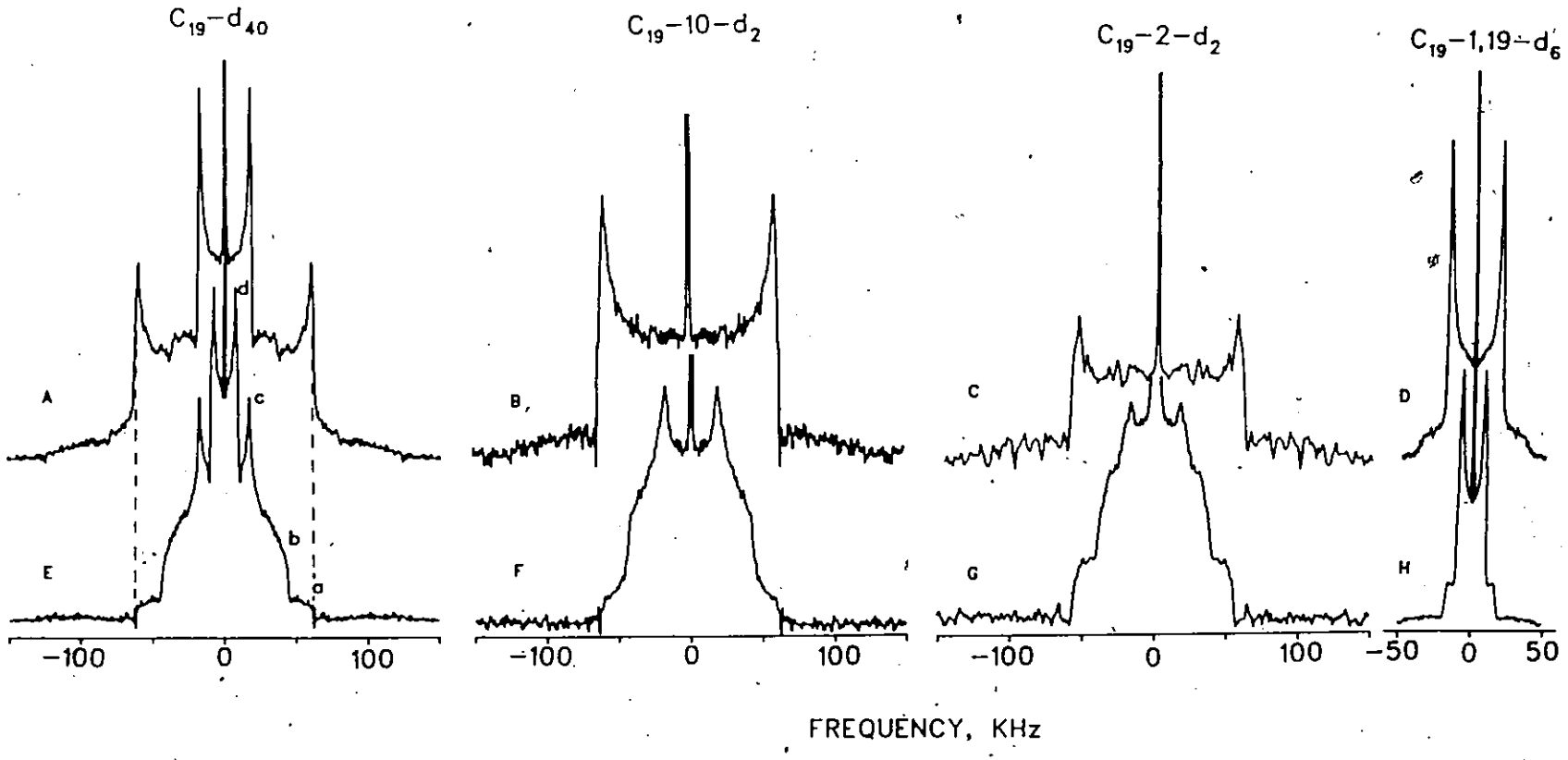

Figure 48. ^2H NMR spectra of phase I (top) and phase II (bottom); $C_{19}-d_{40}$ (A and E); $C_{19}-10-d_2$ (B and F); $C_{19}-2-d_2$ (C and G) and $C_{19}-1,19-d_6$ (D and H). In Figure 48E, a, b, and c represent the spectral features of the methylene deuterons while d represents one of the features of the methyl deuterons.

Table 12

OBSERVED QUADRUPOLE SPLITTING AND SPECTRAL FEATURES (IN kHz)

OF C_{19}-d_{40}, C_{19}-10-d_2, C_{19}-2-d_2 AND C_{19}-1,19-d_6

IN PHASE I AND II

n-Alkane	Phase I (20°C)		Phase II (25°C)			
	C^2H_2	C^2H_3	C^2H_2 Spectral Features	η	C^2H_3 Spectral Features	η
C_{19}-d_{40}	120	35	120; 86; 35	0.43	15.6	
C_{19}-10-d_2	119		119; 84; 37	0.40		
C_{19}-2-d_2	110		119; 74; 35	0.36		
C_{19}-1,19-d_6		36			33.4; 18.8; 15.1	0.11

presence of a narrow central resonance. This peak is of low integrated intensity and is likely due to trace impurities and lattice defects in the sample (47).

VII.3 Discussion

The phase I spectra of the C^2H_2 groups in both C_{19}-d_{40} and C_{19}-10-d_2 are expected from an alkane in a rigid environment. The quadrupole splitting of 119-120 kHz is characteristic of C^2H_2 groups which are static on the ^2H NMR time scale, that is, they are not subject to spatial fluctuations with frequencies greater than 10^5 Hz (47). However, for the deuterons on the penultimate carbon (C_{19}-2-d_2) the quadrupole splitting is only 110 kHz. This is evidence that the ends of the chain in phase I are subject to motional averaging mechanisms which are not operative in the central region of the chain.

The second component of the spectrum of C_{19}-d_{40} in phase I has a quadrupole splitting of 35 kHz. This splitting coincides with that observed in the spectrum of C_{19}-1, 19-d_6 and is assigned to the terminal methyl groups. The reduction in the quadrupole splitting from that observed for the methylene groups results from rapid rotation of the methyl group about the C_3 axis (47). This quadrupole splitting is less than the 40 kHz expected for a methyl group undergoing only C_3 rotation and is consistent with a

further motional averaging mechanism operating on the chain ends. It could also be explained by a distorted tetrahedral arrangement for the methyl group (166). A distortion of approximately 2^{o} could account for the observed quadrupole splitting.

The phase II spectra are characterized by spectral features which are reduced in width compared to those of their counterparts in phase I. The reduction in the spectral features is a consequence of the expansion of the lattice (40), yielding greater intermolecular distance, which allow chain motion about the molecular long axes. However, while the amplitude of this motion is sufficient to reduce the quadrupole splitting it is less than that of a freely rotating chain since the splittings are still larger than 60 kHz. The phase II spectra also exhibit line shapes which suggest that either the three principal components of the electric field gradient tensor are intrinsically different, or that molecular motion occurs which gives rise to three apparently different components (167) (see also Appendix). It is this latter case which gives rise to the spectra observed in phase II.

The degree of motionally induced asymmetry can be measured by an apparent asymmetry parameter, η, defined as

$$\eta = \frac{V_{xx} - V_{yy}}{V_{zz}} \qquad (18)$$

where V_{xx}, V_{yy} and V_{zz} are the principal components of the electric field gradient tensor in the motionally averaged frame of reference. Following convention (47), $V_{zz} > V_{xx} > V_{yy}$ so that η will take values of 0 (no asymmetry) to 1 (greatest asymmetry). The three principal components of the tensor manifest themselves as the spectral features (labelled a, b and c) in Figure 48E and lead to values of η for C_{19}-10-d_2 and C_{19}-2-d_2 of 0.40 and 0.36 respectively. The lower asymmetry of the C_{19}-2-d_2 spectrum indicates that, as in phase I, the amplitude of motion at the chain ends is greater than in the central positions of the chain. The C_{19}-1,19-d_6 spectrum is also asymmetric, with η = 0.11. This also confirms the presence of larger amplitude motions at the chain ends.

Torsional motions involving greater amplitudes near the chain ends provide the most ready explanation of the observed spectral features. It is interesting to note that even in phase I, where the intermolecular distances are minimal and chain packing is such that the chains are interlocked in position, there is an observable difference in the motional behaviour of the chain ends. In phase II, the torsional angles are larger and the spectra are narrower than in phase I, but the amplitudes of motion are again largest at the chain ends.

Rapid gauche-trans isomerisation will also narrow ^2H NMR spectra and the effect of this type of motion on ^2H NMR spectra of gel state lipid bilayers has been analyzed (117). In the case of phase II nonadecane the concentration of gauche bonds is low (39, 45, 46) and localized at the end of the chain (46). It is possible that rapid gauche-trans interconversion contributes to a general narrowing of the phase II spectrum of C_{19}-2-d_2, but better spectra, and several labelled positions are needed to clarify this.

However, torsions will eventually create gauche bonds, thus a clear distinction between these two motional mechanisms cannot be made. In the context of the present work torsional motions alone can account for the results, especially when considering the case of phase I, where no gauche defects have been found. Further studies involving variations in both chain length and temperature will contribute to our understanding of the characteristics of phase II n-alkanes.

VII.4 Simulations

We have used spectral simulation in order to compare the experimental spectra with those expected for different types of motion (47, 167). The results of the simulations are shown in Figure 49.

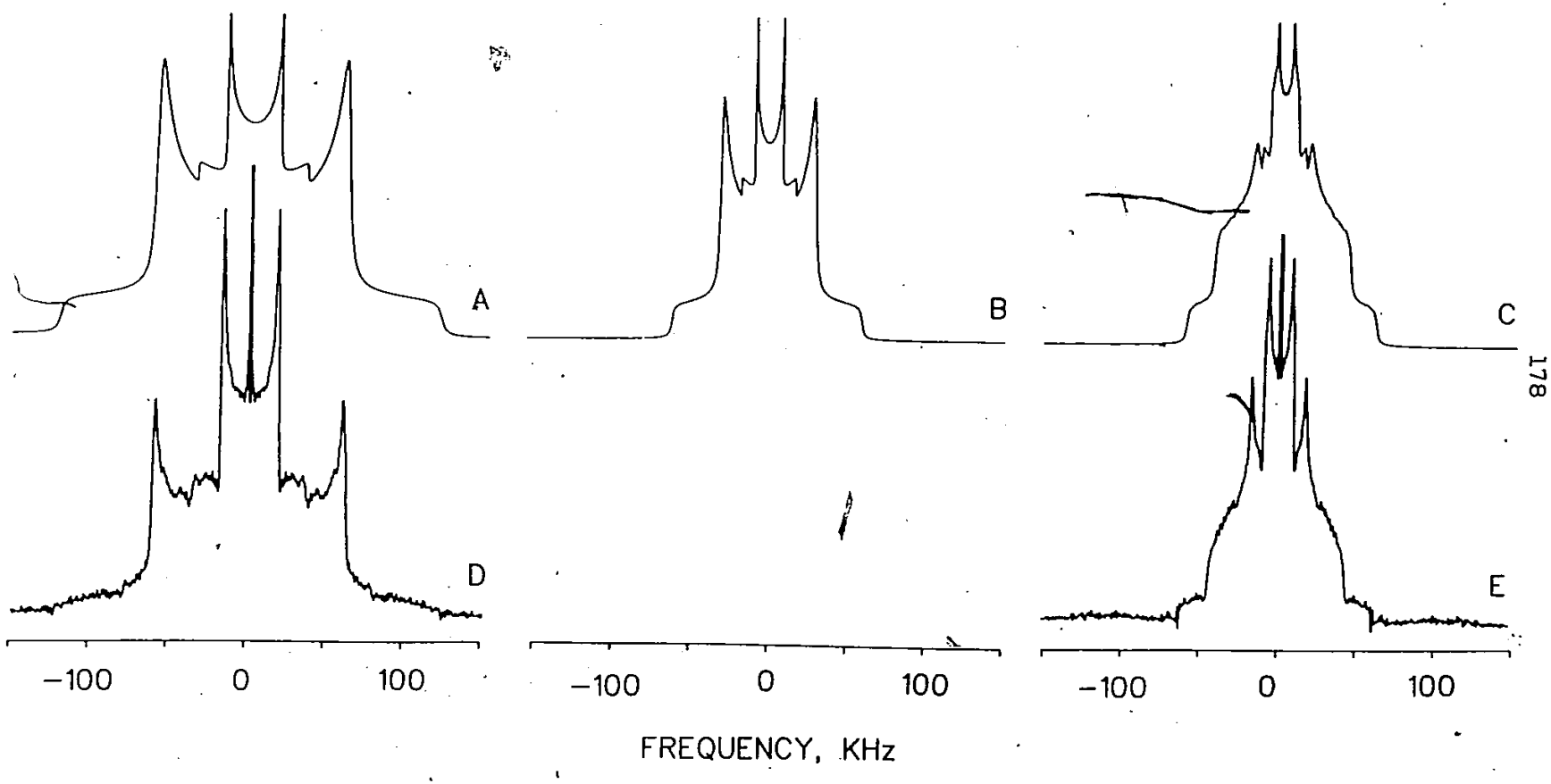

Figure 49. Simulated ^2H NMR spectra of $C_{19}-d_{40}$ A) phase I; B) fully rotating chains (hexagonal); C) very fast 62° jumps between two equivalent sites. Parts D and E are a reproduction of A and E of Figure 48.

Figure 49A shows the spectrum calculated by assuming a set of 34 rigid methylene deuterons and six methyl deuterons rotating about their C_3 axis. This is the spectrum expected for C_{19}-d_{40} in phase I. The agreement with the experimental spectrum is good except for differences in the relative intensities of the two components. There are three possible sources of this discrepancy. Firstly, we have used arbitrary values for the component linewidths in the simulations so that the relative vertical intensities of the methyl and methylene signals may be aberrated. A second source is the distortion which results from an inability to provide equal excitation across the width of the pattern (94). The observed intensity is progressively attenuated as the frequency separation from the central frequency is increased (e.g., Figure 48A). Finally, the C_{19}-2-d_2 alkane shows a quadrupole splitting of 110 kHz and hence our assumption of 34 rigid deuterons is not completely correct. Nonetheless, the results confirm that most of the methylene deuterons are in a rigid environment.

In order to emphasize the point that the motion in phase II is hindered, we have calculated the spectrum expected for freely rotating chains, that is, a phase with true axial symmetry (hexagonal). The result is shown in Figure 49B. The spectral shape is well defined, without the rounded shoulders of the experimental spectrum (Figure 48E and 49E).

The phase II spectra were simulated by adopting a restricted jump model (167), previously employed in the analyses of ^{1}H NMR (42) and inelastic neutron scattering experiments (43), in which no distinction between different positions in the chain was possible. In this model the alkane chain remains all-trans and reorientation occurs by random, restricted jumps between two equivalent sites on a circle located in the plane perpendicular to the long axis of the chains (see Appendix for further details). While our results point to a positional dependence of motional amplitude, the rigid chain, restricted jump model provides a first approximation for comparison with the experimental spectra.

A variety of jump angles were used to simulate the spectrum. The results shown in Figure 49C represent the best fit to the experimental data and were obtained using a jump angle of 82°. A comparison of the features, in Figures 49E and 49C, shows that the calculated spectrum of the $C^{2}H_{2}$ groups agrees well with the experimental spectra of n-$C_{19}D_{40}$ and C_{19}-10-d_{2}. That is, the spectrum of the bulk of the methylene groups is well reproduced. However, the ^{2}H NMR spectrum of the methyl groups is not reproduced adequately with the simple restricted jump of 82°. The observed $C^{2}H_{3}$ spectrum is characteristic of a higher symmetry ($\eta = 0.11$) than the calculated one ($\eta = 0.27$). In addition,

there is not conservation of the tensor component parallel to the chain axis (27.6 kHz). This indicates off C_3-axis motion which, together with torsions are the most likely causes of the differences between the spectra of the centre and the ends of the chain.

Finally, although a single 82° jump provides a reasonable simulation of the central methylene deuterons, we cannot exclude the possibility that the alkane reorients by restricted jumps between several sites. Rapid jumping between several sites could also lead to a spectrum consistent with the experimental data.

VII.5 Conclusions

The picture of the phase I structure of nonadecane that emerges from this study is one in which most of the central portion of the chain is constrained in a rigid crystalline structure and is virtually immobile on a time scale of 10^{-5} s. However, the methyl component of the C_{19}-d_{40} spectrum, and the spectra of C_{19}-2-d_2 and C_{19}-1, 19-d_6, indicate that there are motions near the ends of the chains which cause the observed reduction in the quadrupole splittings.

The phase II spectra reflect the large amplitude rotational motions of the chains and confirm that chain rotation is hindered. As in phase I, comparison of the

labelled compounds demonstrates higher amplitudes of motion at the ends of the chains than at the centre, and torsional motion of the chains provides the most ready explanation. Finally, the simplest model which would explain the behaviour of the central methylene groups is one involving hindered rotation of the chains between sites 82^{o} apart. However, the spectral contributions from the ends of the chains are not reproduced adequately with an 82^{o} jump, confirming our view that the alkane chain does not behave like a rigid rotor.

CHAPTER VIII

MOLECULAR MOTIONS IN THE SOLID PHASES OF C_{21} AND C_{35} n-ALKANES

VIII.1 Introduction

The ^2H NMR studies on deuterated nonadecanes (C_{19}), reported in Chapter VII, provide several new insights into chain motions in the solid state. In phase I the chains are rigid on the ^2H NMR time scale, however, there is evidence of torsional motions at the ends of the chains. The phase II results can be modelled in terms of an alkane chain undergoing fast ($>10^7$ sec^{-1}), 82^o jumps between equivalent sites. However, the results also indicate that these chains do not reorient as a rigid rotater. Rather, the ends of the chain undergo higher amplitude torsional motions than the centre.

For n-alkanes longer than C_{23} there are from one to three other solid phases between phase I and phase II (38, 39, 44). These phases are characterized by increases in the concentration of non-planar alkanes, but there is no hindered rotation. This hindered rotation is limited to the last solid phase observed prior to melting (phase II), but the phase exists over a narrower temperature range than found for shorter alkanes.

In all of the n-alkanes, phase II is also characterized by the appearance of gauche rotamers (38, 39, 46, 169). These rotamers are localized at the ends of the chains and IR studies have shown that the gauche population increases towards the end of the chain and with increasing temperature within phase II (46). As many as 8% of the chains contain a gauche rotamer at the 2 position, just prior to the phase II melt (see Figure 8).

In the present work, the temperature dependence of the ^2H NMR spectra of several specifically deuterated C_{21} n-alkanes was examined. The heneicosanes were specifically deuterated at positions eleven (C_{21}-11-d_2), six (C_{21}-6-d_2), four (C_{21}-4-d_2) and two (C_{21}-2-d_2) and the ^2H NMR spectra were acquired at several temperatures, in both phase I and II. As with the work on nonadecane, the phase II spectra are characteristic of chains undergoing rapid, restricted jumps about their long axis. The spectra in phase II correlate well with the gauche populations reported in a recent IR study of these compounds (46). As well, extra torsional motions are present at the chain ends which are not present at the centre, and these motions increase with temperature. In phase I, the central portion of the chain is rigid on the ^2H NMR time scale (10^5 sec^{-1}); however, at positions 2 and 4 there is evidence of torsional motions which persist down to $-20^{\circ}C$. We have also studied a

specifically deuterated C_{35} n-alkane (C_{35}-18-d_2) in several of its solid phases.

VIII.2 Results and Discussion

C_{21} Alkanes in Phase I

The phase I spectra of C_{21}-11-d_2 and C_{21}-6-d_2 both show broad quadrupole patterns with quadrupole splittings of 122 kHz. These splittings are characteristic of C^2H_2 groups which are static on the ^2H NMR time scale, that is, they are not subject to large amplitude motions on a time scale of $>10^5$ s^{-1} (47). For positions 2 and 4 the quadrupole patterns are reduced in width from that of the rigid limit, indicating the presence of rapid motions. The quadrupole splittings at 25°C, which is below the phase I - phase II transition of 32.5°C, are plotted in Figure 50 as a function of chain position. This reduction in quadrupole splittings at the ends of the chain was also noted in our earlier work on nonadecane. A quadrupole splitting of 110 kHz was measured for C_{19}-2-d_2 just below the phase I - phase II transition.

On careful examination of the C_{21}-2-d_2 and C_{21}-4-d_2 spectra it is apparent that the spectra have a non-zero asymmetry parameter (η). This asymmetry arises from an intrinsic or a motionally induced non-equivalence of the principal components of the electric field gradient tensor

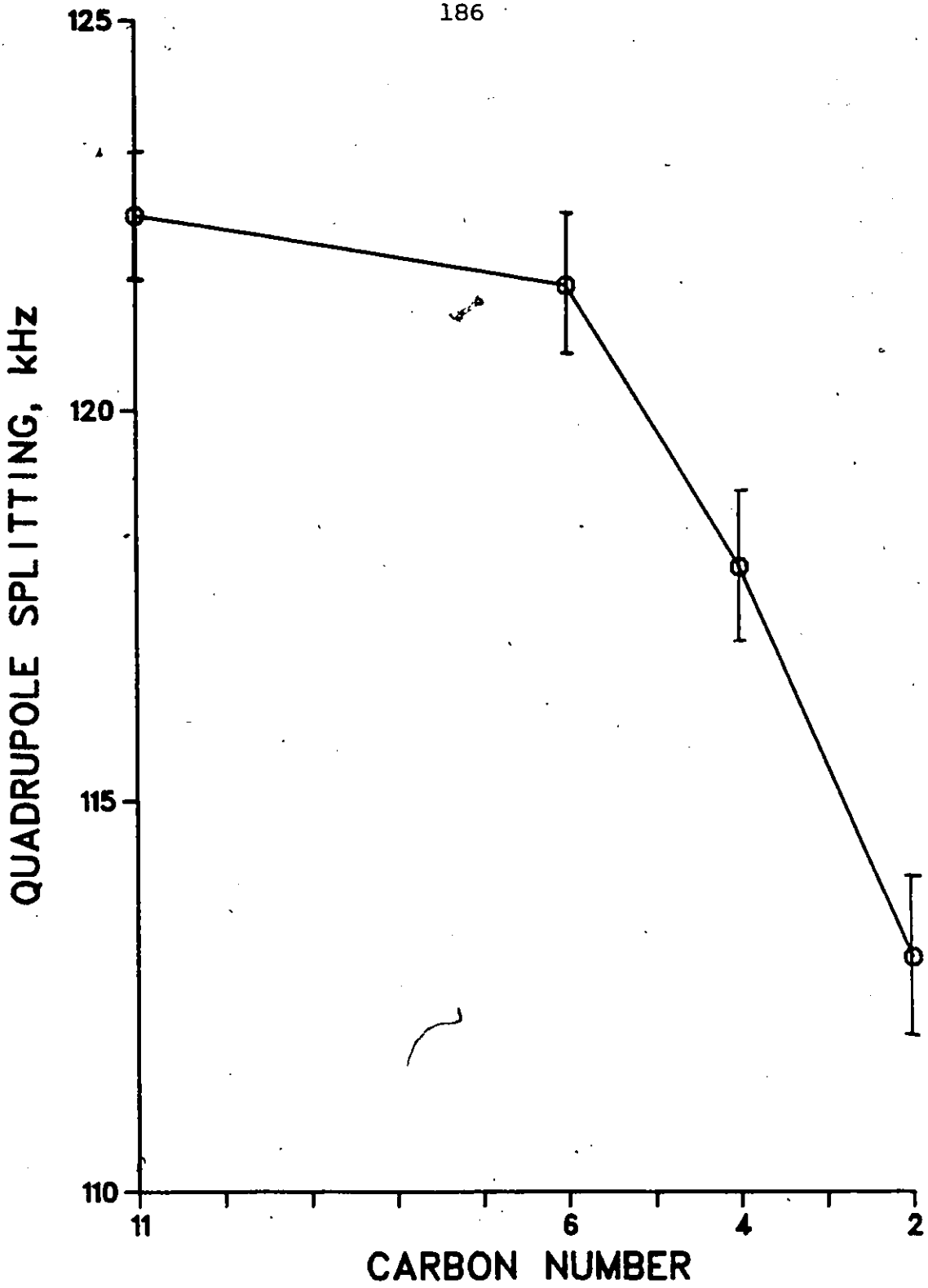

Figure 50. Variation of the quadrupole splitting with chain position for the C_{21} alkanes at 25°C.

(47). The asymmetry is most pronounced at the 2 position just prior to the transition to phase II. Figure 51 shows the spectra of C_{21}-2-d_2 at 25°C and at -30°C. The -30°C spectrum is consistent with the rigid limit spectra obtained for C_{21}-11-d_2 and C_{21}-6-d_2 and indicates that there is no motion on the ^2H NMR time scale. On warming the sample from -40°C to 30°C (just below phase II) the asymmetry parameter increases from $\eta = 0$ to $\eta = 0.06$. Figure 52 shows the variation of the V_{xx} component of the tensor (the quadrupole splitting in the rigid limit) with temperature. It is clear that the motions which average the electric field gradient tensor persist down to at least -20°C.

The observed asymmetry may indicate small angle jumps, for the chain ends, about the alkane long axis. The effect of rapid jumps, between equivalent sites, in a plane perpendicular to the long axis of an alkane chain has been modelled for the C_{19}'s. The components of the electric field gradient tensor (V_{xx}, V_{yy}, V_{zz}), in the two static orientations, before and after a jump of angle θ, can be transformed and averaged into a jumping frame tensor (V^J). The resulting components of the jumping frame tensor will therefore be:

$$V^J_{xx} = V_{xx} \cos^2 \frac{\theta}{2} + V_{zz} \sin^2 \frac{\theta}{2} \qquad (19)$$

$$V^J_{YY} = V_{yy} \qquad (20)$$

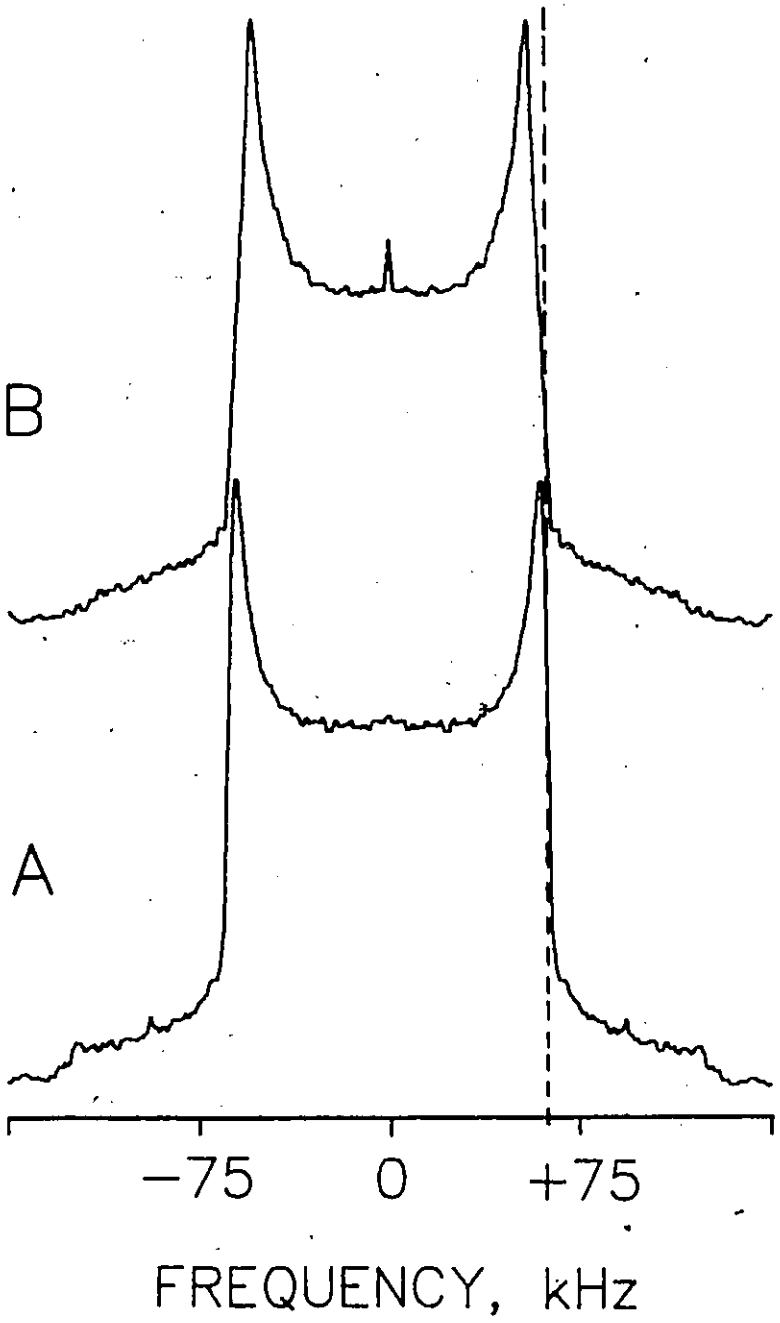

Figure 51. ^2H NMR spectra of C_{21}–2–d_2 at A) −30 °C and B) 25 °C. The broken line is at the rigid limit quadrupole splitting of 122 kHz.

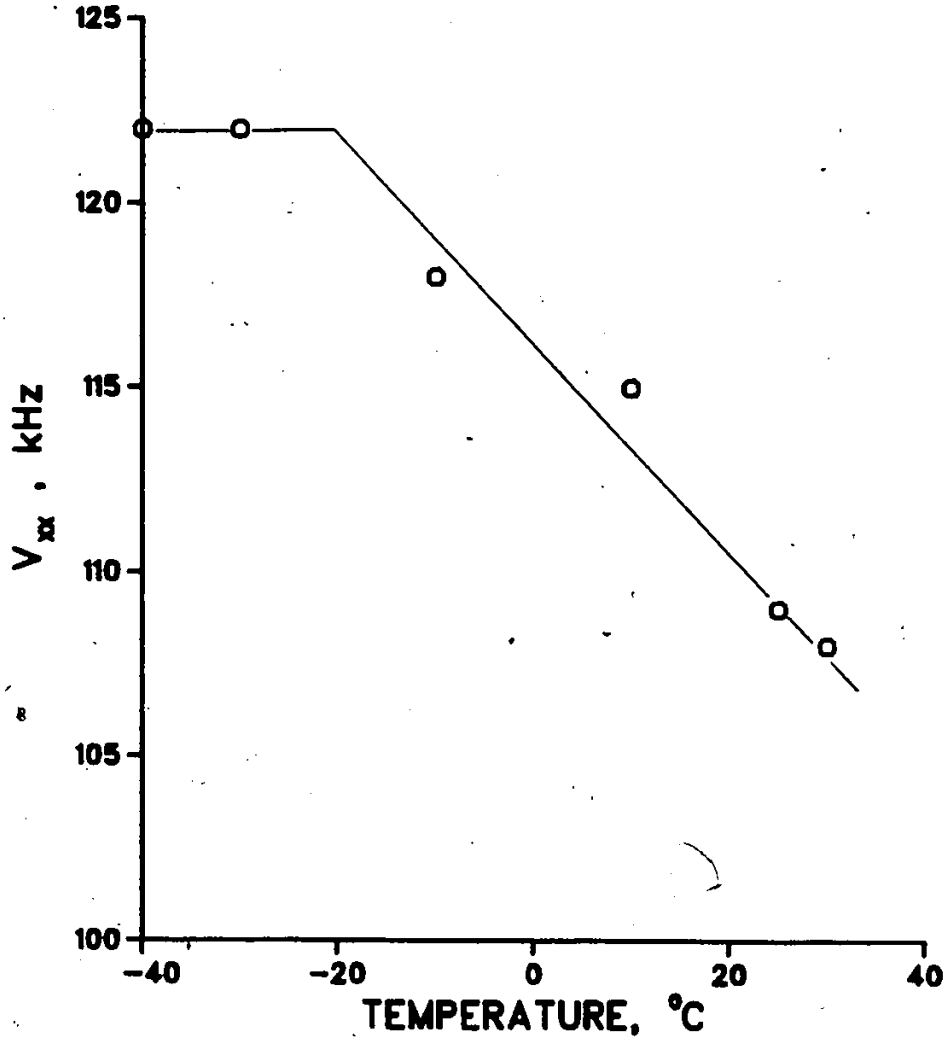

Figure 52. Variation of V_{xx} (quadrupole splitting for rigid limit spectra) with temperature for C_{21}-2-d_2

$$V_{zz}^{J} = V_{xx} \sin^2 \frac{\theta}{2} + V_{zz} \cos^2 \frac{\theta}{2} \qquad (21)$$

For C_{21}-2-d_2, at 25°C, the spectrum has an asymmetry of $\eta = 0.06$ and this corresponds to a jump angle of 22°. For position 4, at the same temperature, the spectrum shows an asymmetry of $\eta = 0.03$ which corresponds to a jump of approximately 10°. The asymmetry observed in the phase I spectra of C_{21}-2-d_2, C_{21}-4-d_2 and C_{19}-2-d_2 indicates that the ends of the chains are subject to small angle jumps which increase in size towards the end of the chain. These jumps are fast relative to 10^5 sec^{-1} and suggest chain packing defects which allow room for some motion. It is possible that the observed, slightly non-tetrahedral, arrangement for the methyl groups of alkanes (166) gives sufficient room for these extra jumping motions to occur.

C_{21} Alkanes in Phase II

In phase II, the spectral features are substantially narrowed from those observed in phase I and the line shapes are characteristic of a non-zero asymmetry parameter (47). This asymmetry has been demonstrated to arise from rapid ($>10^5$ sec^{-1}) jumps of the alkane chains about their long axis. The chain deuterons, subjected to such motions, have their electric field gradient tensor averaged according to Equations 19-21 and the result is a spectrum with a measurable

asymmetry parameter. Convention dictates that $V_{zz} > V_{xx} > V_{yy}$, so it is important to remember that the averaging caused by large jumps will make V^J_{xx} and V^J_{zz} less than V^J_{yy} for some jump angles. In fact, for all of the alkanes studied to date, all of the phase II spectra show x and z tensor components less than the y component. Convention thus requires a rotation of the axis system which simply changes the label assigned to the tensor component. This results in V^J_{yy} being relabelled V_{zz}, V^J_{zz} being relabelled V_{xx} and V^J_{xx} being relabelled as V_{yy}. These three spectral features are labelled as a, b and c respectively in Figure 53.

Figure 53 shows the 33°C and 39°C spectra of C_{21}-11-d_2. At both of these temperatures the alkanes exist in phase II, but it is clear that the degree of asymmetry is decreasing with increasing temperature. This is indicative of an increase in the jump angle from 82°, when $\eta = 0.41$, to 86°, when $\eta = 0.21$. The phase II spectra of all four labelled C_{21} alkanes were recorded at five temperatures in phase II and the η values are plotted in Figure 54 as a function of temperature. It is clear that the value of η decreases with temperature for all positions and there is also a decrease in η as you move towards the chain ends. These observations suggest increasing jump angles with temperature, and increasing jump angles for the chain ends.

In both spectra of C_{21}-11-d_2 the shoulders (marked with the broken line in Figure 53) are at 122 kHz. This

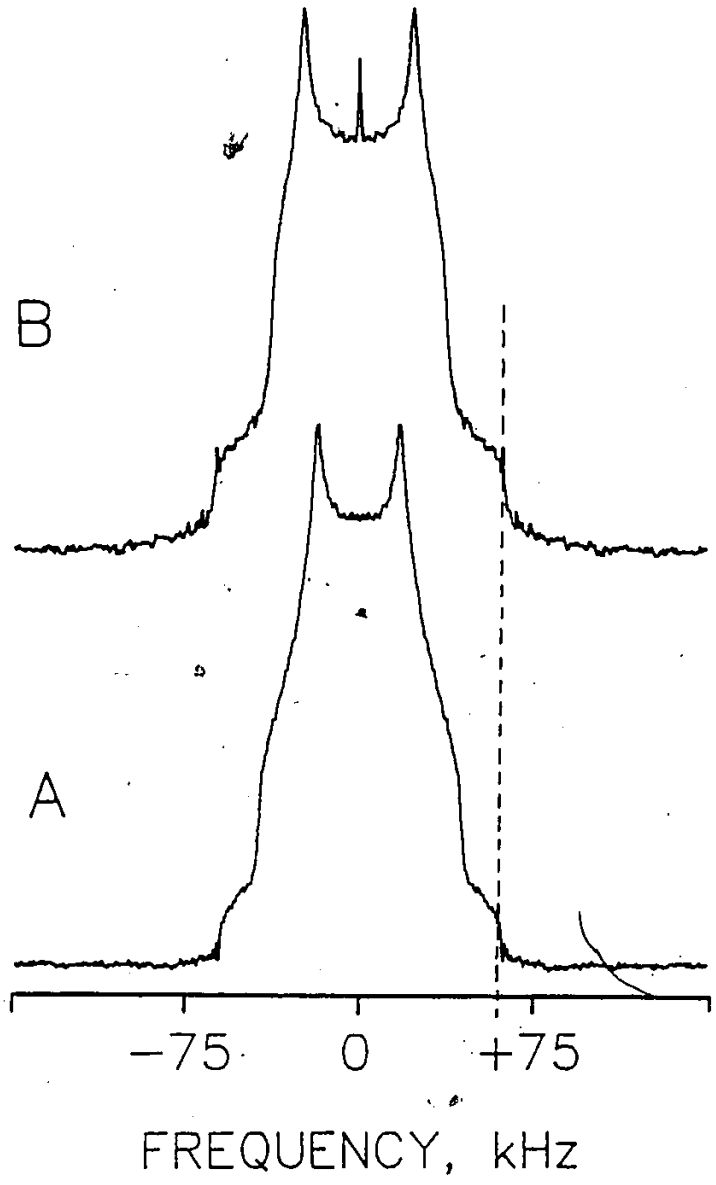

Figure 53. ^2H NMR spectra of C_{21}-11-d_2 at A) 33°C and B) 39°C. The broken line at 122 kHz is the V_{YY}^J component.

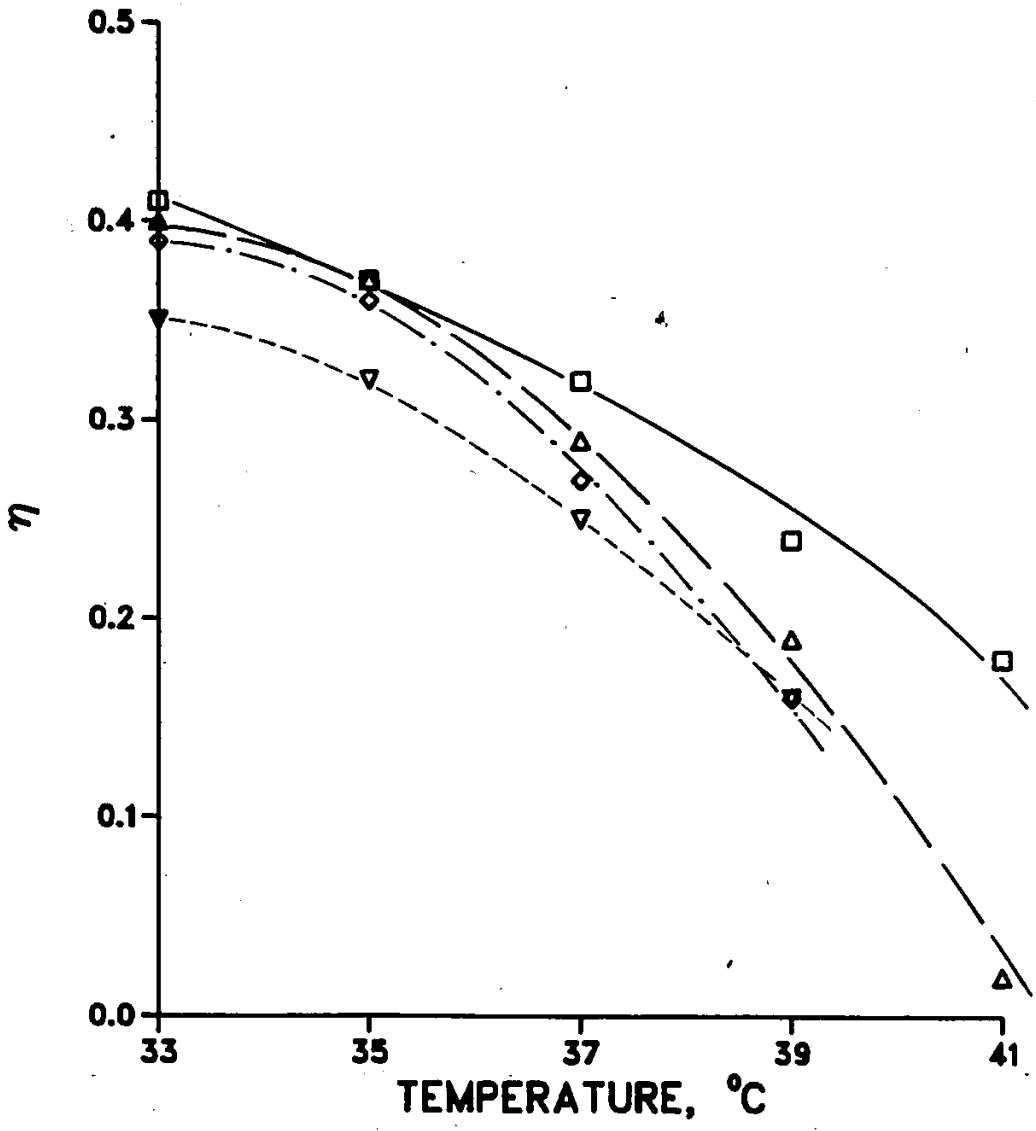

Figure 54. The variation of the asymmetry parameter η, with temperature for the four labelled positions. C_{21}-11-d_2 □ , ———— ; C_{21}-6-d_2 △ , — — — ; C_{21}-4-d_2 ◇ , —·—·— ; C_{21}-2-d_2 ▽ , --------.

represents the component of the electric field gradient which lies along the chain long axis. This component should be invariant with position if there is no motion perpendicular to the chain long axis. This is certainly the case for the central positions of the chain, however, for position 2 it is clear that the 122 kHz component is not conserved (see Figure 55). Furthermore, this off-axis motion becomes more pronounced with temperature. Values of the V^J_{yy} component are plotted in Figure 56 as a function of temperature, in phase II. Clearly, there is little or no off-axis motion in the centre of the chain, but at positions 2 and 4 this motion is quite pronounced. This off-axis motion was also noted for the 2 position of the C_{19} alkane.

Phase II is characterized by the appearance of gauche rotamers in the chain. At position 2 of the C_{21} chain and at 33°C, 4% of the chains have a gauche rotamer adjacent to position 2 (46). As the temperature is increased to 39°C, approximately 9% of the chains have gauche conformer adjacent to the 2 position. These concentrations quickly fall off to less than 1% for positions 6 through to the centre. These fast, trans-gauche interconversions will contribute substantially to the observed reduction of the V^J_{yy} component in phase II. The effect of gauche rotamers on the ^2H NMR spectra of specifically

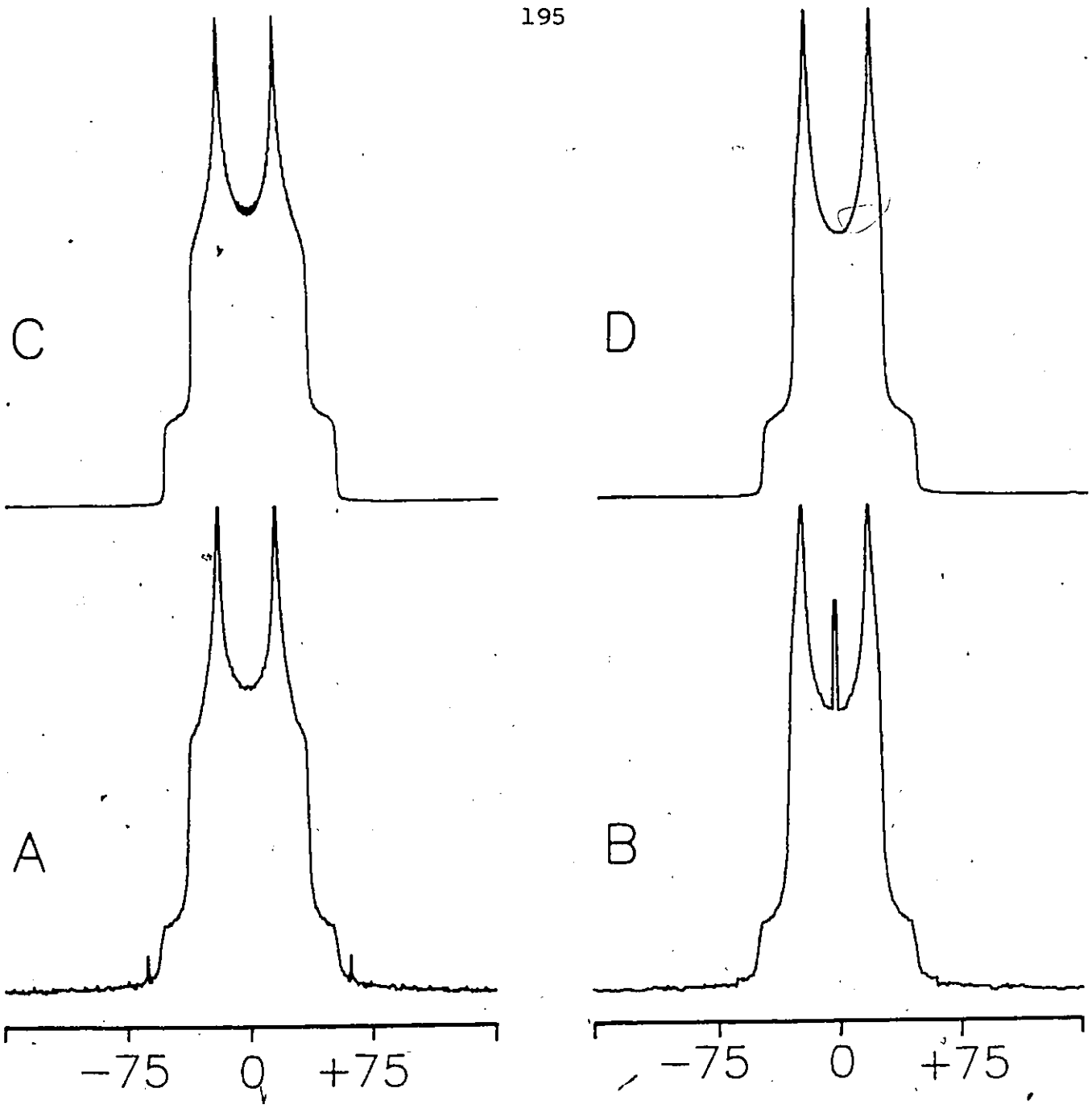

Figure 55. ^2H NMR spectra of C_{21}-2-d_2 at A) 33°C and B) 39°C. Simulations are of the 33°C spectrum C) V_{YY}^J = 105 kHz, η = 0.35, linewidth of 500 Hz, and the 39°C spectrum D) V_{YY}^J = 92.8 kHz, η = 0.16, linewidth = 750 Hz.

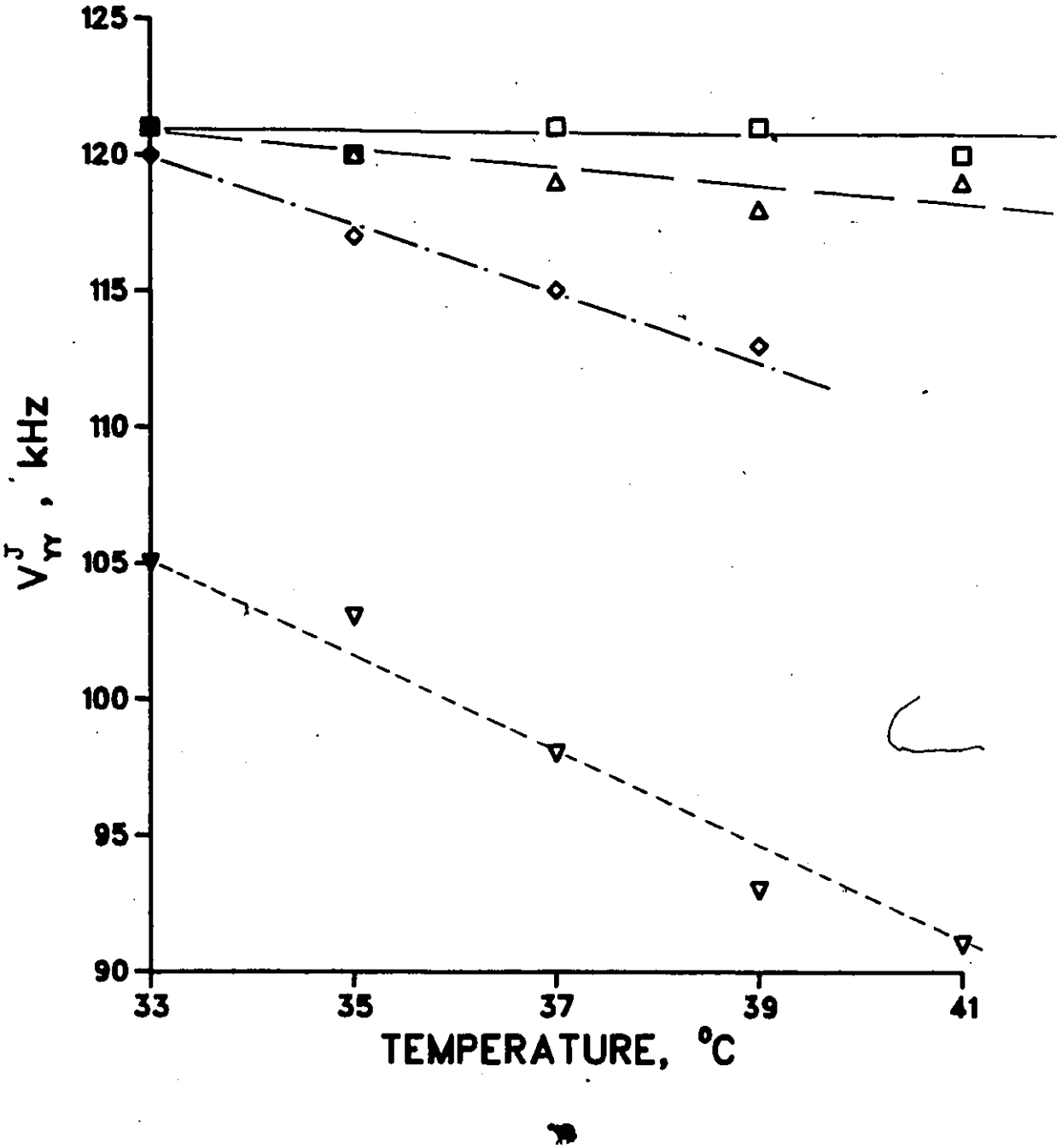

Figure 56. Variation of the V_{YY}^J component of the jumping frame tensor with temperature for the four labelled C_{21}'s. C_{21}-11-d_2, □, ———— ; C_{21}-6-d_2, △, — — —; C_{21}-4-d_2, ◇, —·—·—; C_{21}-2-d_2, ▽, ---------.

deuterated dipalmitoylphosphatidylethanolamines, in the gel phase, has been modelled recently (117). Rather than showing the 120-125 kHz quadrupole splittings expected for acyl chains in a rigid, all-trans environment, the quadrupole splittings decreased with position down the chain. Simulations of the spectra indicated that gauche probabilities of from 1 to 7% could account for the reduced splittings. The observed quadrupole splittings and the calculated gauche probabilities of DPPE correlate very well with the gauche probabilities in the C_{21}'s (46) and the V^J_{yy} components observed in the phase II spectra of this study.

The spectra of the C_{21} n-alkanes in phase II, were simulated by first assuming that rapid trans-gauche isomerization reduces the values of the electric field gradient tensor. These values can be obtained from the shoulders of the phase II spectra, which are invariant to rotation and reflect the influence of gauche rotamers discussed earlier. The phase II spectra were then simulated by assuming rapid jumps of the methylene deuterons in a plane perpendicular to the chain long axis (169). For all the spectra in phase II, different jump angles were required. The angles ranged from 82° for C_{21}-11-d_2 at $33^{\circ}C$ to 89° for C_{21}-2-d_2 at $41^{\circ}C$. It was also necessary to use progressively smaller component linewidths on preceeding to the ends of the chains. This suggests a larger spin-spin relaxation time (T_{2e}) for the

C_{21}-2-d_2 than the C_{21}-11-d_2. The spin-spin relaxation time is sensitive to motions near the deuterium resonance frequency (46.063 MHz), as well as to slower motions. For the chain ends, the torsional motions or trans-gauche isomerizations, which are not present in the centre of the chain, may account for the T_{2e} variation.

Simulations of C_{21}-2-d_2 at temperatures of 33° and 39°C are shown in Figure 55. The simulations are in good agreement with the experimental spectra except for the intensity of the shoulder. The intensity of the shoulder in the experimental spectra is less than in the simulations; this is likely a reflection of pulse roll-off and the inability to provide uniform and complete excitation across a wide pattern (97).

C_{35}-18-d_2

For n-alkanes longer than 23 carbons there are more than two solid phases (39). Spectra of C_{35}-18-d_2 in all the solid phases, but phase II, show only a rigid limit Pake doublet (see Figure 57). This indicates that for the central portions of the C_{35} alkane chain there is no difference which can be observed by deuterium NMR. Studies of n-tritriacontane (n-C_{33}) have shown that the phases between phase I (orthorhomic) and phase II are characterized by the onset of pure 180° rotational jumps (170, 171). If this is the case, and if the jumps are fast (47), the

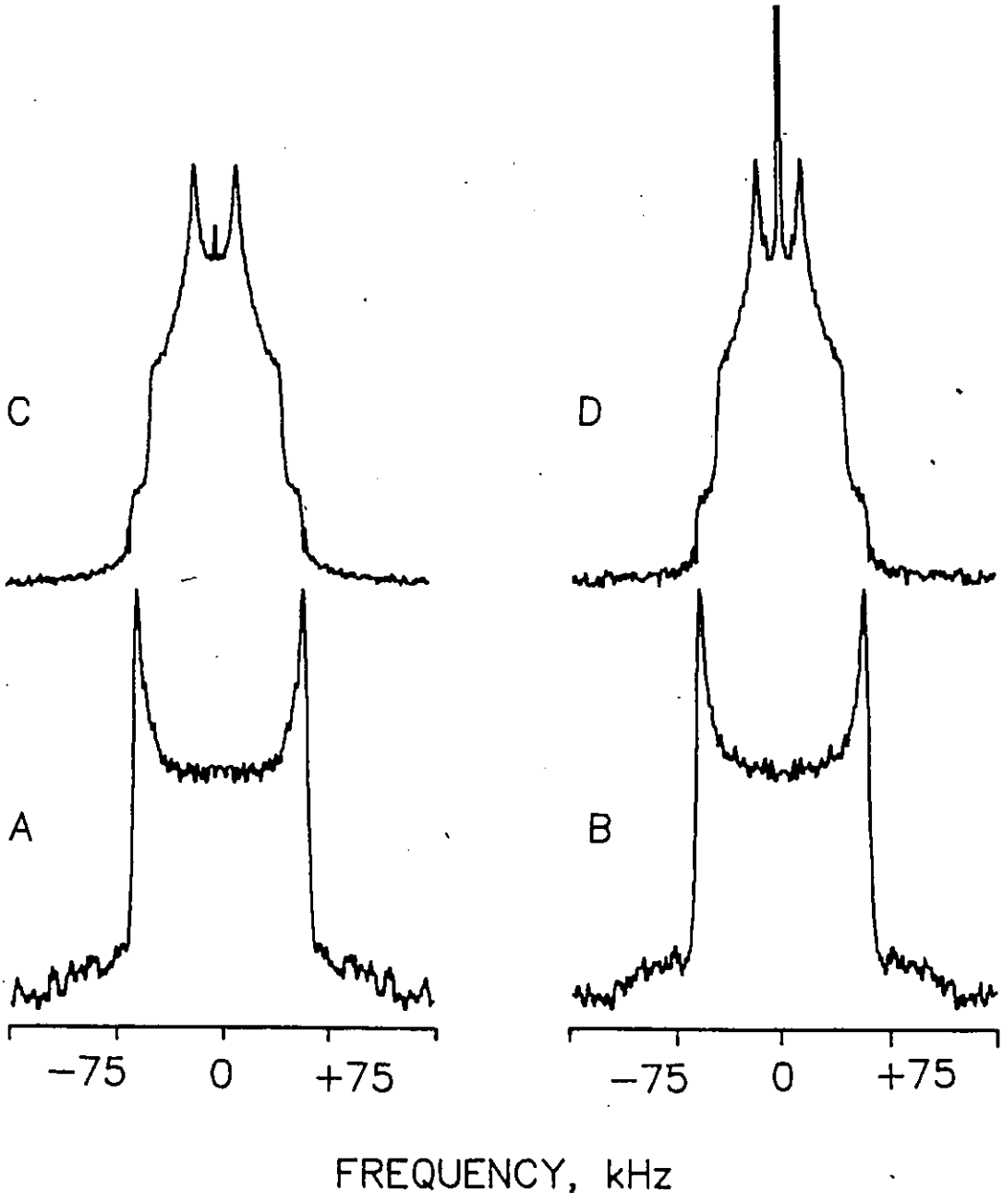

Figure 57. ^{2}H NMR spectra of C_{35}–18–d_2 in A) phase IV, B) phase III, C) phase II at 73 °C and D) phase II at 75 °C.

components of the electric field gradient tensor would be interchanged. This would have the ^2H NMR spectrum apparently unchanged, since the signs of the tensor components cannot be determined.

Phase II for the C_{35} alkane exists over only a 2^o temperature range, prior to melting. The phase II spectra show lineshapes like those observed for the C_{21} n-alkane, however, the asymmetry is larger ($\eta = 0.51$) indicating a jump of 80^o. Like $C_{21}11\text{-}d_2$ the degree of asymmetry increases with temperature, although over a much narrower range. Furthermore, the component of the tensor along the chain long axis is conserved, indicating no off axis motion in the centre of the chain.

VIII.3 Conclusion

In the low temperature, phase I, of the C_{21} n-alkane the central portion of the chain, from carbon 6 to carbon 16 is rigid on the ^2H NMR time scale. However, there is clear evidence for motion at the ends of the chains. These motions are consistent with small angle jumps which increase in size towards the end of the chain. These motions are seen to persist down to -20^oC at the 2 position.

The C_{21} alkane chain in phase II undergoes hindered rotation, but not as a rigid rotator. The chains undergo jumps of 82^o at the centre, but this increases slightly

starting at carbon 6, and reaches 86° for the final methylene. The jump angle is also observed to be temperature dependent in phase II. As the temperature is increased, from just above the phase I - phase II transition to just below the phase II-melt transition, the jump angle increases by approximately 4°. Superimposed on this chain jumping is an off axis motion which effects the final four carbons. It manifests itself in a reduction of the component of the electric field gradient tensor oriented along the chain long axis and it appears to correlate well with the appearance and concentration of gauche rotamers.

For the C_{35} n-alkanes, ^2H NMR cannot distinguish any differences in the central portion of the chain for the various low temperature phases. In phase II the C_{35} undergoes restricted jumps, like the C_{19} and C_{21} alkanes, but with a slightly smaller jump angle.

CHAPTER IX

CONCLUSION AND THOUGHTS FOR FUTURE WORK

IX.1 Anesthetics

The studies of the interaction of the local anesthetics tetracaine and procaine with model membranes have proven quite successful. The exchange of TTC and PRC between model bilayers of phosphatidylethanolamine and water is slow on the ^2H NMR time scale ($<1 \times 10^3$ sec^{-1}). The location of the binding site appears to be governed by the molecular shapes of PE and TTC or PRC and not the charge on the anesthetic. For TTC this binding site involves penetration into the hydrocarbon region, while for PRC the binding site appears to be in the headgroup region only. The major manifestation of the charge on TTC is in the observation of slow lateral diffusion for TTC in PE bilayers, at low pH. The ^2H NMR of labelled TTC, at pH 5.5, shows line shapes which indicate an angular-dependent T_{2e}, while spectra recorded at pH 9.5 have an angular-independent T_{2e}. The ^2H NMR of the labelled PE, with low TTC concentrations, shows two domains of lipid at pH 5.5; one domain of free lipid and one of lipid in contact with TTC. Both of these observations correlate with a slow lateral diffusion of TTC through the PE bilayer, when TTC is charged.

The interaction of TTC and PRC with phosphatidylcholine has been reexamined in order to clear up uncertainty arising from the difficulties in attaining a true equilibrium of the anesthetic between water and lipid (58, 59, 61). The results are supportive of the 3 site model for TTC exchange proposed earlier by Boulanger et al. (58, 59). Tetracaine is in slow exchange between a strongly bound site and a weakly bound site and in rapid exchange between the weakly bound site and free in solution. Unlike the PE model system, the location of TTC in the strongly bound site appears to be governed by the charge on TTC. This is likely a result of the approximately cylindrical shape of PC which has no influence on the wedge shaped TTC molecule.

The studies of the interaction of TTC and PRC with membranes of human erythrocytes and *Acholeplasma laidlawii* B were somewhat disappointing. The exchange rates of the anesthetics between membrane bound and free sites are fast, and quadrupole patterns for the labelled anesthetics are not observed. The increased linewidths for TTC-d_3 and TTC-d_2 labels, relative to TTC-d_6, suggests that the TTC penetrates only partially into the bilayer. The dimethylamino moiety of TTC is therefore located outside of the bilayer where it is subject to increased motional averaging. The results of the deuterated membrane studies confirm that TTC penetrates into the bilayer in large concentrations. This is in sharp

contrast to Conrad and Singer's recent model of the membrane (155, 156) and suggests that the 'internal pressure' proposed by the authors is not present.

In order to extend the model studies, an examination of the interaction of TTC and PRC with model bilayers of phosphatidylserine would be appropriate. Since PS has a net negative charge, it will have characteristics very different from PC or PE. The influence of Ca^{2+} and Mg^{2+} on the anesthetic/lipid systems would also be an interesting extension to this work. Since there are high cation concentrations in real nerves they could have a profound influence on the anesthetic binding and exchange. Finally, studies of PE/PS mixtures with TTC and PRC would be interesting since PE and PS are found on the inside of real membranes.

Future studies on the interaction of anesthetics with real membranes are more difficult. Since the anesthetic exchange rate appears to be much faster in real membranes, further studies could prove difficult. One possibility would be to go to an anesthetic with a bulkier hydrophobic group. Such an anesthetic may exchange more slowly and, thus, be more accessable to study by ^{2}H NMR.

IX.2 Alkanes

The studies of the solid phase-behaviour of long n-alkanes have been quite successful. Previously unobserved motions in the low temperature, orthorhombic phase (phase I)

have been detected. These motions are limited to the final 4 or 5 carbons of the chain and might involve small angle jumps which increase in size as the end of the chain is approached.

In the high temperature phase (phase II) the alkanes are observed to reorient by rapid ($\simeq 82^{o}$) jumps. The chain behaves as a non-rigid rotor, exhibiting higher amplitude jumps at the chain ends. The component of the electric field gradient tensor parallel to the chain long axis shows increased modulation as the label approaches the end of the chain. This appears to correlate well with the recently detected gauche rotamer populations (46).

Future studies of the alkanes should include more careful modelling of the molecular motions, including both the reorientational jumps of the chain and the gauche populations. Relaxation studies of the alkanes might also prove interesting. Finally, studies of even number n-alkanes, n-alkane mixtures and substituted alkanes could be attempted.

APPENDIX

SIMULATION OF THE ^2H NMR SPECTRUM OF C_{19}-d_{40} IN PHASE II

In order to simulate the spectrum of C_{19}-d_{40} in phase II we have assumed that the molecules reorient by random, restricted jumps about the chain long axis. If the jumping is fast (~10^{-9}-10^{-12}s) (42, 43) relative to the ^2H NMR time scale an electric field gradient tensor corresponding to a jumping frame of reference can be calculated. Tensors, corresponding to the two static orientations before and after a jump of angle θ, can be transformed and averaged into this jumping frame (172). For the coordinate system shown in Figure 58, jumps about the chain long axis will leave the component of the tensor in the y direction unchanged. Jumping will cause averaging of the x and z components. The resulting jumping frame tensor (V^J) is diagonal and has the following principal components:

$$V^J_{xx} = V_{xx}\cos^2\frac{\theta}{2} + V_{zz}\sin^2\frac{\theta}{2} \qquad \text{(A1)}$$

$$V^J_{yy} = V_{yy} \qquad \text{(A2)}$$

$$V^J_{zz} = V_{xx}\sin^2\frac{\theta}{2} + V_{zz}\cos^2\frac{\theta}{2} \qquad \text{(A3)}$$

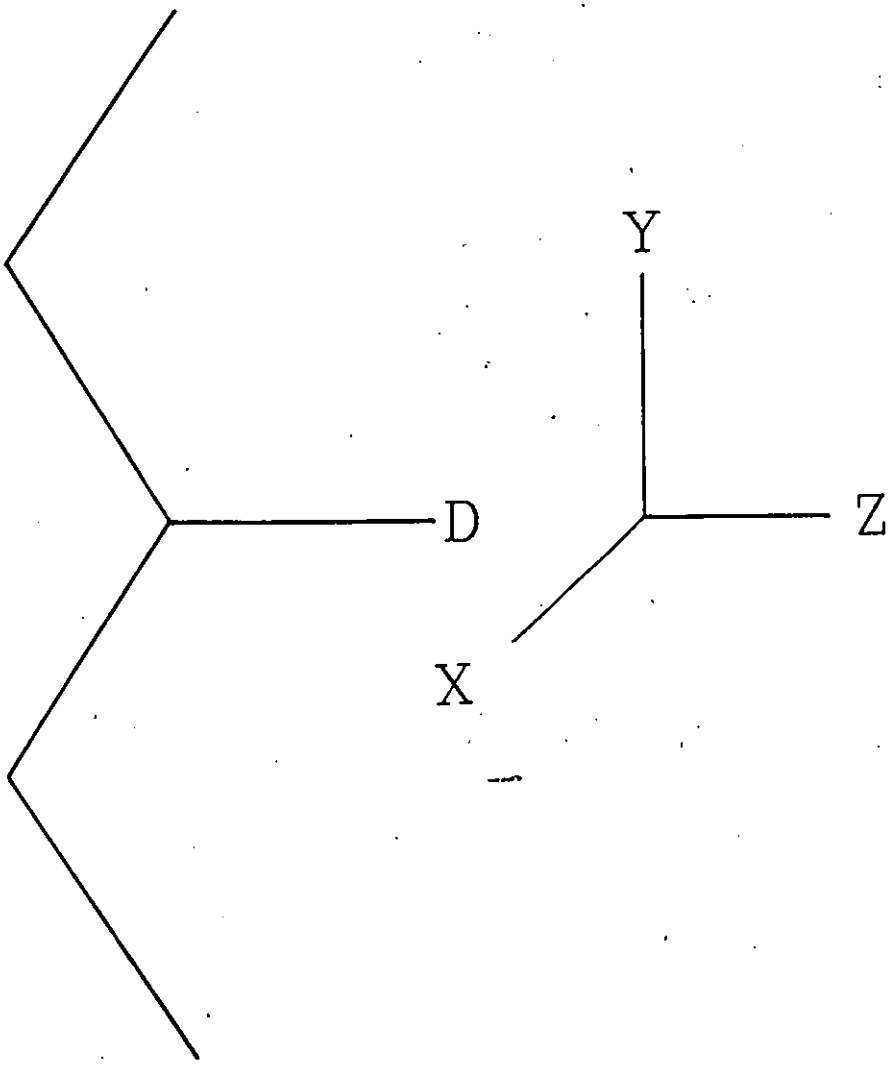

Figure 58. Coordinate system used in the calculation of the effect of chain jumps.

where V_{xx}, V_{yy} and V_{zz} are the principal components of the static tensor and θ is the jump angle. The values of the principal components of the corresponding static quadrupole coupling tensor (Q_{xx}, Q_{yy} and Q_{zz}) can be taken from the phase I spectrum (orthorhombic phase) and can be related directly to the components of the electric field gradient tensor (47). For the methylene deuterons the components are $Q_{xx} = \pm 120$, $Q_{yy} = \pm 120$ and $Q_{zz} = \mp 240$ kHz. (By convention Q_{zz} is assigned to the largest component of the tensor. The correct sign cannot be determined from the spectra.) The effect of the jump is then simulated by allowing the deuterons to jump between two equivalent sites on a circle, perpendicular to the long axis (167, 169). The components of the quadrupole coupling, jumping frame tensor (Equation A1-A3 with V replaced by Q) were solved with a variety of jump angles. These components were then used to simulate the ^2H NMR spectra. The best fit was obtained for $\theta = 82^o$ and the resulting simulation is shown in Figure 49C.

For an 82^o jump, the components of the quadrupole coupling, jumping frame tensor obtained from equations A1-A3 are $Q^J_{xx} = \mp 35$, $Q^J_{yy} = \pm 120$ and $Q^J_{zz} = \mp 85$ kHz. Following the convention that $Q^J_{zz} > Q^J_{xx} > Q^J_{yy}$, then a rotation of the jumping frame of reference yields:

$$Q^J = \begin{vmatrix} \mp 85 & & \\ & \mp 35 & \\ & & \pm 120 \end{vmatrix} \qquad \text{(A4)}$$

with the ±120 kHz representing the tensor component parallel to the chain long axis. This component is invariant to rotation and is indicated by the dashed line in Figures 48A and E. The apparent asymmetry parameter η (Equation 18) is thus a reflection of the difference of the components of the electric field gradient tensor perpendicular to the chain long axis. Since the changes in the observed tensor components, perpendicular to the chain axis, arise as a consequence of the motion, η will be sensitive to the jump angle θ.

The tensor expected for the methyl groups can be calculated by transforming the methyl group tensor to the methylene-deuteron coordinate frame. The resulting tensor is transformed to a jumping coordinate frame and diagonalized in the same manner as the methylene groups to yield (for $\theta = 82^{\circ}$).

$$Q^J = \begin{vmatrix} \pm 17.6 & & \\ & \pm 10.0 & \\ & & \mp 27.6 \end{vmatrix}$$

This results in a spectrum indicative of a greater degree of asymmetry in the axial motion ($\eta = 0.27$) than is observed ($\eta = 0.11$).

REFERENCES

1. S.J. Singer and G.L. Nicolson, Science 175, 720(1972).

2. J.N. Israelachvili and D.J. Mitchell, Biochim. Biophys. Acta 389, 13(1975).

3. J.N. Israelachvili, D,J, Mitchell and B.W. Ninham, Biochim. Biophys. Acta 470, 185(1977).

4. P.R. Cullis and M.J. Hope, Nature 271, 672(1978).

5. B.G. Covino and H.G. Vassalo, "Local Anesthetics: Mechanisms of Action and Clinical Use", Grune and Stratton, New York, 1976.

6. R.H. de Jong, "Local Anesthetics", Charles C. Thomas, Springfield, Illinois, 1977.

7. A.M. Shanes, W.H. Freygang, H. Grundfest and E. Amatniek, J. Gen. Physiol. 42, 793(1959).

8. J. Aceves and X. Machne, J. Pharmacol. Exp. Ther. 140, 138(1963).

9. B. Hille, in "Molecular Mechanisms of Anesthesia, Progress in Anesthesiology", Vol 2, ed. B.R. Fink, Raven Press, New York, 1980, p 1.

10. B. Hille, K. Courtney and R. Dunn, in "Molecular Mechanisms of Anesthesia, Progress in Anesthesiology", Vol 1, ed. B.R. Fink, Raven Press, New York, 1975, p 13.

11. C.Y. Kao and A. Nishiyama, J. Physiol. (London) 180, 50(1965).

12. B. Hille, J. Gen. Physiol. 58, 599(1971).

13. T. Narahashi, N.C. Anderson and J.W. Moore, J. Gen. Physiol. 50, 1413(1976).

14. T. Deguchi, Jap. J. Pharmac. 17, 267(1972).

15. M.J. Halsey, F.F. Brown and R.E. Richards, in "Molecular Interactions and Activity in Proteins", Ciba Foundation, Symposium 60, Excerpta Medica, Amsterdam, 1978.

16. J.M. Ritche, Br. J. Anaesth. 47, 191(1975).

17. D.T. Frazier, T. Narahashi and M. Yamada, J. Pharmacol. Exp. Ther. 171, 45(1970).

18. G.R. Stichartz, J. Gen. Physiol. 62, 37(1973).

19. H.H. Meyer, Arch. Exp. Pathol. Pharmacol. 42, 109(1899).

20. E. Overton, "Studien uber die Narkose", Jena, Fisher, 1901.

21. M. W. Hill, Biochim. Biophys. Acta 356, 117(1974).

22. J.R. Trudell, in "Molecular Mechanisms of Anesthesia, Progress in Anesthesiology", Vol 2, ed. B.R. Fink, Raven Press, New York, 1980, p 261.

23. C.D. Richards, C.A. Keightley, T.R. Hesketh and J.C. Metcalfe, in "Molecular Mechanisms of Anesthesia, Progress in Anesthesiology", Vol 2, ed. B.R. Fink, Raven Press, New York, 1980, p 337.

24. D. Papahadjopoulos, K. Jacobson, G. Poste and G. Shepherd, Biochim. Biophys. Acta 394, 504(1975).

25. A.G. Lee, Biochim. Biophys. Acta 448, 34(1976).

26. M.B. Feinstein, S.M. Fernandez and R.I. Sha'afi, Biochim. Biophys. Acta 413, 354(1975).

27. W.L. Hubbel, J.C. Metcalfe, S.M. Metcalfe and H.M. McConnell, Biochim. Biophys. Acta 219, 415(1970).

28. K.W. Butler, H. Schneider and I.C.P. Smith, Arch. Biochim. Biophys. 154, 548(1973).

29. J.R. Trudell, Anesthesiology 46, 5(1977).

30. G. Camejo, G.M. Villegas, F.V. Burnola and R. Villegas, Biochim. Biophys. Acta 193, 247(1969).

31. B. Maraviglia, J.H. Davis, M. Bloom, J. Westerman and K.W.A. Wirtz, Biochim. Biophys. Acta 686, 137 (1982).

32. A.G. Lee, Nature 262, 545(1976).

33. P. Jost, O.H. Griffin, R.A. Capaldi and G. Vanderkooi, Proc. Natl. Acad. Sci. U.S.A. 70, 480(1973).

34. P.F. Knowles, A. Watts and D. Marsh, Biochemistry 18, 4480(1979).

35. S.Y. Kang, H.S. Gutowsky, J.C. Hsung, R. Jacobs, T.E. King, D. Rice and E. Oldfield, Biochemistry 18, 3257 (1979).

36. C.M. Armstrong, F. Bezanilla and E. Rojas, J. Gen. Physiol. 62, 375(1974).

37. A. Müller, Proc. R. Soc. London Ser. A 138, 514(1932).

38. G.R. Strobl, J. Polym. Sci. Polym. Symp. 59, 121(1977).

39. R.G. Snyder, M. Maroncelli, S.P. Qi and H.L. Strauss, Science 214, 188(1981).

40. J. Doucet, I. Denicolo and A. Craievich, J. Chem. Phys. 75, 1523(1981).

41. E.R. Andrew, J. Chem. Phys. 18, 607(1950).

42. M. Stohrer and F. Noack, J. Chem. Phys. 67, 3729(1977).

43. J.D. Barnes, J. Chem. Phys. 58, 5193(1973).

44. T. Oyama, K. Takamizawa, Y. Urabe and Y. Ogawa, Kyushu Daigaku Kogaku Shuho 52, 129(1979).

45. M. Maroncelli, S.P. Qi, H.L. Strauss and R.G. Snyder, J. Am. Chem. Soc. 104, 6237(1982).

46. R.G. Snyder, M. Maroncelli, H.L. Strauss, C.A. Elliger, D.G. Cameron, H.L. Casal and H.H. Mantsch, J. Am. Chem. Soc. 105, 133(1983).

47. J. Seelig, Quart. Rev. Biophys. 10, 353(1977).

48. G. Büldt and R. Wohlgemuth, J. Membrane Biol. 58, 81 (1981).

49. G.W. Stockton, C.F. Polnaszek, A.P. Tulloch, F. Hasan and I.C.P. Smith, Biochemistry 15, 954(1976).

50. N.O. Petersen and S.I. Chan, Biochemistry 16, 2657(1977).

51. E.J. Dufourc, I.C.P. Smith and H.C, Jarrell, Chem. Phys. Lipids, submitted.

52. M.G. Taylor, T. Akiyama and I.C.P. Smith, Chem. Phys. Lipids 29, 327(1981).

53. M.G. Taylor, T. Akiyama, H. Saitô and I.C.P. Smith Chem. Phys. Lipids 31, 359(1982).

54. H.H. Mantsch, H. Saitô and I.C.P. Smith. Prog. NMR. Spectr. 11, 211(1977).

55. I.C.P. Smith, Bull Magn. Reson. 3, 120(1982).

56. J.H. Davis, Biochim. Biophys. Acta, in press.

57. I.C.P. Smith, in "Biomembranes", Vol 12, eds. L.A. Manson and M. Kates, Plenum Press, New York, 1983, in press.

58. Y. Boulanger, Ph.D. Thesis, University of Ottawa, Ottawa, Canada (1980).

59. Y. Boulanger, S. Schreier, L.C. Leitch and I.C.P. Smith, Can. J. Biochem. 58, 986(1980).

60. Y. Boulanger, S. Schreier and I.C.P. Smith, Biochemistry 20, 6824(1981).

61. J. Westman, Y. Boulanger, A. Ehrenberg and I.C.P. Smith, Biochim. Biophys. Acta 685, 315(1982).

62. C.A. Elliger, J. Label. Compounds and Radiopharmaceuticals, in press.

63. W.S. Singleton, M.S. Gray, M.L. Brown and J.L. White, J. Am. Oil. Chem. Soc. 42, 53(1965).

64. F.M. Davidson and C. Long, Biochem. J. 69, 458(1958).

65. P.R. Cullis and B. De Kruiff, Biochim. Biophys. Acta 436, 523(1976).

66. E.G. Bligh and W.J. Dyer, Can. J. Biochem. Physiol. 37, 911(1959).

67. J.S. Chadha, Chem. Phys. Lipids 4, 104(1970).

68. C.M. Gupta, R. Radhakrishnan and G. Khorana, Proc. Natl. Acad. Sci. U.S.A. 74, 4315(1977).

69. Z. Selinger and Y. Lapidot, J. Lipid Research 7, 174 (1966).

70. M.G. Taylor and I.C.P. Smith, Chem. Phys. Lipids 28, 119(1981).

71. A.P. Tulloch, Lipids 12, 92(1977).

72. Handbook of Biochemistry, The Chemical Rubber Co., CRC Press, Cleveland,,1968.

73. R.F. Nystrom and W.G. Brown, J. Am. Chem. Soc. 69, 2548(1947).

74. W.J. Baumann and H.K. Mangold, J. Org. Chem. 29, 3055 (1964).

75. H. Jarrell, private communication.

76. F. Spener and H.K. Mangold, Chem. Phys. Lipids 11, 215 (1973).

77. M.A. Wells and D.J. Hanahan, Methods in Enzymology 14, 178(1969).

78. E. Oldfield, M. Meadows, D. Rice and R. Jacobs, Biochemistry 17, 2727(1978).

79. E. Baer, J. Maurukas and M. Russel, J. Am. Chem. Soc. 74, 152(1952).

80. Y. Boulanger and L.C. Leitch, J. Label. Compounds and Radiopharmaceuticals 18, 1197(1981).

81. J.T. Dodge, C. Mitchell and D.J. Hanahan, Arch. Biochem. Biophys. 100, 119(1963).

82. G.W. Burton, K.U. Ingold and K.E. Thompson, Lipids 16, 946(1981).

83. C.F. Reed, S.N. Swisher, G.V. Marinetti and E.G. Eden, J. Lab. Clin. Med. 56, 281(1960).

84. J. Folch, W. Lees and G.H. Sloane-Stanley, J. Biol. Chem. 226, 497(1957).

85. A.P. Tulloch, Lipids 12, 92(1977).

86. A.P. Tulloch, Lipids 25, 225(1979).

87. A.P. Tulloch, Chem. Phys. Lipids 24, 391(1979).

88. G.W. Stockton, K.G. Johnson, K.W. Butler, C.F. Polnaszek, R. Cyr and I.C.P. Smith, Biochim. Biophys. Acta 401, 535(1979).

89. K.W. Miller and S.C.T. Yu, Br. J. Pharmac. 61, 57(1977).

90. S. Roth and P. Seeman, Biochim. Biophys. Acta 255, 207 (1972).

91. H.H. Mantsch, A. Martin and D. Cameron, Biochemistry 20, 3138(1981).

92. H.H. Mantsch, S.C. Hsi, K.W. Butler and D.G. Cameron, Biochim. Biophys. Acta 728, 325(1983).

93. P.R. Cullis and A.J. Verkleij, Biochim. Biophys. Acta 552, 546(1979).

94. J.H. Davis, K.R. Jeffrey, M. Bloom, M.I. Valic and T.P. Higgs, Chem. Phys. Lett. 42, 390(1976).

95. M. Bloom, J.H. Davis and M.I. Valic, Can J. Phys. 58, 1510(1980).

96. J.H. Davis, Biophys, J. 27, 339(1979).

97. M.I. Valic, H. Gorrissen, R.J. Cushley and M. Bloom, Biochemistry 18, 854(1979).

98. R.L. Vold, J.S. Waugh, M.P. Klein and D.W. Phelps, J. Chem. Phys. 48, 3831(1966).

99. M. Bloom, J.H. Davis and A.L. Mackay, Chem. Phys. Lett. 80, 198(1981).

100. H.C. Jarrell, R.A. Byrd and I.C.P. Smith, Biophys. J. 34, 451(1981).

101. E.L. Hahn, Phys. Rev. 80, 580(1950).

102. M. Rance and R.A. Byrd, J. Magn. Reson. in press.

103. G. Van Meer, C.G. Gahmberg, J.A.F. Op den Kamp and L.L.M. Van Deenan, FEBS Lett. 135, 53(1981).

104. J.A.F. Op den Kamp, Ann. Rev. Biochem. 48, 47(1979).

105. S.R. Davio and P.S. Low, Biochim. Biophys. Acta 644, 157(1981).

106. P.R. Cullis and B. De Kruijff, Biochim. Biophys. Acta 559, 399(1976).

107. A.P. Hornby and P.R. Cullis, Biochim. Biophys. Acta 647, 285(1981).

108. P.R. Cullis, A.P. Hornby and M.J. Hope, in "Molecular Mechanisms of Anesthesia, Progress in Anesthesiology", Vol 2, ed. B.R. Fink, Raven Press, New York, 1980, p 337.

109. J.L. Browning and H. Akutsu, Biochim. Biophys. Acta 684, 172(1982).

110. H.H. Wang, J. Earnest and D. Chan, in "Molecular Mechanisms of Anesthesia, Progress in Anesthesiology", Vol 2, ed. B.R. Fink, Raven Press, New York, 1980, p 483.

111. M.J. Neal, K.W. Butler, C.F. Polnaszek and I.C.P. Smith, Mol. Pharm. 12, 144(1975).

112. L.E.G. Eriksson and J. Westman, Biophys. Chem. 13, 253 (1981).

113. J. Cerbon, Biochim. Biophys. Acta 290, 51(1972).

114. H.G.L. Coster, V.J. James, C. Berthet and A. Miller, Biochim. Biophys. Acta 641, 281(1981).

115. L.B.A. Johansson ang G. Lindblom, Biophys. J. 36, 735(1981).

116. P. Seeman, Pharmacol Rev. 24, 583(1972).

117. A. Blume, D.M. Rice, R.J. Wittebort and R.G. Griffin, Biochemistry 21, 6220(1982).

118. D. Marsh, A. Watts and I.C.P. Smith, Biochemistry, in press.

119. M. Rance, Ph.D. Thesis, University of Guelph, Guelph, Canada (1981).

120. R.G. Barnes, Adv. Quadrupole Reson. 15, 335(1974).

121. S. Kashino, M. Ikeda and M. Haisa, Acta Crystallogr. B38, 1868(1982).

122. M.F. Brown, J. Seelig and U. Haberlen, J. Chem. Phys. 70, 5045(1979).

123. M.F. Brown, J. Chem. Phys. 77, 1576(1982).

124. M.F. Brown and J.H. Davis, Chem. Phys. Letters 79, 431 (1981).

125. A. Seelig and J. Seelig, Biochemistry 16, 45(1977).

126. P.G. Bradford and G.V. Marinetti, J. Membrane Biol. 67, 211(1982).

127. A.G. Marshall, J. Chem. Phys, 52, 2527(1970).

128. A. Johansson and T. Drakenberg, Mol. Cryst. Liq. Cryst. 14, 23(1971).

129. K.R. Jeffrey, Bull. Magn. Reson. 3, 69(1982).

130. G.L. Turner and E. Oldfield, Nature, 277, 669(1979).

131. J. Seelig and H.U. Gally, Biochemistry 15, 5199(1976).

132. H. Hauser, I. Pascher, R.H. Pearson and S. Sundell, Biochim. Biophys. Acta 650, 21(1981).

133. A. Seelig and J. Seelig, Biochim. Biophys. Acta 406, 1 (1975).

134. M.F. Brown and J. Seelig, Biochemistry 17, 381(1978).

135. H. Akutsu, Y. Kyogoku, H. Nakahara and K. Fukuda, Chem. Phys. Lipids 15, 222(1975).

136. P.B. Hitchcock, R. Mason, K.M. Thomas and G.G. Shipley, Proc. Natl. Acad. Sci. U.S.A. 71, 3036(1974).

137. H. Richards, J. Dufourcq and C. Lussan, FEBS Lett. 45, 136(1974).

138. J.F. Nagle, J. Membrane Biol. 27, 233(1976).

139. S.C. Shen, J.M. Sturtevant and B.J. Gaffney, Proc. Natl. Acad. Sci. U.S.A. 77, 5060(1980).

140. D.A. Wilkinson and J.F. Nagle, Biochemistry 20, 187(1981).

141. M.C. Phillips and D. Chapman, Biochim. Biophys. Acta 163, 301(1968).

142. A. Blume, Biochim. Biophys. Acta 557, 32(1972).

143. J. Frenzel, K. Arnold and P. Nuhn, Biochim. Biophys. Acta 507, 185(1978).

144. A. Blume and R.G. Griffin, Biochemistry 21, 6230(1982).

145. R. Gosh and J. Seelig, Biochim. Biophys. Acta 691, 151(1982).

146. V.T. Marchesi, H. Furthmayr and M. Tomita, Ann. Rev. Biochem. 45, 667(1976).

147. R.F.A. Zwaal, B. Roelofsen, P. Comfurius and L.L.M. Van Deenen, Biochim. Biophys. Acta 406, 83(1976).

148. A. Kahlenberg, C. Walker and R. Rohrlick, Can. J. Biochem. 52, 803(1974).

149. D.A. Butterfield, C.C. Whisnant and D.B. Chesnut, Biochim. Biophys. Acta 426, 697(1976).

150. P.R. Cullis and C. Grathwohl, Biochim. Biophys. Acta 471, 213(1977).

151. P.R. Cullis, FEBS Lett. 68, 173(1976).

152. J.H. Davis, B. Maraviglia, G. Weeks and D.V. Godin, Biochim. Biophys. Acta 550, 362(1979).

153. B. Maraviglia, J.H. Davis, M. Bloom, J. Westerman and K.W.A. Wirtz, Biochim. Biophys. Acta 686, 137(1982).

154. D.D. Koblin, J. Yguerabide and H.H. Wang, in "Molecular Mechanisms of Anesthesia, Progress in Anesthesiology", Vol 2, ed. B.R. Fink, Raven Press, New York, 1980. p 439.

155. M.J. Conrad and S.J. Singer, Biochemistry 20, 808(1981).

156. M.J. Conrad and S.J. Singer, Biochemistry 20, 808(1981).

157. M. Rance, K.R. Jeffrey, A.P. Tulloch, K.W. Butler and I.C.P. Smith, Biochim. Biophys. Acta 600, 245(1980).

158. M. Rance, K.R. Jeffrey, A.P. Tulloch, K.W. Butler and I.C.P. Smith, Biochim. Biophys, Acta 688, 191 (1982).

159. H.C. Jarrell, K.W. Butler, R.A. Byrd, R. Deslauriers, I. Ekiel and I.C.P. Smith, Biochim. Biophys. Acta 688, 622(1982).

160. E.D. Matayoshi, Biochemistry 19, 3414(1980).

161. M.G. Broadhurst, J. Res. Natl. Bur. Stand. Sect. A 66, 241(1962).

162. H.L. Casal, H.H. Mantsch, D.G. Cameron and R.G. Snyder, J. Chem. Phys. 77, 2825(1982).

163. G. Zerbi, R. Magni, M. Gussoni, K.H. Moritz, A. Bigotto and S. Dirlikov, J. Chem. Phys. 75, 3175(1981).

164. N. Boden, L.D. Clark, S.M. Hanlon and M. Mortimer, Faraday Symp. Chem. Soc. 13, 109(1979).

165. J.A. Ripmeester and S.R. Gough, Mol. Cryst. and Liq. Cryst. Letters 64, 133(1981).

166. A distortion of $<2°$ from the tetrahedral angle has been found in propane. R.D. Lide, J. Chem. Phys. 33, 1514(1960).

167. H.W. Spiess, Rotation of molecules and nuclear spin relaxation, in "NMR Basic Principles and Progress", Vol 15,eds. P. Diehl, E. Fluck and R. Kosfeld, Springer-Verlag, Berlin, 1978, p 55.

168. T.H. Huang, R.P. Skarjune, R.J. Wittebort, R.G. Griffin, and E. Oldfield, J. Am. Chem. Soc. 102, 7377(1980).

169. S. Soda and T. Chiba, J. Chem Phys. 50, 439(1969).

170. B. Ewen, G.R. Strobl and D. Richter, Faraday Spec. Discuss. Chem. Soc. 69, 19(1980).

171. B. Ewen, E.W. Fischer, W. Piesczek and G.R. Strobl, J. Chem. Phys. 61, 5265(1975).

172. A. Carrington and A.D. McLachlan, "Introduction to Magnetic Resonance", Harper and Row, New York, 1967.

173. D.I. Hoult and R.E. Richards, Proc. R. Soc. London A 344, 311 (1975).